THE
PHYSICAL REVIEW
A Journal of Experimental and Theoretical Physics Established by E. L. Nichols in 1893
VOL. 50, NO. 9 NOVEMBER 15, 1936 SECOND SERIES

Polarization of Hard X-Rays

ERIC RODGERS,* *Ryerson Physical Laboratory, The University of Chicago, Chicago, Illinois*
(Received September 5, 1936)

A study has been made of the polarization of x-rays scattered at 90° from the primary beam for various voltages ranging from 80 to 800 kilovolts. The scattered rays were again scattered at 90° and a Geiger-Müller counter was used to determine the relative intensities of the tertiary rays in directions parallel and perpendicular to the primary rays. At 80 kilovolts the polarization was found to be practically complete, but it was found to decrease to 69.6 percent as the x-ray tube voltage was raised to 800 kilovolts. Within the limits of experimental error, the results agree with Nishina's theory which predicts an unpolarized component in the secondary x-rays increasing in relative magnitude as the frequency of the primary rays becomes greater.

INTRODUCTION

IN 1928 Klein and Nishina[1] published their well-known formula for x-ray scattering per electron. This formula was derived on the basis of the relativistic quantum mechanics of Dirac. Except in the domain of very short wave-lengths, the predictions of the Klein-Nishina formula differ very little from the predictions of the formula derived by Dirac[2] in 1926, or from those of the formula derived by Compton[3] in 1923. However, when the wave-length of the incident rays is sufficiently short that the mass of a photon of the rays is comparable with the rest mass of the scattering electron, the Klein-Nishina formula gives a scattering coefficient that is considerably greater than that from either of the other formulas. Recent experimental results by several investigators[4] have been in excellent agreement with the Klein-Nishina formula.

Besides predicting different results regarding intensity, there is another feature of the Klein-Nishina formula that differs from the other formulas. The latter require the rays scattered at 90° with the primary beam to be completely plane polarized. According to the Klein-Nishina formula, the rays scattered at 90° are not completely plane polarized, but contain an unpolarized component which is a function of the frequency. For ordinary wave-lengths the unpolarized component is negligible, but it becomes important at wave-lengths at which the intensity predictions of the Klein-Nishina formula begin to differ appreciably from those of the older theories. Dirac's theory shows that the electron has a property which may be interpreted as a magnetic moment, and it is this magnetic moment that leads to the unpolarized component.

* Now at University of Alabama, University, Alabama.
[1] O. Klein and Y. Nishina, Zeits. f. Physik **52**, 853 (1928).
[2] P. A. M. Dirac, Proc. Roy. Soc. **A111**, 405 (1926). Also derived independently by G. Breit, Phys. Rev. **27**, 362 (1926), and by W. Gordon, Zeits. f. Physik **40**, 117 (1926).
[3] A. H. Compton, Phys. Rev. **21**, 491 (1923).
[4] C. Y. Chao, Phys. Rev. **36**, 1519 (1930); J. Read and C. C. Lauritsen, Phys. Rev. **45**, 433 (1934); W. V. Mayneard and J. E. Roberts, Nature **136**, 793 (1935); J. Read, Proc. Roy. Soc. **A152**, 402 (1935); L. Meitner and H. Hupfeld, Zeits. f. Physik **67**, 147 (1930); G. B. T. Tarrant, Proc. Roy. Soc. **128**, 345 (1930).

A. H. Compton[5] notes that from purely classical electrodynamics there should be an unpolarized component if the electron has a magnetic moment. Nishina[6] has considered the polarization of the rays scattered at 90° and has derived an expression for the intensity of the rays after a second scattering at 90°. His result is

$$I_t=\frac{e^8}{2m^4c^8r^2r'^2}\frac{I_0}{(1+2\alpha)^3}\left[\sin^2\theta+\frac{\alpha^2(2+4\alpha+3\alpha^2)}{2(1+\alpha)^2(1+2\alpha)}\right],$$

where $\alpha=h\nu/mc^2$, I_t is the intensity of the tertiary rays, I_0 is the intensity of the primary rays, r is the distance between the two scattering electrons, r' is the distance from the second electron to the point of observation, θ is the angle measured in a plane at right angles to the direction of the secondary rays and is the angle between the direction of observation and a line perpendicular to the direction of the primary rays, and e, h, and ν have their usual meaning. The experiments described below were performed to test Nishina's theory of the unpolarized component.

Source of X-Rays

The large x-ray tube at Mercy Hospital was used as a source of hard x-rays. The use of this equipment was made possible through the kind permission of Dr. Henry Schmitz of Mercy Hospital. Experiments were performed with the large tube operating at voltages from 400 to 800 kilovolts with 10 ma tube current, and with a smaller x-ray tube also at the hospital operated at 200 kilovolts and 25 ma tube current.

Apparatus

A. Counter and circuits

As a means of measuring relative x-ray intensities, a Geiger-Müller counter was used. Several types of counters were tried. The one which worked best consisted of a small cylinder of thin copper with a fine tungsten wire coaxial with it and sealed off in a glass tube at a pressure of 12.5 cm of dry air. The copper cylinder was 3 cm long and 1 cm in diameter. The negative potential applied to the cylinder of the counter tube was supplied by a slightly modified form of the circuit described by Johnson and Street.[7] The impulses from the counter were amplified by a circuit essentially the same as that described by Locher.[8] The specially designed mechanical recorder was capable of responding to 70 impulses per second. Radium tests showed that for gamma-rays the counting rate was directly proportional to the intensity of the rays.

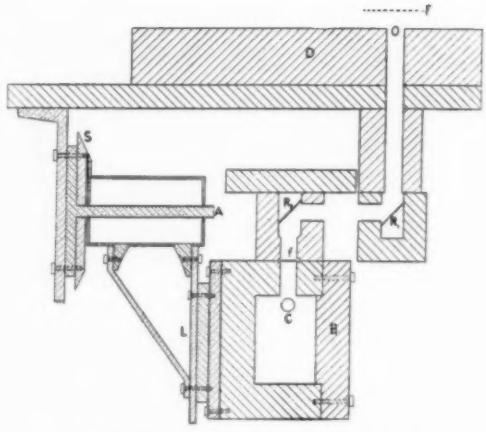

FIG. 1. Apparatus used in studying polarization.

B. Polarization apparatus

The apparatus used in studying the polarization is shown diagrammatically in Fig. 1. The counter tube C was inclosed in the lead box B having walls $1\frac{1}{2}$ inches thick. The lead box was rigidly attached to a steel beam L which could be rotated about the horizontal axis A. A divided circle S was used for angular measurements. A window in the x-ray tube permitted the x-rays to be emitted vertically downward, the target of the tube being surrounded with lead 6 inches thick except for the window. The apparatus was mounted under the x-ray tube so that the x-rays passed through the opening O and reached the counter after being scattered twice at right angles by the scatterers R_1 and R_2. The scatterers were of iron $1\frac{1}{2}$ mm thick and were set so that the incident rays struck them at 45°. The x-rays were filtered through the 3 mm brass window of the x-ray tube, through the filter at f consisting of 1 mm of aluminum and 0.5 mm of copper, the

[5] A. H. Compton and S. K. Allison, *X-Rays in Theory and Experiment* (1935), p. 237.
[6] Y. Nishina, Zeits. f. Physik **52**, 869 (1928).
[7] J. C. Street and T. H. Johnson, J. Frank. Inst. **214**, 155 (1932).
[8] G. L. Locher, J. Frank. Inst. **216**, 553 (1933).

aluminum being nearer the counter, and through additional filters placed at F. The additional filters ranged from 1 mm of aluminum at 400 kilovolts to 1 mm of aluminum, 3 mm of copper and 1 mm of tin at 800 kilovolts. The experimental arrangement with the 200 kilovolt tube was exactly the same, except that the filter at F consisted of 1 mm of aluminum and 0.75 mm of copper and the permanent filter in the window of the tube was different. A small metal box containing the first amplifying tube was attached to the side of the lead box containing the counter.

A large thickness of lead was required to protect the counter from the direct x-ray beam. With 1 inch of lead at D, the direct rays penetrated sufficiently to give 2500 counts per minute when the counter was in the horizontal position. In order to make the effect of the primary rays negligible, it was necessary to increase the thickness at D to $3\frac{1}{2}$ inches.

Experimental Procedure

Four readings were required to make a determination of the polarization. First a count was taken with the counter directly underneath the scatterer R_2. This is the position shown in the diagram. In this case the tertiary rays striking the counter were parallel to the primary rays. The lead box containing the counter was then swung through 90° into the horizontal position and a count taken. The scatterer R_2 was then taken out and counts taken in the two positions. These counts were subtracted from the first two to give net counts in the two positions. The average number of counts during 5 minute intervals as thus observed are given in Table I. Experiment showed that if the scatterer R_1 were removed instead of R_2, practically no radiation at all reached the counter, the counting rate in this case being less than one count per minute above the rate with the x-rays off. This showed that the radiation reaching R_2 that was not scattered from R_1 was negligible.

Table I. *Average number of counts during 5-minute intervals.*

Tube voltage kilovolts	Parallel		Perpendicular	
	R_2 in	R_2 out	R_2 in	R_2 out
200	2028	161	362	138
400	816	74	195	82
500	1090	95	275	92
600	1209	93	307	91
700	1466	113	408	103
800	1347	128	439	121

The counting rate throughout the experiments was sufficiently low to make it unnecessary to correct for impulses lost due to the resolving time of the apparatus. There were two sources of error that had to be taken into account. One resulted from multiple scattering and the other resulted from the fact that the rays were not all scattered at exactly 90°. The latter could be estimated from the geometry of the apparatus. An approximate calculation showed that this error amounted to about 4.5 percent, in the polarization. The multiple scattering error was estimated experimentally by using different thicknesses for the scatterers R_1 and R_2. This error was estimated to amount to about 6.5 percent.

The effective wave-length at each voltage was estimated from absorption measurements. With the counter tube set in the parallel position, the reduction in intensity due to different thicknesses of copper placed just above the filter F was determined. The effective mass-absorption coefficient was then computed. The value for the mass-absorption coefficient obtained in this way is too large because of strong absorption at the longer wave-lengths. An approximate correction for this error was estimated by using assumed spectral energy distributions in the primary beam. Such a correction, however, cannot be expected to be very accurate because of lack of knowledge of the exact spectral distribution.

Results

The polarization was computed from the defining relation

$$P=(I_{\parallel}-I_{\perp})/(I_{\parallel}+I_{\perp}),$$

where the net counts in the parallel and perpendicular directions were used for $I_{\parallel}$ and $I_{\perp}$, respectively. Table II shows the uncorrected and corrected values of the polarization. The results of the first series of experiments are relatively unreliable, due chiefly to lack of constancy of the x-ray tube. During the second series of experiments, referred to in Table II, the same counter tube was used throughout. No change could be detected in its residual count or in its response to

TABLE II. *Comparison of results with values calculated from Nishina's formula.*

X-ray tube voltage (kv)	Observed Polarization		Estimated wave-length A.U.	Corrected polarization results	Calculated from Nishina's formula
	1st series of experiments	2nd series of experiments			
	Percent	Percent		Percent	Percent
80	89.0	—	—	—	—
200	—	78.6	0.100	89.6	92.6
400	72.8	73.5	.060	84.5	84.2
500	63.9	68.9	.052	79.9	80.9
600	62.2	67.5	.050	78.5	80.0
700	60.8	63.2	.042	74.2	74.7
800	59.9	58.6	.039	69.6	73.1

radium tests throughout the period taken to do the experiments. Special precautions were also made to keep the x-ray tube operating under constant conditions. Due to the conditions under which the first set of results was obtained, they are not averaged with the results of the second set of experiments. The corrected results were obtained by adding a correction of 11 percent to each of the results of the second series of experiments. This is the estimated value for the two sources of error mentioned above. Each of the given experimental results represents an average of several separate trials. The value given for 80 kilovolts was obtained at Ryerson Laboratory with carbon scattering blocks before the apparatus was moved to the hospital. The corrected result at this voltage is not given because no effort was made to find the effect of multiple scattering in the carbon blocks. It would seem reasonable to assume that the correction in this case should be of the same order of magnitude as that at other voltages, and consequently the corrected result at this voltage should be approximately 100 percent. This would be in accord with earlier precision experiments on polarization, such as those of Compton and Hagenow.[9]

The last column in Table II gives the percentages of polarization predicted by Nishina's theory for the assumed wave-lengths. The estimated wave-lengths are rather uncertain, but they do not differ greatly from those which had previously been determined by Dr. Schmitz from absorption measurements in the primary beam. It is believed that these experiments furnish conclusive evidence that an unpolarized component of the predicted order of magnitude does exist.

The writer wishes to express his appreciation to Professor A. H. Compton for suggesting the problem and for much valuable advice, to Dr. Henry Schmitz of Mercy Hospital through whose cooperation this work was made possible, to the diagnostic x-ray department of Mercy Hospital for furnishing a room in which to keep the apparatus, and to Mr. F. W. Eims for many hours spent in operating the large x-ray tube.

[9] A. H. Compton and C. F. Hagenow, J. O. S. A. and R. S. I. **8**, 487 (1924).

NOVEMBER 15, 1936 PHYSICAL REVIEW VOLUME 50

Scattering of X-Rays by a Spinning Electron

ARTHUR H. COMPTON, *University of Chicago, Chicago, Illinois*

(Received October 5, 1936)

A theory based upon classical electrodynamics is presented for the scattering of x-rays by an electron which is spinning and has a magnetic moment. The radiation scattered by such a magnetic doublet is found to be almost completely unpolarized. Being proportional to ν^2, it is negligible for ordinary x-rays, but should comprise the major part of the scattering according to classical theory for wave-lengths as short as hard gamma-rays. The rays thus scattered by one electron should be incoherent with those from every other. In all of these features the radiation thus magnetically scattered is closely similar in properties to that described by the added term of Klein and Nishina's quantum theory of scattering. Only in the distribution of scattered rays with angle does there appear a fundamental difference between the results of the two theories. Insofar as the two theories agree, we may consider the classical interpretation of Klein and Nishina's added term to be scattering due to the electron's spin. In particular, an interpretation according to classical electron theory of Rodger's experimental discovery of an important unpolarized component in scattered x-rays of very high frequency is that the electron is a magnetic doublet, which for these frequencies is comparable in importance with its electric charge.

THE concept of a spinning electron[1] which because of its spin has a magnetic moment has been useful in accounting for several physical phenomena, especially the fine structure of spectral lines.[2] When such an electron is traversed by an electromagnetic wave it should scatter radiation in a distinctive manner. The characteristics of the radiation thus scattered, as calculated according to classical electrodynamics, are similar to those of the scattered radiation described by Klein and Nishina's quantum-mechanics theory of the phenomena.[3] This theory, it will be recalled, added a term, which to the second power of α is

$$I_{KN}=I_e\alpha^2\frac{(1-\cos\varphi)^2}{1+\cos^2\varphi}, \qquad (1)$$

to that given by the earlier formula of Breit, Gordon and Dirac.[4] Here I_e is the scattering per electron as calculated by Thomson's classical electron theory

$$I_e=I_0\frac{e^4}{m^2r^2c^4}(1+\cos^2\varphi), \qquad (2)$$

φ being the angle between the primary and the scattered rays, r the distance from the electron to the observer, e, m, c and h have the usual significance, and

$$\alpha\equiv h\nu/mc^2=h/mc\lambda, \qquad (3)$$

where λ is the wave-length of the incident rays. This term arose from the use of Dirac's relativistic form of quantum mechanics, whose classical analog contains a spin term and an imaginary electric moment term. Presumably a part at least of the added scattering predicted by Klein and Nishina should thus be attributable to electron spin. The fact that classical electrodynamics, when applied to a spinning electron gives rise to a very similar expression (Eq. (9)), supports this presumption.

Following the successes of the Klein and Nishina formula in describing the intensity of scattering and the absorption of x-rays of short wave-length, Rodgers has recently[5] shown also that for these short wave-lengths an unpolarized component of the scattered x-rays appears. According to the Klein and Nishina theory,[6] it is only the component described by Eq. (1) which is incompletely polarized when scattered at 90°. On classical theory, as is well known, the scattered rays due to the electron's charge are completely polarized, while, as we see below, those due to its magnetic moment have an important unpolarized component. Rodger's experimental discovery of an unpolarized component thus gives specific confirmation of the new term in the Klein-Nishina formula, and affords new and direct evidence for the spin and the magnetic moment of the electron.

Precession of a Spinning Electron

Let $\mathbf{p}$ be the angular momentum of the electron's spin, and $\boldsymbol{\gamma}$ be its magnetic moment. The torque exerted on the electron by the electromagnetic wave which traverses it is then

$$\mathbf{T}=\boldsymbol{\gamma}\times\mathbf{H},$$

where $\mathbf{H}$ is the magnetic vector of the wave. The result is a precession of the spin axis about $\mathbf{H}$ such that

$$d\mathbf{p}/dt=\mathbf{T},$$

and a change of magnetic moment at the rate

$$\dot{\boldsymbol{\gamma}}=(\gamma/p)[\boldsymbol{\gamma}\times\mathbf{H}].$$

If now the magnetic vector of the primary is expressed by

$$\mathbf{H}_0=\mathbf{A}_0\cos 2\pi\nu t$$

we have, assuming that the rate of rotation of the spinning electron is high compared with ν,

$$\ddot{\boldsymbol{\gamma}}=(\gamma/p)[\boldsymbol{\gamma}\times(d\mathbf{H}/dt)]$$
$$=-2\pi\nu(\gamma/p)[\boldsymbol{\gamma}\times\mathbf{A}_0]\sin 2\pi\nu t.$$

But the magnitude of the magnetic vector of the wave radiated by this changing magnetic doublet is

$$H_s=(\ddot{\gamma}/rc^2)\sin\theta,$$

[1] Cf. A. H. Compton, Phil. Mag. **41**, 279 (1921).
[2] E.g., L. Pauling and S. Goudsmidt, *The Structure of Line Spectra* (1930), p. 54.
[3] O. Klein and Y. Nishina, Zeits. f. Physik **52**, 853 (1929).
[4] For a summary of this work, cf. e.g. A. H. Compton and S. K. Allison, *X-Rays in Theory and Experiment* (1935), p. 234.
[5] E. Rodgers, preceding paper, this issue.
[6] A detailed discussion of the polarization characteristics of the rays scattered according to their theory has been given by Y. Nishina, Zeits. f. Physik **52**, 869 (1929).

where θ is the angle between $\ddot{\boldsymbol{\gamma}}$ and $\mathbf{r}$, i.e., between $\mathbf{T}$ and $\mathbf{r}$. The instantaneous intensity of the scattered wave is then

$$I'=\frac{c}{4\pi}H_s^2=\frac{c}{4\pi}\frac{4\pi^2\nu^2}{r^2c^4}\frac{\gamma^2}{p^2}[\boldsymbol{\gamma}\times\mathbf{A}_0]^2\sin^2\theta\sin^2 2\pi\nu t.$$

The average value of this intensity taken over a complete cycle, assuming that the period of the electron's precession is long compared with the period of the wave, is

$$I''=I'/2\sin^2 2\pi\nu t.$$

The corresponding average intensity of the primary wave traversing the electron is

$$I_0=(c/8\pi)A_0^2.$$

We may thus write

$$I''=I_0\frac{4\pi^2\nu^2}{r^2c^4}\frac{\gamma^4}{p^2}\sin^2\xi\sin^2\theta, \qquad (4)$$

where ξ is the angle between $\boldsymbol{\gamma}$ and $\mathbf{A}_0$.

We next proceed to average I'' over all possible orientations of the spin axis. Let us refer to Fig. 1, in which the X axis is the direction of propagation of the primary beam, and the XY plane is chosen to include OP, the direction of the scattered ray under consideration. The primary magnetic vector $\mathbf{H}$ is then normal to OX and at an arbitrary angle ζ with the Y axis, and the magnetic doublet $\boldsymbol{\gamma}$ is at an angle ξ with $\mathbf{H}$. The torque $\mathbf{T}$ is perpendicular to $\boldsymbol{\gamma}$ and $\mathbf{H}$. The angle θ between $\mathbf{T}$ and $\mathbf{r}$ is given by

$$\cos\theta=-\cos\varphi\sin\psi-\sin\varphi\cos\psi\sin\zeta.$$

Thus, $$\sin^2\theta=1-\cos^2\varphi\sin^2\psi-2\sin\varphi\cos\varphi$$
$$\times\sin\psi\sin\zeta-\sin^2\varphi\cos^2\psi\sin^2\zeta. \qquad (5)$$

The average intensity for all orientations of the spin axis is,

$$I_s=\frac{1}{4\pi}\int_0^{\pi}\int_0^{2\pi}I''\sin\xi\,d\psi\,d\xi.$$

Substituting the value of I'' and of $\sin^2\theta$ given in Eqs. (4) and (5), we obtain on integration

$$I_s=I_0\frac{4}{3}\pi^2\frac{\nu^2\mu^4}{r^2c^4p^2}[1+\sin^2\varphi\cos^2\zeta]. \qquad (6)$$

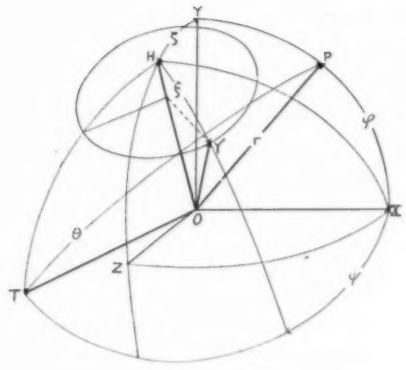

FIG. 1.

STATE OF POLARIZATION

For the ray scattered at $\varphi=90°$, if the primary ray is polarized with the magnetic vector along the Y axis, $\zeta=0$, and the factor in brackets becomes equal to 2. In this case reference to Fig. 1 shows that the direction of $\mathbf{T}$ and hence of $\ddot{\boldsymbol{\gamma}}$ is perpendicular to the Y axis, which is the direction of scattering, and that the probability distribution of this direction is axially symmetrical about Y. Thus the scattered ray is in this case completely unpolarized.

If the primary ray has its magnetic vector along the Z axis, $\zeta=90°$, and the bracketed factor becomes 1. In this case $\ddot{\boldsymbol{\gamma}}$ lies in the XY plane. This gives rise to a component of the ray scattered along the Y axis which is polarized in the same plane as is the ray scattered by the electric charge of the electron.

Since for an unpolarized primary beam the average magnitudes of the Y and Z components of the magnetic vector are equal, this means that when an unpolarized ray is scattered at 90° the scattered ray may be thought of as consisting of an unpolarized component of intensity 2 upon which is superposed a polarized component of intensity 1. If this ray is scattered again at 90° by a magnetic doublet, as in the usual technique for studying polarized x-rays, it can be shown that the ratio of $I_{\parallel}$ to $I_{\perp}$ is 5/4. Thus the magnitude of the polarization of rays scattered only by the magnetic moment of the electron, as defined in the usual manner, should be

$$P\equiv(I_{\parallel}-I_{\perp})/(I_{\parallel}+I_{\perp})=1/9. \qquad (7)$$

Nishina has shown[6] that the corresponding polarization of the added term in the Klein-Nishina formula is 0.

Intensity

In the theory of spectra, it is found necessary to assume that the effective value of the electron's angular momentum and magnetic moment are, respectively,[2]

$$p=\sqrt{(\tfrac{3}{4})}h/2\pi$$

and
$$\gamma=\sqrt{(\tfrac{3}{4})}(h/2\pi)(e/mc). \tag{8}$$

Substituting these values in Eq. (6), and taking the average value of $\sin^2\zeta$ as $\frac{1}{2}$ for unpolarized radiation, we obtain,

$$I_\gamma=\frac{1}{8}\frac{e^4}{m^2r^2c^4}\frac{h^2\nu^2}{m^2c^4}(3-\cos^2\varphi).$$

Using relations (2) and (3), this may be written,[7]

$$I_\gamma=I_e\alpha^2\frac{3-\cos^2\varphi}{4(1+\cos^2\varphi)}. \tag{9}$$

Noting that $\alpha=0.024/\lambda$, if λ is expressed in angstroms, this means that for wave-lengths shorter than about 0.024A, in the middle gamma-ray region, the magnetic moment of an electron is responsible for more scattering than is its electric charge.

[7] This result, except for an error of a factor of 2, has been given in footnote 166, p. 237, of A. H. Compton and S. K. Allison's *X-Rays in Theory and Experiment* (1935), where a comparison with the results of Klein and Nishina's theory is also given. The derivation of the expression has, however, not been presented.

It will be seen that this magnetic scattering is of the same order of magnitude as the added term (1) of Klein and Nishina's theory. It is noteworthy however that while both theories give the same type of variation of intensity with frequency, the variation with angle of scattering is fundamentally different. The factor $(1-\cos\varphi)$ present in Klein and Nishina's formula suggests on classical theory an incoherent scattering which vanishes at $\varphi=0$ because of exactness of phase relationships. Such a process has no place in the present theory of scattering by a magnetic doublet.

Phase Relationships

It will be seen from Fig. 1 that for every orientation of **T** there is an equally probable orientation in the opposite sense. It follows that if the squares of the sum of the amplitudes of the waves scattered by a group of spinning electrons is averaged over all possible orientations, all the product terms must vanish, leaving only the sum of the squared terms. Thus each doublet scatters a wave which is incoherent with that from every other doublet. Because of this incoherence it is legitimate to assume, as we have done, that the scattering by an electron's magnetic doublet is independent of that by its electric charge.

This feature is also characteristic of the scattering represented by Klein and Nishina's added term. In their case incoherence follows from the fact that the initial and final states of the scattering atoms are of different energy, implying an increased wave-length, so that no exact phase relationships can exist.

Cosmic-Ray Shower Production and Absorption in Various Materials

J. E. MORGAN AND W. M. NIELSEN, *Duke University, Durham, North Carolina*

(Received, August 31, 1936)

Measurements have been made of shower production in thin pieces of carbon, aluminum, copper, tin and lead. The results as shown by a study of three and twofold showers for thicknesses of 0.58 and 0.29 cm lead mass equivalent thickness and for several different experimental arrangements, indicate that the increase in counting rate associated with each atom in the producing material varies as the 2.0 ± 0.2 power of the atomic number of the element concerned. Our measurements indicate that the increase in counting rate for heavy elements such as lead increases faster than the first power of the thickness of producing material. The departure from linearity seems to be a function of atomic number, being greater for elements of large Z. Absorption measurements of showers from lead, in lead, tin, copper, aluminum and carbon show that the absorption per atom varies between the first and second powers of the atomic number. Rossi transition curves for lead, iron and aluminum are presented. In the case of iron and aluminum these measurements are extended to larger thicknesses than in previous investigations.

1. INTRODUCTION

DURING the past several years, a great deal of attention has been paid to the so-called cosmic-ray shower production.[1] Experiments of this kind are of importance not only because of the relation between showers and the general cosmic-radiation, but also because such studies give valuable information on the nature of the interaction between high energy particles and matter.

We have had in progress, during the past few years, a series of experiments concerned with the production and absorption of cosmic-ray shower particles in various materials. In this paper we present (1) our observations on shower production in small thicknesses of various materials as a function of atomic number; (2) shower production as a function of the thickness of producing material; (3) our measurements on the absorption of showers in various materials, and (4) measurements on the Rossi transition curve for lead, iron and aluminum.

2. EXPERIMENTAL ARRANGEMENTS

The apparatus used is a modification of the circuit of Johnson and Street[2] adapted for selective detection of double, triple, or quadruple coincidences of the Geiger-Müller counter discharges.

The counters were made by Mr. A. G. Nester, with the aid and supervision of Dr. G. L. Locher of the Bartol Research Foundation of the Franklin Institute. In most of the work we have used counters approximately 5 cm in diameter and 20 cm in effective length. In Section 6 and in the observations given in Fig. 7 of Section 4 we have also used counters $2\frac{1}{2}$ cm in diameter and 20 cm in effective length. In the latter case the counters are connected together in groups of three to each input channel.

Counts and time interval marks are recorded on a moving paper tape. This automatic recorder allows easy statistical analysis of count distribution over any desired interval from the permanent record.

Highly accurate voltage regulation is accomplished in the power pack by means of a constant current ballast tube, saturated core reactors, and a thermionic tetrode regulator of the type of Street and Johnson[3] for the direct counter voltage. Sufficient constancy is obtained so that all readings are repeatable, within normal statistical error, after several months elapsed time.

All apparatus is housed in a small cabin of very light construction in order to minimize the background shower count as much as possible. While we have never observed a definite change in sensitivity of our counters with temperature, we have, as a precaution, maintained the temperature within the cabin reasonably constant by thermostatic control.

The location of this experimental station is approximately 410′ above sea level.

[1] H. Geiger, Ergeb. d. Exakt. Naturwiss. **14**, 42 (1935).
[2] T. H. Johnson and J. C. Street, J. Frank. Inst. **215**, 239 (1933).
[3] J. C. Street and T. H. Johnson, J. Frank. Inst. **214**, 155 (1932).

TABLE I. *Shower production in various materials. In all cases the showers are produced in plates of same area and have a mass per unit area equivalent to 0.58 cm of lead.*

Element	Z	Total Count	Total Time (hr.)	Counts per hr.	A	$\Delta(0.58)$	$A\Delta(0.58)$
Background		14,139	2376.4	5.95±0.02			
Carbon	6	1,778	281.3	6.32± .12	12	0.37±0.12	4.5± 1.5
Aluminum	13	1,045	150.0	6.93± .11	26.97	0.98± .11	26.4± 3.1
Copper	29	1,290	160.0	7.91± .13	63.55	1.96± .13	124.5± 8.7
Tin	50	1,214	115.4	10.52± .18	118.7	4.57± .18	538. ±21
Lead	82	4,121	319.8	12.90± .17	207.2	6.95± .17	1440. ±35

3. SHOWER PRODUCTION AS A FUNCTION OF ATOMIC NUMBER

The dependence of shower production on the nature of various materials was investigated by means of the experimental arrangement shown in Fig. 1. The plate of material above the three counters was approximately 22 cm×30 cm with a mass per unit area equivalent to 0.58 cm of lead. These dimensions were kept constant for each of the elements investigated. Since only triple coincidences were recorded, inspection of the figure referred to above will show that any shower from the material must consist of at least three particles in order to be detected by the apparatus as a count. The series of elements carbon, aluminum, copper, tin and lead gave the data of Table I.

The large number of hours of operation with no producing material in position is due to the fact that this condition is used at frequent intervals to check the over-all efficiency of the apparatus. The differences $\Delta(0.58)$ between the number of observed coincidences when the material in question is placed above the counters and when it is removed is shown in column 7 for each of the elements investigated. In view of current theories of pair production we have also expressed these data in terms of the number of coincidences produced per hour per atom of material in the producing plate, by multiplying the above quantities by factors corresponding to their individual atomic weights. The results are given in column 8.

The curve A of Fig. 2, plotted from these data, represents the increase in counting rate per nucleus as a function of atomic number.

Using the same experimental arrangement, a similar set of data was obtained for a producing plate of 0.29 cm lead equivalent thickness. These results are plotted as curve *B* of Fig. 2. It will be apparent from an inspection of these curves that the observed increase in counting rate per atom increases rapidly with increase in atomic number. The log-log plot of these data

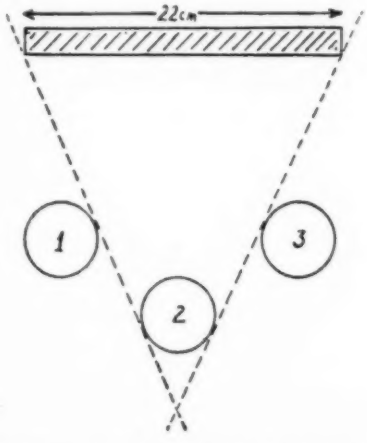

FIG. 1. Arrangement for investigation of shower production as a function of atomic number and thickness.

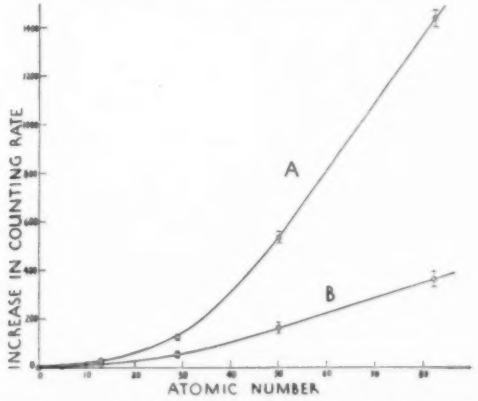

FIG. 2. Increase of counting rate, multiplied by atomic weight, as a function of atomic number.

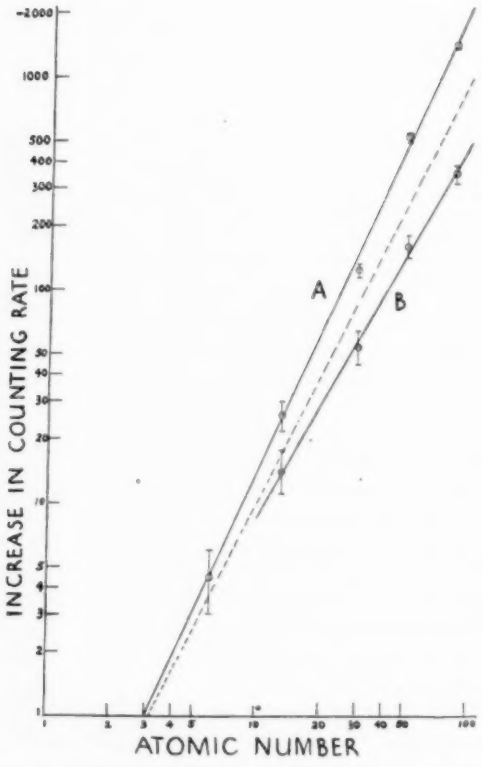

FIG. 3. Logarithmic plot of the data of Fig. 2. Dotted curve has a slope of 2.0.

shown in Fig. 3 indicates that this increase varies approximately as the second power of the atomic number. The data for a thickness of 0.29 cm indicate a power of Z of 1.85 while the data for the full thickness of 0.58 cm lead equivalent show a power of Z of 2.2. This difference is hardly outside the probable errors involved. In a later section we discuss some of our experiments on the absorption of cosmic-ray showers. At this point we wish only to point out that any detectable effects of absorption either of background or of the showers created in the producing material would lead one to expect a greater slope for the plot of observed data associated with the smaller thickness of producing material. This follows because of the greater coefficient of absorption, expressed in cm^2/g, for the elements of higher atomic number. That both sets of data give a dependence of shower production on Z in substantial agreement is a point of some interest.

We have also made measurements on the increase in counting rate for double coincidences produced in layers of materials of 0.58 cm lead equivalent. In this work we have recorded double coincidences between counters 1 and 3 of Fig. 1. These data are given as A of Fig. 4 in which log A $\Delta(0.58)$ is plotted as a function of log Z. The background count in this case was 47.18 counts per hour. The increase associated with 0.58 cm of lead was 31.1 counts per hour. The slope of the straight line drawn through the data points of A is 1.95.

In order to increase the importance of the producing material compared to the background we have also used the arrangement shown in Fig. 5. In this case the background count was 0.84 count per hour and the increase in counting rate with 0.58 cm of lead was 11.51 counts per hour. Measurements with copper and lead have been made and are plotted as B in Fig. 4, the slope of which is the same as that of A within the limits of error.

It would appear then that all of our measurements on shower production in different ma-

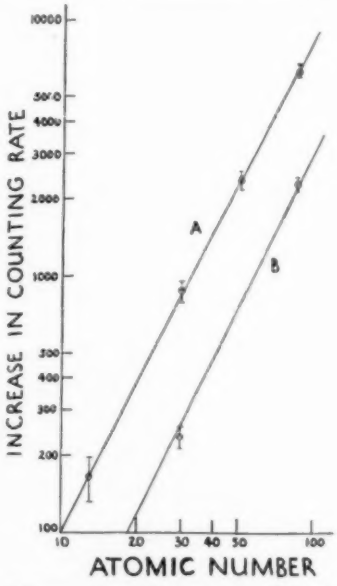

FIG. 4. Increase of counting rate, multiplied by atomic weight, for twofold coincidences. Data for curve A obtained with counters 1 and 3 of Fig. 1. Data for curve B obtained with arrangement of Fig. 5.

terials lead to the conclusion that the effectiveness of the various atoms in their contribution to the increase in counting rate varies quite closely as the 2.0 ± 0.2 power of the nuclear charge.

4. Shower Production as a Function of Thickness

A comparison of the two curves shown in Fig. 2 at the abscissa corresponding to lead shows the surprising result that at $Z=82$ the ordinate of A has a value much more than twice that of B which corresponds to the smaller thickness. This fact has already been referred to in a previous note.[4] These data raise the question as to whether or not the contribution of a given thickness of material to the increase in counting rate is a function of the material above it. In this connection it is therefore of some interest to compare the increase in counting rate due to the second 0.29 cm lead equivalent of material placed above the counters with that due to the first 0.29 cm. To that end we give in Fig. 6 a plot of the ratio, R, which we define as the observed difference in counting rate $(\Delta(0.58)-\Delta(0.29))$ divided by the increase $\Delta(0.29)$, the contribution from the first increment in thickness. If the contributions measured in this way were equal, one would expect a constant ratio of unity. The points shown in Fig. 6 indicate, however, that this ratio increases with Z from a value of approximately unity for the elements of small Z to approximately three in the case of lead. While the probable error is necessarily large in such treatment of data the departure from unity for the heavy elements would seem to be quite definite.

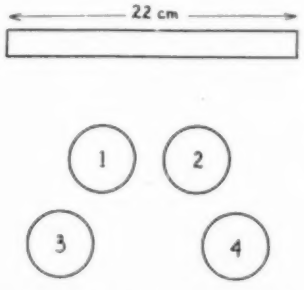

Fig. 5. Experimental arrangement for study of twofold coincidences.

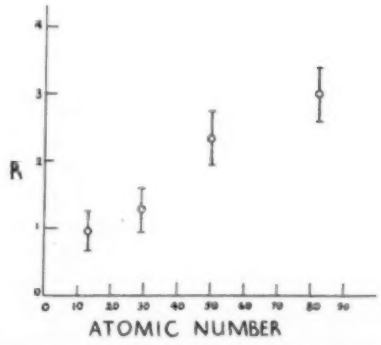

Fig. 6. Ratio R as a function of atomic number.

While there is no doubt that the absorption of shower particles plays some part in the quantitative nature of the results obtained, it appears that it is not of sufficient importance to modify the conclusions arrived at from these data.

Our work on the absorption of shower particles will be discussed in detail in the next section. At this point we refer to the results of these experiments only insofar as they have a direct bearing on the conclusions of this section.

It is shown both in our own and in other work on the absorption of cosmic-ray shower particles that over the region of 0.0 to 0.5 cm the absorption is approximately exponential. Our work is also in agreement with that of others in showing that the coefficient of absorption per gram/cm^2 of the material in question is less for the lighter elements. Experiments also indicate that shower particles which have their origin in elements of smaller atomic number are more penetrating, that is, have a smaller value of the coefficient of absorption.

There are three possible ways in which the values of R may be affected by absorption. We propose to discuss them in order.

We first consider the absorption of shower particles in the material in which they are produced. It is quite obvious from geometrical considerations that any correction for such absorption must be of such a kind as to increase the ratio R. It is also clear from a consideration of the absorption coefficients given in the next

[4] J. E. Morgan and W. M. Nielsen, Phys. Rev. **48**, 773 (1935).

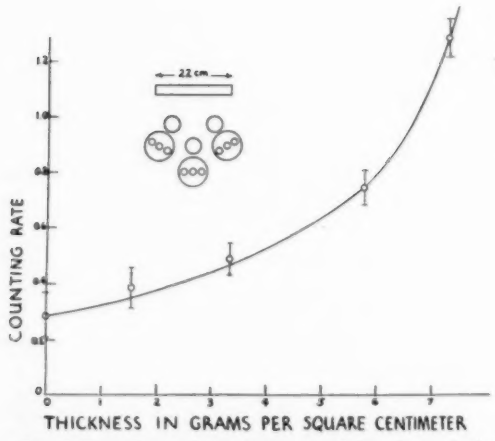

FIG. 7. Experimental arrangement and data for variation of the rate of occurrence of showers of at least three particles as a function of lead thickness.

section that such corrections will be larger for elements of higher atomic number.

We turn next to the absorption of the so-called background. If one assigns a coefficient μ per cm of material to the absorption of shower particles effective in the discharge of the counters it can be shown that the corrected value of R takes on the form

$$\frac{\Delta(0.58)-\Delta(0.29)+N_0(e^{-0.29\mu}-e^{-0.58\mu})}{\Delta(0.29)+N_0(1-e^{-0.29\mu})}$$

where N_0 represents the background count. Rossi[5] using an arrangement (Arrangement II of his paper) essentially the same as that shown in our Fig. 8*b* was unable to determine any absorption. In fact, for some thicknesses his results indicate an increased counting rate, presumably because of the presence in the background of particles which are capable of causing new showers.

Arguments will be presented in the next section which indicate that arrangements such as shown in Fig. 8*b* give values of the coefficient of absorption which are too high. For the present, it is of interest to take a value of 1.2 per centimeter of lead, suggested by the results of Zeiller with arrangement *b* of Fig. 8 without the "Trennwand." We have multiplied the value of 0.8 per cm of lead as obtained by Zeiller by 3/2 in an attempt to correct for the difference between 3- and 2-fold shower coincidences. There is evidence[6] that showers originating in light material are more penetrating, so there is the possibility that we are here using too large a value for the coefficient of absorption. Substituting the values of 6.95, 1.74 and 5.95 for $\Delta(0.58)$, $\Delta(0.29)$ and N_0 in the above corrected expression for R we obtain a value of about 1.9.

To test still further this departure from linearity in the shower contribution from different layers of producing material of high atomic number we have also measured triple coincidences using the arrangement shown in Fig. 7, in which at least three particles from the lead are necessary to give a count. The experimental data obtained with this arrangement are plotted in the curve of Fig. 7. One of the important features of this curve is that the increase due to the lead is much larger compared to the background than in the former arrangement. The increase in counting rate for the two thicknesses, 7.6 g/cm² and 3.35 g/cm² are 1.0 and 0.21 counts per hour, respectively. The ratio R as previously defined has then a value of approximately four while the ratio of the two thicknesses is approximately 2.3. If we take the same value of μ as used previously the corrected value of R has the value 2.9. If we make the extreme and unlikely assumption that all of the background is absorbed in the first 3.35 g/cm² of lead the ratio would be 1.6. It is quite apparent that if the absorption of the background were a critical factor in our qualitative estimates of the ratio R, one would expect a marked dependence on the magnitude of the so-called background.[7] This fact, together with other considerations previously noted, points to the definite conclusion that the increase in counting rate associated with a given thickness of producing material is for small thicknesses of lead very definitely a function of the thickness of lead above it. From Fig. 6 one would infer that this increased contribution to the counting rate from the second

[5] B. Rossi, Zeits. f. Physik **82**, 151 (1933).

[6] J. A. Priebsch. Zeits. f. Physik **95**, 102 (1935).

[7] It is clear from an inspection of Fig. 1 and Fig. 7 that the absorption of the background is of greater importance in the latter case. This follows because in the former arrangement some of the background counts are very probably caused by particles which do not pass through the region occupied by the producing material. We would therefore not expect the corrected values of R obtained in the two experiments to agree with each other but only regard the departure from unity as of significance.

increment of material decreases with decrease in atomic number.

Finally, it is necessary to say a word about the absorption of the so-called shower producing radiation. It is customary in discussing the Rossi transition curve to postulate such a producing radiation and to assign absorption coefficients to it. In any case, the intensity of such producing radiation would normally be expected to decrease with depth beneath the top of the slab of material. On such a view one would therefore expect a decreased contribution from the second or lower layers of material. The point involved here would seem to be whether or not there is a unique cosmic-ray shower producing radiation. Our results would indicate that any such shower producing radiation must undergo modifications, either in quality or in intensity, of such a kind as to increase the recorded coincidences from the second increment of thickness.

5. The Absorption of Shower Particles

Our experiments on absorption of shower particles have extended over a number of different geometrical arrangements and cover most of the elements under investigation in this paper.

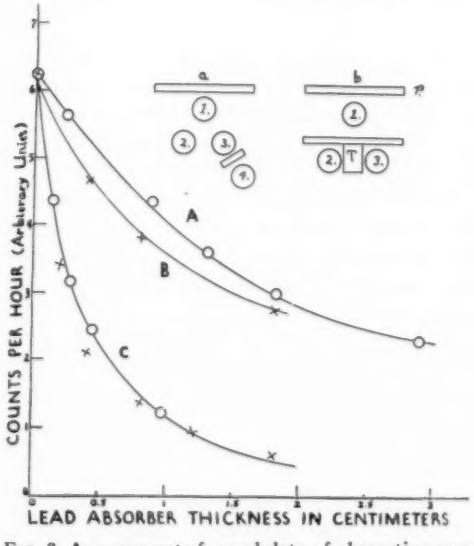

FIG. 8. Arrangements for and data of absorption measurements. Curve *A* represents our data using arrangement *a*. Curve *B* represents plot of Zeiller's data using arrangement *b* without "Trennwand." Crosses and circles on curve *C* represent Zeiller's and our observations, respectively, using arrangement *b* with "Trennwand."

We give at *a* in Fig. 8 the arrangement used in our earlier attempts. The results obtained with this arrangement are shown in the curve *A* of Fig. 8. A semi-log plot of these data indicates that the absorption in the first 5 mm is approximately exponential, the coefficient of absorption being 0.47 per centimeter of lead. It is of interest to compare this curve with some work of Zeiller[8] the arrangement and data of which are shown in Fig. 8 at *b* and *B*, respectively. From data obtained from his plotted curve without Trennwand *T* (curve *B* of Fig. 8) we have computed an absorption coefficient of 0.8 per centimeter of lead. The difference between this value and that given by our own data is about what one might expect from Zeiller's results on the absorption of two and threefold showers. In our case only one counter is shielded by absorbing lead, whereas, in the case of Zeiller both lower counters are shielded. Zeiller has also presented an absorption curve obtained with the Trennwand *T* in place as indicated. We have multiplied his data by a constant factor and plotted it on curve *C* of Fig. 8. Our data obtained by the use of an identical arrangement are also plotted on this curve. Both sets of data are in very good agreement. Our results lead to a coefficient of absorption of approximately 3.2 per centimeter of lead. The marked difference between the absorption coefficients obtained with and without the Trennwand in place is interpreted by Zeiller[8] and Geiger[1] as indicating that radiation from the plate *P* ejects secondary radiation (*D* radiation in the nomenclature of Geiger) from the absorbing plate as it passes from counter 1 towards counter 2 or counter 3. The presence of the Trennwand then results in a reduction of the number of coincidences which can occur when it is not placed between the lower counters. Zeiller has also plotted the difference between the curves obtained without and with the Trennwand in position. This curve shows a saturation value at a thickness of about 0.5 cm as do the so-called backward scattering curves.[1] It is of some importance that using an arrangement as in *a* of Fig. 8 we have obtained results which are of the same general character as those obtained by Zeiller without the Trennwand for, if it be true that the differences between curves

[8] O. Zeiller, Zeits. f. Physik **96**, 121 (1935).

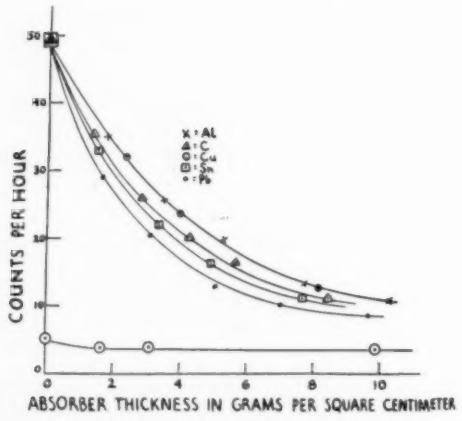

FIG. 9. Absorption in various elements of showers produced in lead. The lower curve corresponds to the absorption of the background. (Symbols for carbon and copper data should be interchanged.)

A and *C* are due to a secondary radiation (*D* radiation) then it seems reasonable to assume that this same radiation is also effective in the discharge of our counters. From the geometry of our arrangement this implies that a part of this *D* radiation is scattered in the backward direction.[1] It would also seem that if one were to correct in a detailed manner the data presented in previous sections of this paper for shower absorption such corrections would have to be made using coefficients of absorption obtained by the use of arrangements in which such secondary *D* or other radiation contributes to the counting rate as in the actual experiment.

We have already referred to our measurements of the absorption coefficient of lead showers in lead using an arrangement similar to that of Zeiller.[8] Using the same arrangement we have also measured the absorption coefficient of copper showers in copper and aluminum showers in aluminum with the results indicated in Table II. We have also made similar measurements on the absorption of lead showers in carbon,

TABLE II. *Coefficients of absorption of showers generated in various materials. In all cases the coefficients refer to absorption in the same element as producing material.*

Producing and Absorbing Material	μ (cm^{-1})	μ (cm^2/g)
Lead	3.2	0.28
Copper	2.4	.27
Aluminum	.54	.20

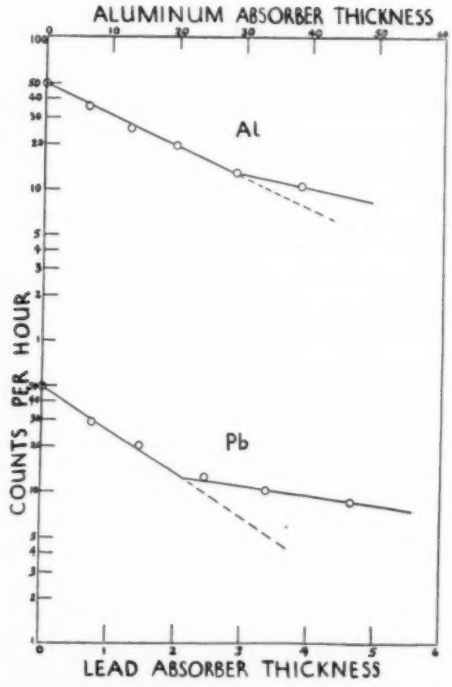

FIG. 10. Logarithmic plot of lead and aluminum data of Fig. 9. The abscissae are proportional to the absorber thickness in g/cm^2 divided by the atomic weight of the element concerned.

aluminum, copper, tin and lead. The absorption data are plotted in Fig. 9. A semi-log plot of the data for lead and aluminum is shown in Fig. 10. The abscissae here are proportional to the number of atoms in question per unit area of absorbing material. As previously noted by others[8] such plots indicate a more penetrating type of radiation in addition to the softer radiation represented by the initial approximately linear decrease.

In Fig. 11 we have plotted the absorption coefficients of the less penetrating showers as a function of atomic number. Our results indicate that the absorption coefficient of such shower particles varies with a power of Z between the first and second. A similar conclusion follows from a less extensive series of measurements of Woodward.[9] The straight line drawn in Fig. 11 has a slope corresponding to the 1.4th power of Z. The point for carbon indicates, however, that for

[9] R. H. Woodward, Phys. Rev. **49**, 711 (1936).

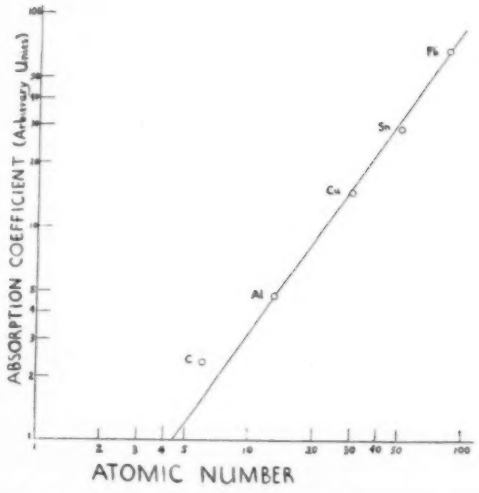

FIG. 11. Absorption coefficient as a function of atomic number of absorber.

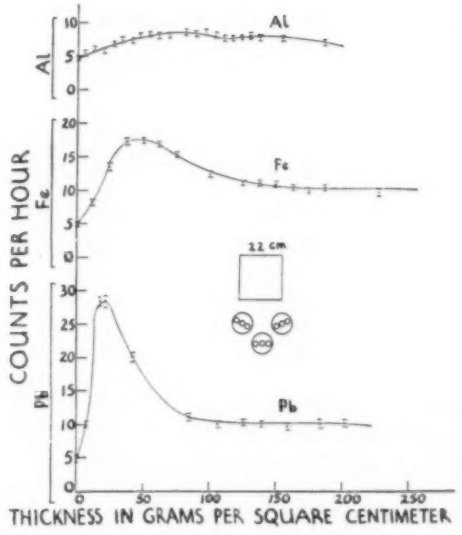

FIG. 12. Rossi transition curves for lead, iron and aluminum.

elements of low atomic number the dependence upon Z is not as high as this.

6. Rossi Transition Curves in Lead, Iron and Aluminum

The Rossi transition curves of lead, iron and aluminum have been the subject of several investigations. Our measurements on iron and aluminum have apparently been carried to larger thicknesses than heretofore. The curves shown in Fig. 12 were obtained with an arrangement shown in the inset. In the case of lead and aluminum the producing blocks were 660 square centimeters in area while the results for iron are for a producing block of 22.9 cm×38 cm area. In adding successive layers, the position of the lower layers remained fixed in all cases. The positions of the first maxima for lead and iron are in agreement with the results of previous investigations. Our results for aluminum show a broad maximum at a thickness of approximately 75 g/cm². This is considerably greater than observed by Fünfer, presumably because of the presence of extraneous scattering material in his experiments.[10] The relative positions and magnitudes of the maxima in the cases of lead and aluminum are apparently in fair agreement with the theoretical calculations of Oppenheimer.[11]

The transition curve for iron at the larger thicknesses does not decrease as rapidly as it does near the thickness of maximum counting rate. The interpretation of similar observations with lead has been associated with the presence of a second maximum in the transition curve.[12] This feature of the Rossi transition curve will be discussed in a future contribution from this laboratory.

We wish to thank Mr. Roy A. Hunt of the Aluminum Company of America for providing the necessary aluminum in this investigation. We are also indebted to the Research Council of Duke University for providing funds with which to carry out this work.

[10] E. Fünfer, Zeits. f. Physik **83**, 92 (1933).
[11] J. R. Oppenheimer, Phys. Rev. **50**, 389 (1936).
[12] M. Ackermann, Zeits. f. Physik **94**, 303 (1935); J. N. Hummel, Naturwiss. **22**, 170 (1934); H. Kulenkampff, Physik. Zeits. **22**, 785 (1935); R. H. Woodward, reference 9.

The Transmutation of Potassium, Chlorine and Phosphorus by Th C′ Alpha-Particles

ERNEST POLLARD* AND CHARLES J. BRASEFIELD, *Sloane Physics Laboratory, Yale University, New Haven, Connecticut*

(Received June 22, 1936)

The transmutation of the three similar $(4n+3)$ type elements K, Cl, P under alpha-particle bombardment has been studied by observing the energy distribution of emitted protons. These are found to occur in groups corresponding to discrete values of the nuclear energy changes which have been determined and tabulated. A general similarity between the behavior of the three elements is observed: They each give groups with energy changes differing by 1.5 Mev on the average, which fit in with the groups from the similar type elements F, Na, Al as found by May and Vaidyanathan. The values 33.9799 ($\pm$0.0015) and 37.9753 ($\pm$0.0016) for the masses of S^{34} and A^{38} are deduced.

RECENT experiments by Haxel[1] and by May and Vaidyanathan[2] on the transmutation of elements differing in nuclear structure by the equivalent of an alpha-particle have shown that for reactions in which an alpha-particle enters and a proton is ejected, the excited states of the product nucleus are similar. Haxel's experiments were performed on the $4n$-type elements Mg^{24}, Si^{28} and S^{32} while May and Vaidyanathan worked with F^{19}, Na^{23}, Al^{27} and P^{31} of the type $4n+3$. The similarity of the proton groups emitted by the $4n$-type elements is quite striking: the groups occur in sets of three with separations of a little under a million electron volts. The three elements F^{19}, Na^{23} and Al^{27} give four groups with an average separation of a million and a half electron volts. Phosphorus has been found to give three groups by both May and Vaidyanathan[2] and Paton,[3] having a mean separation roughly the same as the three previous elements, but with the longest range group absent. We considered it of interest to examine the elements chlorine ($Cl^{35, 37}$) and potassium (K^{39}) which have not been investigated since the early scintillation experiments of Rutherford and Chadwick,[4] as well as phosphorus to see whether the similarity between elements of the $4n+3$ type continues.

The masses of chlorine and phosphorus are known and the transmutation of these elements therefore should enable the masses of argon and sulphur isotopes to be determined by measuring the limiting energy of the proton groups.

APPARATUS

The essential features of the apparatus have been described in a previous paper.[5] In the experiments here reported we have made two important changes. The first was an improvement in the counter which was designed to permit evacuation of the outer grounded case, thus eliminating the need for an insulating mica foil over the counter itself. For the foil covering the counter opening (1.8 cm diameter) we used aluminum of 4.1 cm air equivalent. The axial wire was of tungsten, 0.013 cm diameter. The major improvement was in the use of argon instead of air in the counter: This operates at a lower case voltage and permits higher gas pressures with higher ionization per proton and also gives much more uniform multiplication over the counter opening. With argon at atmospheric pressure the potential of the case of the counter is -2000 while with air at 50 cm, -4000 is needed. The lower voltage renders operation simpler and the counter has given no trouble in five months of steady operation.

The second improvement, made possible by the trouble-free operation of the detection apparatus, was an automatic screen-changing device which interposed successively, between target and counter, ten different sets of absorption screens at regular intervals. The protons are recorded by a thyratron circuit actuating a magnet which deflects a metal point running on waxed (Stylograph) paper.

The targets we used were as follows. Potassium was bombarded as KOH melted on gold foil or

* Sterling Fellow.

[1] O. Haxel, Physik. Zeits. **36**, 804 (1935).

[2] A. N. May and R. Vaidyanathan, Proc. Roy. Soc. **A155**, 519 (1936).

[3] R. F. Paton, Zeits. f. Physik **90**, 586 (1934).

[4] Rutherford and J. Chadwick, Nature **113**, 457 (1924).

[5] C. J. Brasefield and E. Pollard, Phys. Rev. **50**, 296 (1936).

copper according to whether the layer was required to transmit protons or not. Chlorine was used as lithium chloride in the right angle arrangement (we first satisfied ourselves that lithium gives no protons of ranges as great as our minimum); or as "Arochlor"—a chlorinated diphenyl which is used commercially as an insulator for condensers. This latter is remarkably suitable for our purpose; it melts easily and flows into smooth uniform layers of any desired thickness. Phosphorus was bombarded as red phosphorus and layers were made by mixing it with vaseline into a paste and warming it on the backing surface until it flowed out uniformly. A thin layer can be obtained fairly easily in this way.

Experimental Procedure and Results

The experimental procedure is similar to that previously described.[5] Protons ejected from targets under bombardment by alpha-particles from a Th C′ source are detected by the counter and their energies measured by absorption. The sources used varied in strength between one and three millicuries as measured by direct counting of the number of alpha-particles emitted in a small solid angle. In order to eliminate natural protons from the source and recoil protons from hydrogen in the target, the counter, target and alpha-particle source were so arranged that the detected protons were moving in a direction which was approximately at right angles to the incident beam of alpha-particles.[6] This "right angle" arrangement was used in two modifications. In the first, the alpha-particle source was placed very near and parallel to the target; curves *A* of Figs. 1, 2 and 3 were thus obtained. In the second modification the source was so placed that the spread in the angle between alpha-particle trajectory and path of ejected proton was as small as possible (44°); this tends to minimize the distortion of the groups. Since the target now subtends a smaller solid angle the yield of protons is less as curves *B* of the same figures indicate.

In order to measure the maximum energy of the ejected protons, counter, target and source were arranged in line[6] so that the minimum angle between the alpha-particle and counted proton paths was zero. This "forward" arrangement is particularly suitable for examining groups of protons of range greater than 40 cm; for it permits greater solid angles between source and target and therefore greater yields of protons. Natural and recoil protons from source and target mask all groups of range less than 40 cm. The principal difficulty with the "forward" method is obtaining a target of uniform stopping power which is sufficiently thin to transmit protons.

The results obtained, with these three arrangements for targets of potassium, chlorine and phosphorus, are shown in Figs. 1, 2 and 3, respectively. In each case the number, *N*, of protons ejected per minute per millicurie of Th C′ is plotted as ordinate against the range *R* of the protons in centimeters of standard air. Due to the different geometrical conditions of each arrangement, a certain group of protons may be better resolved in one curve than in another. Curves *A* are to be regarded as relatively rough at absorptions less than 40 cm. Between 100 and 500 particles were counted at each point plotted. The rather low number of 100 particles at a point applies only to the long range low yield groups where the main interest is in the presence or absence of a group. Our counter background, due to contamination, etc., was not more than four counts per hour: the background to be subtracted when a strong source is near the counter was around twelve per hour. At the extreme ranges the actual yield was therefore generally double the background. For the groups at smaller absorptions we found it preferable to use better geometrical conditions and smaller counts. Even so, the fact that the separation in range grows less for smaller energies (due to the range energy relation) means that there is some doubt about the precise end point of groups having short ranges. This is particularly true in the case of phosphorus and the analysis of the results for that element is to be regarded as less certain than for the two previous elements. As, however, this element has been previously analyzed by Paton, and May and Vaidyanathan, we contented ourselves with confirming their work, and so showing our findings are consistent with the other workers in this field.

[6] See, for example, Fig. 1 of our previous paper (reference 5).

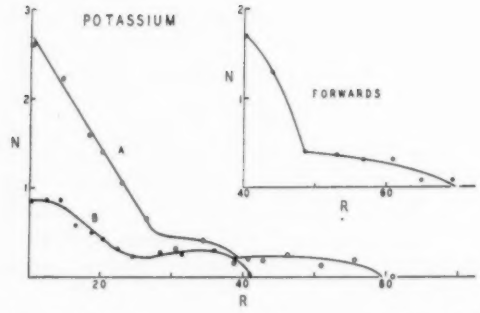

FIG. 1. Yield of protons per minute per millicurie (N) *versus* absorption in centimeters air equivalent (R).

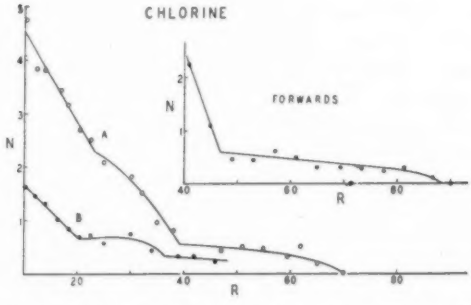

FIG. 2. Yield of protons per minute per millicurie (N) *versus* absorption in centimeters air equivalent (R).

Potassium

Potassium yields three groups of protons as shown in Fig. 1. The most energetic group (here called group 1) has a range of 70 cm forward and 59 cm at right angles; the second group has a range of 49 cm forward and 41 cm at right angles in curve B, or 39 in curve A where it is badly resolved; the third group has a range of 25 cm at right angles in curve B or 27 cm (curve A). Its range in the forward direction is too low to be measured as already explained.

These protons result from the reaction:

$$K^{39}+He^{4}\rightarrow Ca^{42}+H^{1}(+Q).$$

Knowing the velocities of alpha-particle and proton and the masses of all particles involved in the reaction, it is possible to compute[7] the energy change Q corresponding to each group of protons. The values (in Mev) thus found for this reaction are given in Table I together with the relative yields of each group in the last column. The letters (A) and (B) indicate the values corresponding to curves (A) and (B), respectively.

TABLE I. *Values of Q and relative yields for the three proton groups from potassium.*

	Forward		Right Angle		Best Value of Q	Relative Yield
	Range (cm)	Q value	Range	Q value		
Group 1	70	−1.0	59	−1.1 (A)	−1.0	1
Group 2	49	−2.3	41 39	−2.4 (B) −2.3 (A)	−2.3	4
Group 3			25 27	−3.7 (B) −3.4 (A)	−3.6	12

[7] This is discussed in more detail in our previous paper.

Chlorine

The results obtained for chlorine are shown in Fig. 2. The most energetic group (1) has a range of 88 cm forward and 70 cm at right angles; the second group a range of 47 cm forward, at right angles 38 cm (curve A) and 36 cm (curve B); the third group a range at right angles of 21 cm (curve A) and 20 cm (curve B). It is assumed that the most abundant isotope of chlorine is responsible for all three groups (this assumption is further justified in the discussion) which are consequently emitted according to the reaction

$$Cl^{35}+He^{4}\rightarrow A^{38}+H^{1}(+Q)$$

in which the calculated nuclear energy change (Q) values are given in Table II.

Phosphorus

Fig. 3 shows the results obtained for phosphorus. The dotted line indicates the natural and recoil protons which have a range of 40 cm in the forward direction. The region containing the protons of medium range is not easy to analyze. The way in which we have drawn our lines appears to us to fit our results best, but it is clear from the figure that too great a reliance cannot be placed

TABLE II. *Values of Q and relative yields for the three proton groups from chlorine.*

	Forward		Right Angle		Best Value of Q	Relative Yield
	Range	Q	Range	Q		
Group 1	88	+0.1	70	−0.3	+0.1	1
Group 2	47	−2.4	38 36	−2.5 (A) −2.7 (B)	−2.5	3
Group 3			21 20	−4.1 (A) −4.2 (B)	−4.2	3

on exact values of ranges. We feel the most likely analysis is into four groups of protons arising from the reaction:

$$P^{31}+He^{4}\rightarrow S^{34}+H^{1}.$$

The most energetic group (1) has a range of 85 cm forward and 72 at right angles; the second a range of 64 cm forward and 56 at right angles; the third a range at right angles of 35 cm (curve *A*) and 34 cm (curve *B*)—it may possibly show at 47 cm forward; the fourth a range of 15 cm according to both curves. The calculated energy change values are given in Table III. The first three groups appear in the experiments of Paton[3] and May and Vaidyanathan,[2] the fourth gives protons of energies too low to be detected in their work. Their values are, respectively, 0.0; −1.5; 3.0; and −0.1; −1.4; −2.9. The agreement with our figures is reasonably good, particularly as in none of the experiments is a perfect resolution of groups 2 and 3 obtained. We found no evidence of a very long range group of positive Q value.

Possibility of resonance effects

The possibility of resonance effects was tested by repeating absorption curves at lower incident particle energies. We found that the yield falls rapidly for all groups as the incident energy is reduced and that the ranges also vary rapidly in about the way expected if the groups are due to excited states and not critical incident particle energies. The detection of groups arising from resonance levels probably demands still better resolution, using thin targets and more prolonged counting. The study of such levels was not attempted in this work. Energy change values calculated from reduced range experiments are: potassium, $Q=-2.6$; phosphorus, $Q=-2.5$; chlorine, $Q=-2.2$, which agree reasonably well with the predicted values −2.4; −2.6; −2.4; considering the necessarily rough nature of the measurements.

TABLE III. *Values of Q and of relative yields for the four proton groups from phosphorus.*

	Forward		Right Angles		Best Value of Q	Relative Yield
	Range	Q	Range	Q		
Group 1	85	−0.1	72	0.0	0.0	1
Group 2	64	−1.3	56	−1.1	−1.2	4
Group 3	47?	−2.4	35 34	−2.6 (A) −2.7 (B)	−2.6	12
Group 4			15	−4.6 (A, B)	−4.6	12

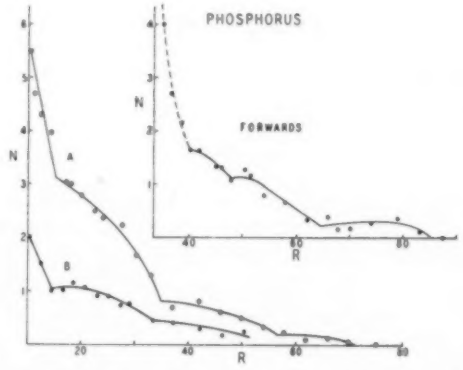

FIG. 3. Yield of protons per minute per millicurie (N) *versus* absorption in centimeters air equivalent (R).

The ranges are given in centimeters air equivalent. We used aluminum screens for absorption, taking 1.64 mg/cm² as equivalent to one centimeter of air. The velocities were derived from the ranges by means of the curves used in the Cavendish Laboratory which are applicable over the ranges measured in our experiments. We give the outside limit of error for all our Q values as 0.3 Mev for K and Cl and groups 1 and 4 for P. Groups 2 and 3 for P cannot very well be assessed as their analysis is uncertain.

Relative yields for different elements

To compare the yields from the different elements we made some additional experiments in which an aluminum target was bombarded under identical conditions. We found the following total yields relative to Al as standard:

Al	1	
P	0.9	
Cl	0.9	(if all due to Cl^{36} 1.20)
K	0.6.	

The experiments on Al suggested the existence of a new group of range about 19 cm which might

TABLE IV. *Values (in Mev) of nuclear energy changes in various reactions.*

$F^{19}\rightarrow Ne^{22}$	$Na^{23}\rightarrow Mg^{26}$	$Al^{27}\rightarrow Si^{30}$	$P^{31}\rightarrow S^{34}$	$Cl^{35}\rightarrow A^{38}$	$K^{39}\rightarrow Ca^{42}$
1.4	1.9	2.1	—	—	—
−0.1	−0.4	−0.2	0.0	0.1	—
−2.1	−2.1	−1.5	−1.2	—	−1.0
−3.2	−3.1	−2.8	−2.6	−2.5	−2.3
		−4.0	−4.6	−4.2	−3.6

mean a new Q value of -4.0 Mev. We wish to investigate this more thoroughly since there is a likelihood that resonance effects are prominent in the aluminum nucleus.

Discussion

We give in Table IV our values for the nuclear energy changes together with those found by May and Vaidyanathan[2] for F^{19} and Na^{23} and Duncanson and Miller[8] for Al^{27}. The possible new Q value for Al^{27} is indicated in italics. There is clearly a tendency for the same groups to appear in each element, the Q value for a particular group rising slightly in general as heavier elements are considered. The most positive Q value disappears at phosphorus and the next at potassium: this is probably because the product nuclei become relatively heavier as the atomic weight increases.

The group at about -1.2 Mev expected in the case of chlorine is absent according to our analysis of our results. In the forward curve there appears a dip at 64 cm range which would give a Q value of -1.4 Mev. We did not find any evidence of a corresponding dip in the right-angle experiments (where the yields were, however, rather low) and so prefer to regard the presence of the group as uncertain. Our experiments do show that some selection rules must operate since the yield of this group, if it is present, is abnormally low.

The average separation of the levels is approximately 1.5 Mev which is greater than the value 0.9 found in the $4n$-type elements studied by Haxel.

Masses of A^{38} and S^{34}

The Q values corresponding to the least energy in the product nuclei, that is the least negative or most positive Q's, permit the derivation of the masses of A^{38} and S^{34} from our experiments on Cl and P. Using the assumed reaction

$$Cl^{35}+He^4 \rightarrow A^{38}+H^1+Q$$
$$34.9796+4.0039=A^{38}+1.0081+0.0001$$
$$(\pm 0.0012)(\pm 0.0002) \qquad (\pm 0.0002)$$

we find $A^{38}=37.9753\pm 0.0016$. Here we have used Bainbridge's value[9] for the mass of Cl^{35}. If we ascribe the long range group to Cl^{37} we find (again using Bainbridge's value) the mass 39.9734 ± 0.0016 for the mass of A^{40}. Aston's recent value[10] is 39.9754 which lies beyond the limits of error. We therefore feel some confidence in ascribing the groups here found to the more abundant isotope. In view of the fact that the yield is small for great energy release it is unlikely that any proton group due to Cl^{37} would show among the greater yields of the proton groups from Cl^{35}.

The reaction investigated by Haxel[1]

$$Si^{28}+He^4 \rightarrow P^{31}+H^1(+Q)$$

and that here studied

$$P^{31}+He^4 \rightarrow S^{34}+H^1(+Q)$$

enable first the mass of P^{31} to be computed from Aston's value for Si^{28} and from this the mass of S^{34}. Putting in the experimental values we find $P^{31}=30.9844\pm 0.0015$ and $S^{34}=33.9802\pm 0.0015$, the limits of error being somewhat roughly estimated.

The masses of S^{34} and A^{38} are of some interest in view of the experiments of Libby, Peterson and Latimer[11] who find an alpha-ray emitter of gaseous form resulting from the decay of radiochlorine. They suggest that this emitter is A^{38} which passes into S^{34} after losing an alpha-particle. The difference between the masses which we find for these isotopes is insufficient to permit the emission of an alpha-particle so that it may be necessary to suppose the existence of two forms of A^{38}.

We wish to express our thanks to Professor A. F. Kovarik for his interest in the work and to Professor L. W. McKeehan for help in writing the manuscript.

[8] W. E. Duncanson and H. Miller, Proc. Roy. Soc. **A146**, 408 (1934).

[9] K. T. Bainbridge, Phys. Rev. **43**, 378 (1933).

[10] F. W. Aston, Nature **137**, 613 (1936).

[11] W. F. Libby, M. D. Peterson and W. M. Latimer, Phys. Rev. **48**, 571 (1935).

The Artificial Radioactivity of Copper, a Branch Reaction

S. N. VAN VOORHIS,* *Radiation Laboratory, Department of Physics, University of California, Berkeley, California*

(Received September 10, 1936)

The artificial radioactivity of longer half-life produced in copper by deuteron bombardment is studied. It is found to emit both electrons and positrons in the ratio 1.6 to 1. The half-life is found to be 12.8 ± 0.1 hours. The excitation curve of positrons and electrons for deuterons of different energies is studied and found to agree with the theoretical expression of Oppenheimer and Phillips. The upper limits of the energy distribution of the positrons and electrons are obtained from cloud chamber photographs, and are found to be 0.79 and 0.83 Mev, respectively. The results are interpreted as showing that this activity is due to Cu^{64} which branches in disintegrating, going either to zinc or nickel.

WHEN copper is bombarded with high energy deuterons, two radioactive isotopes are produced, one from each of the stable isotopes of copper. The reaction is the capture of a neutron, with the emission of a proton. Lawrence, McMillan and Thornton[1] have measured the excitation curve for deuterons up to 3.1 Mev energy. The same radioactive isotopes may be formed by neutron bombardment of copper. Fermi[2] and others have studied this reaction. In the work to be described, a more detailed study of the isotope of longer half-life has been made.

Deuterons were accelerated to energies of 5 to 6 Mev in the magnetic resonance accelerator or cyclotron. In the first experiment, a solid block of copper was bombarded with 10 μa of deuterons of 25 cm range for fifteen minutes. It showed a large activity with a half-life of about $12\frac{3}{4}$ hours. An absorption curve in lead showed the presence of radiation of about the hardness of annihilation radiation, decaying at the same rate as the electron activity. This absorption curve showed no evidence for any other gamma-radiation. The sample was then placed in a Wilson chamber traversed by a magnetic field. Visual examination showed the presence of both positrons and electrons in roughly equal numbers.

In order to get some quantitative separation of the effect due to positrons and to electrons the following procedure was adopted. Observations were made with a pressure ionization chamber and FP-54 Pliotron, first with the sample directly exposed to the ionization chamber, then with the sample covered with 1.5 cm of paraffin, this being sufficient to stop all electrons encountered here. For calibration purposes two artificial radioactive substances are available, radio-nitrogen produced by deuteron bombardment of carbon which emits only positrons, and radio-phosphorus produced by deuteron bombardment of phosphorus which emits only electrons. Neither substance is known to emit any gamma-rays.

Samples of these two substances were measured with the ionization chamber, first with the sample bare, then covered with paraffin. For the radio-nitrogen (positron emitter) the ratio of ionization with the sample bare to that with it covered was found to be about twenty, while with the radio-phosphorus (electron emitter) this ratio was found to be over a thousand. Therefore if a sample emitting both positrons and electrons but no gamma-rays is examined in this way, the ionization observed with the sample bare is a measure of the sum of the two activities while that observed with the sample covered when multiplied by the factor twenty is a measure of the positron activity alone. For the copper sample, this ratio was found to be about sixty, indicating twice as many electrons as positrons. As mentioned above, the half-life of both positron and electron activities was found to be exactly the same, a more exact measurement giving the value 12.8 ± 0.1 hours.

Next the excitation curves for the two activi-

* National Research Fellow.

[1] Lawrence, McMillan and Thornton, Phys. Rev. **48**, 493 (1935).

[2] Amaldi, d'Agostino, Fermi, Pontecorvo, Rasetti and Segrè, Proc. Roy. Soc. **A149**, 522 (1935).

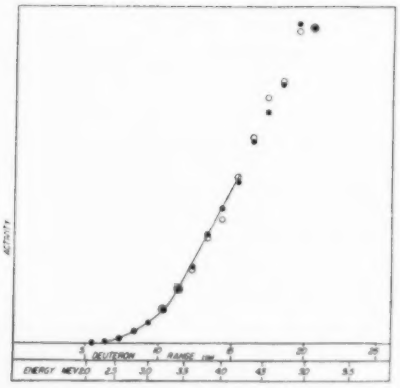

FIG. 1. Excitation curve of Cu^{64} by deuterons. Open circles, positrons; black circles, total (+ and −); line, Oppenheimer and Phillips theory.

ties were determined by the method of bombarding a stack of thin copper foils. The foils used had an average stopping power of 9 mm. They were measured individually with alpha-particles and the corrections given by Mano[3] for the variation of stopping power with velocity were applied. In this case the deuteron beam had a range of 21 cm, the current was 4 μa, and the time of bombardment one hour. Fig. 1 shows the excitation curves so obtained, the open circles representing the positron activity alone, and the solid circles the combined activity. The ordinates have been adjusted to agree at the highest energy point. The curve is the theoretical expression given by Oppenheimer and Phillips[4] with the binding energy of the deuteron set equal to 2.1 Mev. It has been adjusted to fit at its high end, 4.2 Mev, this being the upper limit of the calculations given by Oppenhiemer and Phillips.

Next another solid copper target was bombarded and placed in a hydrogen-filled Wilson chamber which was traversed by a magnetic field. Photographs were taken of the tracks, and their radius was measured by reprojection. These results are shown in Fig. 2 as a histogram, the solid line representing the electrons and the dotted line the positrons. In this series of pictures there were 557 negatives and 353 positives, this ratio agreeing with the ionization chamber analysis as closely as could be expected. These results were analyzed by the method described by Kurie, Richardson and Paxton[5] on the basis of the Konopinski-Uhlenbeck modification of the Fermi theory. The upper limits so found, 0.79 Mev for the positives and 0.83 Mev for the negatives, are indicated on Fig. 2. The straight line plots given by this method of analysis are shown in Fig. 3. It will be noted that the fit is about the same for positives and negatives on these straight line plots but that the histograms are somewhat different in form, that for the positives having its maximum at a slightly higher energy. This is the result of the action of the positive charge of the nucleus, and is noticeable because the emitted particles have comparatively low energy.

Since stable isotopes of both nickel and zinc of mass 64 have been reported,[6] it seems that these observations can best be explained by assuming that radio-copper of mass 64 can disintegrate in either of two ways, going to zinc with the emission of an electron, or to nickel with the emission of a positron. The activity

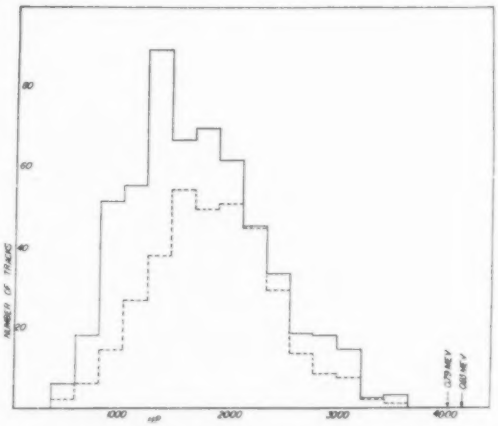

FIG. 2. Distribution of $H\rho$ of positrons and electrons from Cu^{64}. Positrons, broken line; electrons, solid line.

[3] Mano, J. de phys. et rad. **5**, 628 (1934).
[4] Oppenheimer and Phillips, Phys. Rev. **48**, 500 (1935).
[5] Kurie, Richardson and Paxton, Phys. Rev. **49**, 368 (1936).
[6] Aston, *Mass Spectra and Isotopes;* de Gier and Zeeman, Proc. K. Akad. Amsterdam **38**, 8, 810 (1935); Dempster, Phys. Rev. **50**, 98 (1936).

reported by Fermi[2] with a half-life of 5 minutes would then be associated with the disintegration of radio-copper of mass 66, going to zinc 66 with the emission of an electron.

The yield of this reaction is about one atom of Cu^{64} in 5×10^6 deuterons of 5.1 Mev energy.

In conclusion, I wish to express my thanks to Professor Lawrence for the privilege of working in the laboratory, to the other members of the Radiation Laboratory for help and advice, in particular to Dr. Kurie for the Wilson chamber photographs, and to the National Research Council for financial support. Support of the laboratory work by the Research Corporation, the Chemical Foundation, and the Josiah Macy, Jr. Foundation is also gratefully acknowledged.

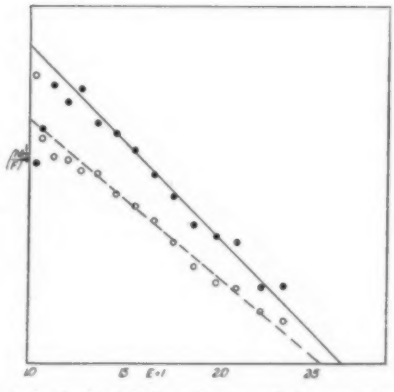

FIG. 3. Analysis of Cu^{64} positrons and electrons for upper limit. Copper K-U plot. Open circles, positrons; black circles, electrons.

NOVEMBER 15, 1936 PHYSICAL REVIEW VOLUME 50

On the Slowing Down of Neutrons in Water

GABRIEL HORVAY, *Columbia University, New York City, and Talladega College, Talladega, Alabama*

(Received August 31, 1936)

The diffusion of neutrons in water is considered, and a simple method is given which permits an approximate estimation of initial neutron energies when the final energy and the mean square distance of travel are known.

IF we have a source of neutrons in water the escaping particles collide with the surrounding molecules. The free paths between successive collisions form zig-zag trajectories, and there is a tendency to keep the forward direction because the mean scattering angle is small. Fermi[1] has considered this case in detail and found that the relation between distance traveled, r, mean free path, λ, and the number of collisions, a, is given by the formula

$$(r^2)_{av}=2\Big\{\lambda^2(0)[1+\rho(0)]+\int_0^a\lambda^2(x)[1+\rho(x)]dx+\lambda^2(a)[1+\rho(a)]$$
$$+\frac{\lambda(0)}{1+\rho(0)}\int_0^a\lambda(x)\exp\Big[-x/2-\int_0^x\rho(\xi)d\xi\Big]dx+\frac{\lambda(0)\lambda(a)}{1+\rho(0)}\exp\Big[-a/2-\int_0^a\rho(x)dx\Big]$$
$$+\lambda(a)\int_0^a\frac{\lambda(x)}{1+\rho(x)}\exp\Big[-(a-x)/2-\int_x^a\rho(\xi)d\xi\Big]dx+\int_0^a\frac{\lambda(x)dx}{1+\rho(x)}\int_0^{a-x}\lambda(x+\xi)$$
$$\times\exp\Big[-\xi/2-\int_0^\xi\rho(x+\zeta)d\zeta\Big]d\xi\Big\},\quad\Big(\lambda=\frac{1}{N_H\sigma_H+N_0\sigma_0},\ \rho=\frac{N_0\sigma_0}{N_H\sigma_H}.\Big)\quad(1)$$

[1] E. Fermi, Ric. Scient. July, 1936.

Several approximations were made in the derivation of this expression: only elastic impacts were considered, the mass of hydrogen was taken equal to the mass of the neutron, and the mass of oxygen infinitely large compared with that of the neutron. Furthermore, the atoms were considered as free and stationary. This means that (1) is valid only if the energy of the neutron exceeds considerably the energy of chemical binding (1/3 volt) and that of thermal agitation (1/30 volt).

As the neutrons collide with the hydrogen atoms they will lose part of their energy, and after a impacts the original energy, w_0, will be reduced to a value w_a. In formula (1) the variable x is connected with the energy by the relation

$$x=\log\,(w_0/w). \tag{2}$$

Hence it follows that if λ and ρ are known functions of the energy, the integral (1) can be evaluated and an expression will be obtained for $(r^2)_{av}$ in terms of w_0 and w_a. Conversely, an experimental knowledge of $(r^2)_{av}$ and of w_a will permit a determination of the initial energy w_0. (Naturally, we must have $w_a \gg 1/3$ volt.) Thus (1) can be used as a check on the correctness of the assumed diffusion process. It also will permit comparison of other methods of determining neutron energies, and will give an indication as to the validity of the formulae for collision cross sections of hydrogen and oxygen with neutrons.

The functions $\lambda(x)$ and $\rho(x)$ are fairly well known. σ_H has been calculated by Bethe and Peierls:[2]

$$\sigma_H=\frac{4\pi\hbar^2}{M}\left[\frac{3}{4}\frac{1}{\epsilon+w/2}+\frac{1}{4}\frac{1}{\epsilon'+w/2}\right]$$

$$(\epsilon=2.2\text{ Mev},\quad \epsilon'=0.116\text{ Mev}). \tag{3}$$

For σ_0 Dunning's measurements[3] are available: σ_0 is about 1 to 2×10^{-24} cm^2, and can be approximately considered as constant.

Thus the integral (1) can be evaluated,[4] and this has been done for a number of initial energies ranging from 1000 volts to 7 Mev. The curves of $(r^2)_{av}$ as a function of $-\log_w$ first rise rapidly and then become straight lines. This latter fact is immediately obvious from (1): $(r^2)_{av}$ increases linearly with a at energies for which $\lambda=$const., $\rho=$const., and a sufficiently large ($a\gtrsim2$). (λ and ρ are constant when $w\ll\epsilon$, ϵ', i.e., when $w\lesssim10{,}000$ volts.)

Since the neutrons are captured by several detectors for energies of the order of magnitude of one volt, we are interested in the value and slope of the curves in this region.

In Table I we tabulate $(r^2)_{av}$ for initial energies ranging from e^{-7} to e^2 Mev and final energy of 1 volt. We have performed the calculation for values of $\sigma_0=0$, 1, $1\frac{1}{2}$, 2×10^{-24} cm^2. $\Delta(r^2)_{av}$ denotes the increment in $(r^2)_{av}$ between two collisions in the linear region, i.e., it gives the change of $(r^2)_{av}$ in an energy interval w, w/e and thus determines the slope of the lines.

The data obtained can probably be regarded as reliable up to energies of about 1 Mev. For higher energies the $(r^2)_{av}$'s obtained are too large. This is in agreement with the limitation of the validity of the Bethe-Peierls formula to energies for which the de Broglie wave-length is comparable to the range of nuclear forces, the formula giving too small cross sections for higher energies. It is also interesting to note the marked dependence of $(r^2)_{av}$ on the value of σ_0. The presence of oxygen cuts down considerably the range of the neutrons at energies for which the m.f.p. in hydrogen reaches the order of magnitude of that in oxygen.

TABLE I. $(r^2)_{av}$ *in cm² for* $w_a=1$ *volt.*

w_0 (Mev)	$10^{24}\sigma_0$ 0	1	$1\frac{1}{2}$	2
e^2	1596	873	720	608
$e^{1.6}$	969	607	516	444
$e^{1.2}$	633	434	380	332
$e^{.8}$	432	319	287	255
$e^{.4}$	311	245	222	201
e^0	236	194	180	163
$e^{-.4}$	188	159	149	137
$e^{-.8}$	158	134	126	118
$e^{-1.6}$	124	107	102	95
$e^{-2.4}$	103	92	87	82
$e^{-3.2}$	92	82	77	73
e^{-4}	84	75	71	67
e^{-5}	76	67	63	60
e^{-6}	67	60	56	53
e^{-7}	59	53	50	47
$\Delta(r^2)_{av}$	7.9	6.9	6.5	6.1

[2] H. A. Bethe and R. Peierls, Proc. Roy. Soc. **A148**, 146 (1934); **149**, 176 (1934).

[3] E. R. Dunning, Phys. Rev. **45**, 586 (1934).

[4] The writer wishes to express his thanks to Professor Fermi for having suggested these calculations and for his interest in them.

On the Absorption and the Diffusion of Slow Neutrons

E. AMALDI AND E. FERMI, *Royal University of Rome, Rome, Italy*

(Received September 5, 1936)

The study of the absorption properties of slow neutrons establish the existence of absorption bands which correspond to energy intervals sufficiently narrow to allow one to isolate relatively homogeneous neutron groups. In this work, we describe several experiments and considerations designed to disclose the characteristics of the absorption and scattering properties of the various groups. Summary: 1. Introduction. 2. Measurements and their reduction. 3. Selective absorptions. 4. Slow neutron groups. 5. Systematic absorption measurements. 6. Albedo. 7. Scattering of the neutrons of a single group. 8. Mean free path of thermal neutrons. 9. Groups as a function of the distance from the source; energy ratios. 10. Passage of the neutrons from one group to another. 11. Behavior of the groups in the neighborhood of the surface of the paraffin. 12. Width of the energy bands corresponding to the groups. Total number of neutrons. 13. Summary and discussion.

1. INTRODUCTION

THE purpose of this work is to describe systematically the researches we have carried out on the absorption and scattering properties of slow neutrons.[1] It is known that the simplest theory[2] on the probability of capture of a neutron by a nucleus leads to the prediction that the capture cross section is, for small neutron velocities, inversely proportional to the velocities. However, the constant of proportionality can vary between large limits from element to element.

If this were true, thicknesses of two different elements inversely proportional to their constants would be exactly equivalent as absorbers of slow neutrons independently of neutron velocity, and of the substance used as detector. That the phenomenon was not so simple was early observed by various authors,[3] who showed that generally the absorption by an element was greater when the slow neutrons were detected by means of the activity induced in the same element.

The thermal experiments of Moon and Tillman and others,[4] which showed that different detectors exhibit different sensitivities with a variation of the temperature of the paraffin, lead to a similar conclusion. Finally, more recently, Rasetti, Segrè, Fink, Dunning and Pegram[5] have measured the dependance of the absorption coefficient of thermal neutrons on their velocity by means of a mechanical arrangement, and have found that, at least for Cd, the $1/v$ law is not fulfilled. In a systematic study of these phenomena, we have found that the selective absorption of slow neutrons is accentuated by filtering with a sheet of cadmium of sufficient thickness.[6] This fact, observed independently by Szilard,[7] pointed to the possible existence of relatively narrow absorption bands characteristic of various elements.

A systematic description of these phenomena can be obtained by means of an analysis of the slow neutron radiation into groups which are approximately homogeneous with respect to their absorption properties.[8] Such analysis could be performed by decomposing the absorption

[1] E. Amaldi and E. Fermi, Ric. Scient. **VI-II**, 334, 443 (1935); **VII-I**, 56, 223, 310, 393, 454 (1936); see also: E. Fermi, E. Amaldi, O. D'Agostino, F. Rasetti and E. Segrè, Proc. Roy. Soc. **A146**, 483 (1934); E. Amaldi, O. D'Agostino, E. Fermi, B. Pontecorvo, F. Rasetti and E. Segrè, Proc. Roy. Soc. **A149**, 522 (1935).

[2] E. Amaldi, O. D'Agostino, E. Fermi, B. Pontecorvo, F. Rasetti and E. Segrè, Proc. Roy. Soc. **A149**, 522 (1935); H. A. Bethe, Phys. Rev. **47**, 747 (1935); F. Perrin and W. M. Elsasser, Comptes rendus **200**, 450 (1935).

[3] P. B. Moon and J. R. Tillman, Nature **135**, 904; **136**, 136 (1935); T. Bjerge and C. H. Westcott, Proc. Roy. Soc. **A150**, 709 (1935); L. Arsimovitch, I. Kourtschatow, L. Missowski and P. Palibin, Comptes rendus **200**, 2159 (1935); B. Pontecorvo, Ric. Scient. **VI-II**, 145 (1935); L. N. Ridenour and Don M. Yost, Phys. Rev. **48**, 383 (1935).

[4] P. B. Moon and J. R. Tillman, Nature **135**, 904 (1935); Dunning, Pegram, Fink and Mitchell, Phys. Rev. **48**, 265 (1935); P. B. Moon and J. R. Tillman, Proc. Roy. Soc. **A153**, 476 (1936).

[5] F. Rasetti, E. Segrè, G. A. Fink, J. R. Dunning and G. B. Pegram, Phys. Rev. **49**, 104 (1936); Rend. Linc. **23**, 343 (1936).

[6] E. Amaldi, E. Fermi, Ric. Scient. **VI-II**, 344 (1935).

[7] L. Szilard, Nature **136**, 950 (1935).

[8] E. Fermi and E. Amaldi, Ric. Scient. **VI-II**, 443 (1935).

curves into exponentials. We also studied different groups of neutrons by means of their scattering properties in hydrogenated substances.

In §2, we describe the methods used in performing the experiments and the reduction of the results. In §§3, 4, 5, we have collected some systematic data on the absorption properties and on the intensity of the activation produced by the various groups in several detectors. In §6, we describe the measurement of the reflection coefficient (albedo) for the neutrons of different groups; in §§7 and 8, we study the mean free paths and the average number of impacts of a neutron of a given group in paraffin. In §9, we show how the intensity of the activation due to several groups varies as a function of the distance from the source inside a large mass of water; from this relation we can deduce the energy sequence of the various groups and we are also able to evaluate the ratio of the energies of different groups. In §§10 and 11, we describe some diffusion experiments. In §13, all the results are collected and discussed.

In this work, we will often make use of some theoretical relationships that have been derived by one of us.[9] We shall refer to this paper in what follows by F.

2. Measurements and Their Reduction

As neutron source, we always used small glass bulbs about 4 mm in diameter and 15 mm in length which contained Rn (up to 800 mc) and powdered beryllium. Since our researches were extended over a period of several months, it was clearly necessary to establish some standard method of comparing results obtained with different sources and at different times.

We now describe the criteria employed for this purpose: The measurements of activity were made with an ionization chamber represented schematically in Fig. 1, which also contains the scale. The chamber was filled with carbon dioxide at three atmospheres and was closed by a window of aluminum 0.1 mm thick and 7 cm in diameter. Since the aluminum window is greatly curved by the pressure, it was covered by a Cellophane foil which served the double purpose

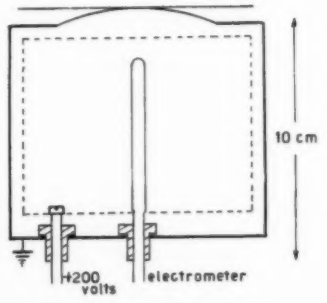

Fig. 1. Ionization chamber.

of protecting the chamber from possible contamination and providing a flat surface upon which to place the detectors. The ionization was measured with an Edelmann electrometer, the wire of which was projected on a scale; it was possible to vary the sensitivity of the electrometer and the magnification of the image of the wire so that we obtained from 5 to 250 divisions per volt. To check the readings we used a uranium oxide preparation contained in a packet of aluminum 5×5 cm^2. We will designate this preparation and its activity by U.

The ionization produced in our chamber by the U is equivalent to that obtained from a solution of 0.96 g of uranyl nitrate ($UO_2(NO_3)_2+6H_2O$) in 25 cm^3 of water contained in a dish of aluminum 0.1 mm thick and 5×5 cm^2 base. Correcting the activity of this solution for the absorption in the solution and in aluminum, we find that it is equal to 0.066 g of uranium element, that is 840 disintegrations per second.

In order to make the readings more rapidly and to be able to use different sensitivities of the electrometer and different scale intervals, we constructed a nomogram which permitted us to find directly, given the sensitivity of the electrometer and the number of divisions used in the reading, the time it would take the U to produce the same ionization. In this way one obtains automatically the correction for the nonlinearity of the instrument and for the dependance of the capacity on the sensitivity. Naturally the readings were corrected for the zero effect which was about 15 percent of the U. The activity of a given detector placed in a definite position with respect to the source and the surrounding objects is evidently proportional

[9] E. Fermi, "Sul moto dei neutroni nelle sostanze idrogenate," Ric. Scient. VII-II, 13 (1936).

to the number of neutrons emitted by the source. In order to have comparable data, it is always necessary to divide the activity by the intensity of the source measured in neutrons (neutron intensity). In order to measure the neutron intensity, it is not sufficient to assume it to be proportional to the quantity of radon contained in the source, which can be measured for example by the γ activity; in fact small differences in the size of the beryllium granules or in the preparation of the source produce considerable variations in the number of emitted neutrons. Because of this it is convenient to measure the neutron intensity directly by means of the radioactivity induced in a suitable detector. Our usual procedure was as follows: a sheet of rhodium of 5×5.6 cm^2 and 10.15 g was activated by placing it in the center of the top surface of a paraffin cylinder

$$25 \text{ cm diameter}, \qquad 15 \text{ cm height}; \qquad (1)$$

on top of the sheet of rhodium was placed a second cylinder of paraffin of 13 cm diameter and 10 cm height; the source was placed on the axis of the lower cylinder 3 cm below its upper surface.

We will designate by S the initial activity of the 44 sec. period of Rh obtained under these conditions after irradiation for an infinite time. We will call neutron intensity I the ratio of this initial activity S to the U:

$$I = S/U. \qquad (2)$$

It should be noted that this definition depends, though not very markedly, on the ionization chamber used. The strongest source we have used had a neutron intensity of 144.9. A neutron intensity 1 corresponds to a source which contains from 5 to 6 mc radon.

We are now able to define what we shall call *activability* A of a given detector (referring, when necessary, to one of its periods) placed in a definite position with respect to the source and the surrounding objects.

Let a be the initial activity of a detector irradiated for an infinite time; we define the activability A of this detector in a given position by the expression

$$A = 1000a/S = 1000a/I\times U. \qquad (3)$$

In practice, naturally, we have calculated the activability by means of this last formula; the neutron intensity was measured once for each source with very high accuracy, and from this value the intensity at any later time was calculated by means of the period of radon.

The initial intensity a was measured by irradiating for a finite time, and was reduced to infinite time by well-known formulae.

In the case of elements of short period, it is convenient to establish a standard for the measurement of the initial activity in order to be as independent as possible, at least for relative measurements, from the possible errors in the value of the period. Therefore, in the case of rhodium (44 sec.) and of silver (22 sec.), which we have used as detectors in a very large number of experiments, we have performed the irradiation for 1 minute; in the case of silver, the readings were made from 20 sec. to 80 sec. after the end of the irradiation, and the activity so measured multiplied by an appropriate factor, gave the initial activity. In reality, a measurement of this kind gives not only the 22 sec. period, because there is a disturbance due to the 2.3 min. period; this disturbance was not very large and ordinarily was not corrected for (see also §5).

In the case of rhodium we have always irradiated 1 min. and we have taken the readings from about 30 sec. to 60 sec. after the end of irradiation; the initial activity was rapidly calculated by means of a nomogram. Also in this case we have neglected the small disturbance due to the 4.2 min. period.

In the course of this work we have performed a large number of measurements of absorption of slow neutrons in different substances. The criteria adopted in these measurements have been the following: The measurements were performed outside of the paraffin because otherwise a large fraction of the neutrons pass through the absorber many times (see §6). The source of Rn+Be was usually inserted in the paraffin cylinder (1), 3 cm below the center of the upper face on which were placed the various detectors. Most of the detectors were squares of 5 cm side.

We will call normal activability A_n of a detector its activability under these conditions. This furnishes an indication of the efficiency of the

different detectors. As examples, in Table I we give the normal activabilities of some of the detectors which we have used.

For absorption measurements, the absorbers were inserted in layers as thin as possible between the paraffin and the detectors.

In order to correct the error due to the height h of the detector from the top of the paraffin, we have measured the variation of the activity of a rhodium detector as a function of h; the practical rule found for reducing the activability to $h=0$, consists in dividing the results of the measurements by $1-h/7$, where h is the height in cm; this rule is sufficiently correct for h up to a little more than 1 cm.

Rigorously, the correction for height would depend on the absorber used and on the group of neutrons with which we work. For the present, we have neglected these refinements. Even if the neutrons leaving the paraffin were homogeneous, the absorption curves obtained under the conditions which we have described, would not be exponential, because the neutrons which come out with different inclination θ traverse different thicknesses of the absorber. In the calculation of the absorption coefficients from the experimental data, it is necessary to take these facts into account; for a long time we have calculated this correction on the assumption that the neutrons leave the paraffin according to the cosine law.

On this assumption, the absorption curve with a thin detector, as a function of $K\delta$ (K = absorption coefficient of the neutrons, δ = thickness of the absorber) instead of being the exponential $e^{-K\delta}$ (curve a of Fig. 2) is the function

TABLE I. *Activability A_n of various detectors.*

Substance	Period	Weight (in g)	Area (cm²)	A_n
MnO_2	2.5 hr.	30	26	30
Cu	5 min.	13	38	2
Ga	20 min.	2.6	7	1.3
As	26 hr.	7	20	24
NaBr	18 min.	26	25	9.2
Rh	44 sec.	10.15	28	282
Ag	22 sec.	8	27	135
In	54 min.	0.76	9	21.2
In	16 sec.	0.76	9	14.2
I	25 min.	25	25	16.9
Ir	19 hr.	14.5	25	78
Au	2.7 d	6.6	25	26

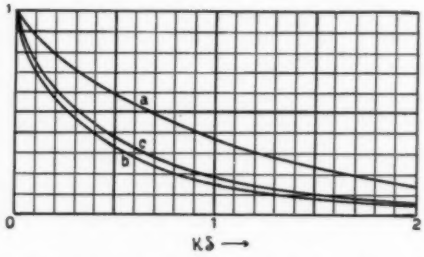

FIG. 2. Absorption curves following different laws. Curve (a) $a(K\delta)=e^{-K\delta}$; curve (b) $b(K\delta)=\int_0^1 e^{-K\delta/x}dx$; curve (c) $c(K\delta)=2/(2+\sqrt{(3)})\int_0^1 e^{-K\delta/x}(1+\sqrt{(3)}x)dx$.

$$b(K\delta)=\int_0^1 e^{-K\delta/x}dx \qquad (4)$$

represented by the curve b of Fig. 2. We now believe that for the neutrons of group C, (see F §6) it is better to assume that the number of neutrons emerging per unit solid angle instead of being proportional to $\cos\theta$, is approximately proportional to

$$\cos\theta+\sqrt{(3)}\cos^2\theta. \qquad (5)$$

If we take this angular distribution of the neutrons, the absorption curve as a function of $K\delta$ is given by the expression

$$c(K\delta)=\frac{2}{2+\sqrt{(3)}}\int_0^1 e^{-K\delta/x}(1+\sqrt{(3)}x)dx \qquad (6)$$

represented by the curve c of Fig. 2. This curve probably represents the behavior of the absorption of the C neutrons fairly well; for the neutrons of other groups, it is probable that the absorption curve will be between b and c; however all reductions have been made with curve c. In the case of thick detectors, in other words when the absorption of the neutrons in the useful thickness was considerable, the data obtained from curve c was further corrected.

The differences between the absorption coefficients given in this work and those reported in preliminary communications, are due, in large part, to the fact that the reductions have been made with curve c instead of curve b of Fig. 2.

3. SELECTIVE ABSORPTIONS

We have already mentioned that, as was observed by different authors, the absorption of slow neutrons in an element is generally

stronger when one uses a detector of the same element. For instance, Table II indicates the percentages of the activity transmitted by absorbers of 0.36 g/cm² of rhodium and 0.96 g/cm² of silver when the detector is a rhodium target of 0.36 g/cm² or a silver target of 0.80 g/cm². Data of this kind concerning a larger number of elements have been published, by various authors.[10]

These facts suggest the existence of selective absorptions of the slow neutrons. The most obvious method of studying these selective absorptions consists in measuring and analyzing the absorption curves. In Fig. 3, are given the absorption curves of cadmium with rhodium detector (0.36 g/cm²) and silver detector (0.057 g/cm²). It is clear from these curves that the radiations which are responsible for the activity of both these detectors are not homogeneous, but consist of a fraction which is absorbed very strongly in cadmium, and a fraction which is very weakly absorbed. Taking into account the fact that with our geometrical disposition the absorber is traversed obliquely by the neutrons, (see §2) it is possible to calculate the absorption coefficient of the strongly absorbed fraction from each of these curves.

In this way we obtain, from the curve with silver detector $K=16$ cm²/g, and from the curve with rhodium detector $K=13.5$ cm²/g. The absorption coefficient of the hard fraction is certainly less than 1/100 of these values; so, for instance, in the case of the rhodium detector we find $K=0.05$ cm²/g.

From the examination of the curves of Fig. 3, it can be seen that in our silver detector half of the activity is due to the component which is strongly absorbed in cadmium and half to the hard component. Instead, in our rhodium detector 72 percent of the total activity is due to

TABLE II. *Absorption of slow neutrons as measured by different detectors.*

Absorber	Rh	Ag
Detector		
Rh	54	67
Ag	68	45

[10] P. B. Moon and J. R. Tillman, Nature **136**, 66 (1935); B. Pontecorvo, Ric. Scient. **VI-II**, 145 (1935); E. Amaldi and E. Fermi, Ric. Scient. **VI-II**, 344 (1935).

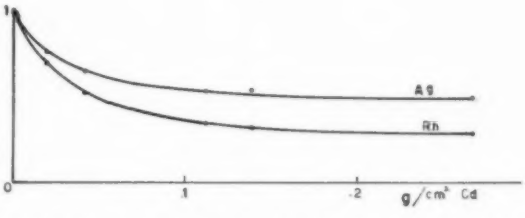

FIG. 3. Absorption curves for Cd as determined by Ag and Rh detectors.

the soft component and the remainder to the hard component. Therefore the absorption by cadmium makes it possible to divide the slow neutrons which come out of a paraffin block containing a source of neutrons into two fractions: that fraction which is strongly absorbed by cadmium will be hereafter designated as group *C*. We will discuss its absorption properties in more detail in §5.

We will now study the properties of the radiations which traverse a thickness of cadmium sufficient to totally absorb the C group. For this purpose we have repeated some absorption experiments on the radiations filtered by 0.27 g/cm² cadmium using rhodium and silver absorbers and detectors.[11] Table III, similar to Table II, is given as an example of the results of such experiments; the results summarized in Tables II and III were obtained with the same absorbers and detectors.

Comparison of Tables II and III shows that the selectivities are accentuated for the radiation filtered by cadmium, which indicates that the component weakly absorbed by cadmium is not homogeneous. In order to further investigate the properties of the radiation filtered by cadmium, we have measured the absorption curve of silver with silver detector (2.2 g/28 cm²) both for the unfiltered radiation and for the radiation filtered by 0.27 g/cm² of cadmium. These curves are

TABLE III. *Absorption of radiations filtered by 0.27 g/cm² Cd.*

Absorber	Rh	Ag
Detector		
Rh	33	84
Ag	88	29

[11] E. Amaldi and E. Fermi, Ric. Scient. **VI-II**, 344 (1935); L. Szilard, Nature **136**, 950 (1935).

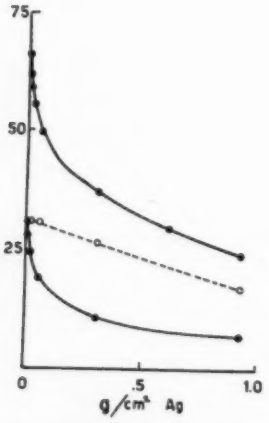

FIG. 4. Upper curve, absorption curve for Ag, unfiltered radiation. Lower curve, absorption curve for Ag, radiation filtered by 0.27 g/cm² of Cd. Ordinates are the activability of Ag detector. Dotted curve is difference of upper and lower curves.

given in Fig. 4 where the abcissa represents the thickness of the silver absorber and the ordinate represents the activability of the detector. The upper curve refers to the unfiltered radiation and the lower curve to the radiation filtered by 0.27 g/cm² of cadmium.

In both curves, we see that the radiation which is responsible for the activity of silver contains a component strongly absorbed in the same element, which component is present with the same intensity both in the filtered and in the unfiltered radiations. This means that this component is not strongly absorbed by cadmium. We will call this component group *A*. The absorption coefficient of the neutrons of group *A* in silver is $K=20$ cm²/g.

Curves of similar character have also been found with a thicker silver detector; in this case however the percentage of activity due to the radiation strongly absorbed in silver is naturally smaller, since it is saturated in less than 0.1 mm of thickness of the detector.

The dotted curve of Fig. 4 is the difference of the two other curves; it therefore represents the behavior of that fraction of the silver activity that is absorbed by 0.27 g/cm² of Cd. It is, therefore, the absorption curve of silver with silver detector due only to the neutrons of group *C*. From this we obtain as value of the absorption coefficient of silver for the *C* neutrons, $K=0.3$ cm²/g.

4. Slow Neutron Groups

We have seen from the examples of the preceding paragraph, that the analysis of the absorption curves permits us to classify slow neutrons into components which are differently absorbed in different elements. It is well known that the analysis of absorption curves into exponentials can be considered reliable only when the accuracy of the individual measurements is very high, and also the geometrical disposition of the absorber and detector with respect to the source, corresponds to accurately calculable conditions. In our case, neither of these conditions were exactly satisfied, and therefore we seek the possibility of checking accurately the homogeneity of each component. For this reason, we have limited ourselves to the description of the properties of groups of approximately homogeneous neutrons.

The differences of behavior from group to group are so marked that it is possible to assign to each of them an individuality, despite the small internal inhomogeneity. The analysis into groups is made possible by the following circumstances:

(a) For some absorbers there exist very large differences in the absorption coefficients from group to group.

(b) It is possible to use different absorbers and detectors which behave quite differently.

(c) It is possible to filter the slow neutrons with absorbers so as to reduce the inhomogeneity.

The most obvious assumption concerning the physical nature of the difference between the various groups is that it is due to a difference in velocity. In a paraffin block the fast neutrons, which escape from the source suffer a progressive slowing down due to the successive collisions with the hydrogen atoms until they arrive at the energy of thermal agitation; therefore, in paraffin there are present at each instant neutrons of all velocities, from the energy of thermal agitation to the energy with which they leave the source. Likewise, neutrons of all these velocities diffuse out of the paraffin block. Hence we may think that the different groups correspond to neutrons of different energy intervals. Selective absorptions must be interpreted as due to irregular variations of the absorption coefficient as a function of the neutron velocity.

The possibility of an irregular dependance of the absorption coefficient on the neutron velocity has been demonstrated by recent considerations of Bohr, Breit and Wigner.[12] We will return to the discussion of the physical origin of the groups after we have described the absorption experiments and also the scattering properties of the various groups.

Already in the preceding paragraph, we have called the radiation strongly absorbed in cadmium ($K=13.5\div16$ cm²/g) group C; and the radiation strongly absorbed in silver ($K=20$ cm²/g) group A.

We have also seen that only 50 percent of the activity of our silver detector (0.057 g/cm²) is due to group C; of the remaining 50 percent about one-half is due to group A, while the rest is due to a radiation which is only slightly absorbed in cadmium and in silver (see Fig. 4); this radiation we have called group B, which is very probably complex. Up to now we have not been able to analyze it into approximately homogeneous components, since we have not found any elements which absorb group B with a high absorption coefficient.

In the preceding section, we have shown that 72 percent of the activity of our rhodium detector (0.36 g/cm²) is due to group C; the remaining 28 percent constitutes a new group, which we have called group D, which is very slightly absorbed by cadmium. In studying a PbI_2 detector (19 g/25 cm², normal activability 11.4), we have found that only about 25 percent of its activity is due to group C and less than 10 percent is due to group A; the remainder is due to a component which is very weakly absorbed in all elements that we have studied up to date, except iodine; this radiation which is responsible for about 70 percent of the activity of our detector has been called the I group.

Frisch, Hevesy and McKay[13] have studied the absorption of gold with gold detector using the cadmium filtered neutrons and have obtained results similar to those we obtained for silver (see Fig. 4). We have tried to analyze the activity of a gold detector (1.75 g/25 cm²) in terms of the groups already mentioned; we have found that the activity of gold is due in part to group C, A and B; the high absorption coefficient of gold with gold detector is probably due to a radiation distinct from all the preceding groups.

[12] N. Bohr, Nature **137**, 344 (1936); G. Breit and E. Wigner, Phys. Rev. **49**, 519 (1936).
[13] O. R. Frisch, G. Hevesy and H. A. C. McKay, Nature **137**, 149 (1936).

5. Systematic Absorption Measurements

Group C

Of all groups the group C is the best known, because it is responsible in almost all detectors for a large percentage of the activity; there are many reasons for believing (see §13) that this group is composed, in large measure, of neutrons having energy of thermal agitation; for this reason we will often refer to it as the thermal group. The study of the C group is particularly easy because of the fact that a thickness of $0.3\div0.4$ g/cm² of cadmium absorbs it practically completely without appreciably absorbing any of the other groups. In order to obtain the fraction of the activity due to the C group, it is sufficient to obtain the difference in the activity observed without and with a filter of cadmium of the above thickness.

In Table IV we give the absorption coefficients in cm²/g for the C neutrons, observed with various detectors (always forming the difference between the activity without and with a cadmium filter) and various absorbers. It is to be noted that the absorption coefficients of the same element measured with different detectors are approximately the same. The differences are due in part to errors in measurements; however we believe that they are not completely accounted for by this reason.

Despite this, if we remember the large differences of the absorption coefficients of an element for the neutrons of different groups, we see that the C group actually has a notable internal homogeneity.

Group D

The D group is easily observed by using rhodium or indium as detector; with both these elements precise measurements are possible.

The fact that it is possible to characterize the D group by using one or the other of these detectors indicates that the corresponding absorption bands are nearly coincident; naturally there is no reason to believe that this coincidence

TABLE IV. *Absorption coefficients in cm²/g for group C neutrons (those strongly absorbed by Cd).*

Absorber	Rh	Ag	Cd	In	Ir	Au	Hg
Detector							
Mn 2.5 hr.	0.9	0.3	–	–	–	–	–
Rh 44 sec.	0.6	0.2	13.5	0.6	1.0	0.2	0.7
Ag 22 sec.	0.7	0.3	16	–	0.9	0.25	0.9
In 54 min.	0.6	0.2	44	0.9	1.0	0.2	0.6
Ir 19 hr.	1.0	0.3	–	–	–	–	0.6

TABLE V. *Absorption coefficients in cm²/g for group D neutrons (those strongly absorbed in Rh).*

Absorber	B	Rh	Ag	Cd	In	Ir	Au	Hg
Detector								
Rh 44 sec.	4.7	2.0	0.06	0.05	3.0	1.0	0.03	0.07
In 54 min.	–	1.6	0.09	–	3.8	1.0	0.04	0.04

is complete; we will see in §9 that of all the groups we have studied, the D group has smaller energy than any, except the C group.

We have already mentioned that 28 percent of the activity of our detectors of rhodium is due to the D group. In an indium detector of 0.76 g/9 cm², 42 percent of the activity of the 54 min. period is due to the D group; the remaining 58 percent is due to the C group. In order to study group D, it is therefore sufficient to use one of these detectors, filtering the radiation by $0.3 \div 0.4$ g/cm² of cadmium in order to eliminate the C group. In Table V some absorption coefficients in cm²/g of the D neutrons are given.

Group A

This group, characterized by the large absorption coefficient in silver ($K = 20$ cm²/g), is ordinarily studied by using a thin sheet of silver as detector.

As was mentioned above, 25 percent of the normal activability of a silver detector of 0.057 g/cm² is due to the A neutrons. In order to isolate this group it is sufficient to form the difference of the activability of a silver detector without and with a silver filter sufficiently thick to absorb completely the A group and not thick enough to appreciably absorb the other groups. In practice it is convenient to eliminate the C group by means of a cadmium filter.

The A group is also detected by gold; a gold detector of 1.535 g/25 cm² has a normal activability of 21, of which 13 percent is due to group A; the absorption coefficient of gold for this group is 4 cm²/g. The absorption coefficient of the A group in boron is 3 cm²/g.

Not much is known concerning the properties of the other groups mentioned in the preceding section. We have performed a few measurements of absorption coefficients which we give here:

Group B: boron $K = 2.3$ cm²/g; gold $K = 1.7$ cm²/g.
Group I: boron $K = 1$ cm²/g; iodine $K = 0.7$ cm²/g.

We have seen that despite the fact that the C group almost always constitutes more than 50 percent of the activity of the different detectors, placed outside of the paraffin, the other groups are found in a smaller number of detectors and are responsible for a smaller percentage of the activities.

This is not due to the fact that the coefficient of absorption of the different elements are greater for the neutrons of group C than for the neutrons of the other groups; we have already encountered numerous examples to the contrary. It is rather due to the fact that the number of C neutrons which come out of paraffin is much larger than the number of neutrons of the other groups.

Therefore, a very important datum for characterizing a group is its *numerosity*. We will define this quantity for practical purposes as follows: the numerosity N_0 of a group is the number of neutrons which are emitted per second per square centimeter and per unit of neutron intensity of the source, averaged over 25 cm² at the center of the top surface of the paraffin (1) containing the source (neutron intensity I) 3 cm below the center of the top.

The principle on which the measurement of the numerosity of a group is based is as follows: We place on the center of block (1) a thin detector of area s; the number of neutrons which strikes this detector is

$$N_0 I s.$$

If we designate the absorption coefficient of the detector by K, assuming that its thickness δ is very small, it is possible to see that the number of neutrons captured by the detector is

$$\sqrt{(3)} N_0 I s K \delta,$$

where the factor $\sqrt{(3)}$ is due to the obliquity of the neutrons, which is taken into account according to Eq. (5).

If we designate by η the efficiency of the ionization chamber, that is the ionization current due to one disintegration per second on the surface, the normal activability (see Eq. (3)) of our detector is

$$A = 1000\sqrt{(3)}sN_0K\delta(K_1/K)(\eta/840\eta_U), \quad (7)$$

where η_U is the efficiency of the chamber for the β-rays emitted by the uranium preparation we used, which, as already has been mentioned, corresponds to 840 disintegrations per second at the surface.

The factor K_1/K is introduced in order to take into account that when a detector absorbs neutrons of a given group (with an absorption coefficient K) it is possible that a fraction of these gives rise either to nonradioactive isotopes or to radioactive isotopes with periods different from that studied; we indicate by K_1 the absorption coefficient due only to the process which is responsible for the studied activity; it is evident that although K is the coefficient which determines the absorption of the neutron in the detector, K_1 determines its activity.

From (7) we find the numerosity of the group under examination.

$$N_0 = 0.485\frac{\eta_U}{\eta}\frac{K}{K_1}\frac{A}{sK\delta}. \quad (8)$$

In this expression for N_0, the quantities A, s, K, δ are directly measurable; in most cases it is possible to put K_1 equal to K; in the other cases where an element has more than one mean life, the ratio of their activabilities corrected for the absorption of the β-rays and for the different efficiencies η, allows one to evaluate K/K_1.

A considerable error in the measurement of N_0 is due to the insufficient knowledge of the ratio of the efficiency of the chamber for β-rays of different hardness. From the relatively small variations which are found in the calculated numerosities for different detectors on the assumption of a constant efficiency η, it can be concluded that this quantity does not vary between very large limits. In the following calculations we have always put $\eta = \eta_U$.

In Table VI we give the values of the numerosities of the various groups calculated using different detectors; as absorption coefficients we have used the averages of the data of the preceding tables. The values given in Table VI have been calculated with a formula similar to (8) in which however the absorption of the neutrons and the electrons in the detector have been taken into account. We have also introduced a small correction in order to take into account the reflection of the electrons from the upper layers of the detector.

The data for indium have been calculated by adding the contributions of the two periods of 16 sec. and 54 min. and by neglecting the weak period of 4 hours. For rhodium and for silver we have made the calculations by taking into account not only the 44 sec. and the 22 sec. periods, but also the 4.2 min. and 2.3 min. periods.

If we try to calculate the numerosity of group C from the activity of iridium (19 hr.), we find a value of about 10; this value seemed to us much too small to be attributed to errors in measurements. Therefore we have tried to find another activity strong enough to justify the previous small value of the numerosity. In reality, this suspicion was well grounded since we have found a second iridium activity with a period of 68 days whose activability, although not yet measured, is of the order of magnitude of the activability of 19 hr. period. The β-particles of this new activity have very small penetrating power.

It is very interesting to determine for elements which have two or more periods, both due to slow neutrons, whether or not the activities of the different periods are due to the same groups.

Therefore we have studied the following detectors; rhodium (0.36 g/cm² 44 sec., 4.2 min.), silver (0.057 g/cm² 22 sec., 2.3 min.), indium (0.065 g/cm² 16 sec., 54 min.), sodium bromide (1 g/cm² 18 min., 4.2 hr.) and we have compared for each of them the activability of the two periods with and without appropriate filters.

In the case of rhodium, the ratio of the activabilities of the 44 sec. and of the 4.2 min. periods remains the same (about 10) with and without a filter of cadmium sufficient to absorb the C group.[14] In the case of silver, however, we have

[14] E. Fermi and E. Amaldi, Ric. Scient. **VI-II**, 443 (1935); E. Segrè, Ric. Scient. **VII-I**, 389 (1936).

TABLE VI. *Numerosity (N_0) for various neutron groups.*

Detector	Group C	D	A	I
Rh	43	9	—	—
Ag	51	—	0.6	—
In	31	6	—	—
I	—	—	—	5
Au	33	—	0.5	—

found a marked difference in the behavior of the two periods; in group C the activability of the long period is 24 percent of the total activity; in group B, 19 percent; finally in group A we have found 3 percent which, within the limits of experimental error could be zero; we can therefore say that the group A is characteristic of the 22 sec. period of silver.

In the case of indium the percentage of activation of the two periods due to group C and D are approximately equal. Similarly for bromine, a cadmium filter does not considerably change the ratio of the activability of the two periods.

We have also replaced the paraffin cylinder on which the measurements were usually made, by an equal cylinder of water and using rhodium, silver and lead iodide detectors and appropriate filters, we have determined the percentages of activation due to the different groups. In this way we have been able to show that the ratios of the numerosity of the various groups are the same in water as in paraffin. Also the absolute values do not vary considerably. However it should be noted that the ratios of the intensities of the various groups undergo a variation at different distances from the source, as will be discussed in more detail in §9.

Finally we have tried to see whether the ratio of intensity of the various groups is affected by using different source of fast neutrons.[15] For this purpose we have determined the activability of rhodium and silver detectors with and without cadmium and silver filters, using a source newly prepared, in which the radium C was not yet in equilibrium; and we have followed the increase of activability during the formation of radium C. We have not found any difference in the ratio of the groups for silver and rhodium during the formation of radium C, although the activability increased from 40 (effect due to the particles of Rn+Ra A) to 100 (effect due to the particles of Rn+Ra A+Ra C). In Fig. 5 we give the curve of the increase of the activity as a function of the time. One should note the high efficiency of the radium C α-particles for producing neutrons from beryllium; their efficiency is three times greater than that of the α-particles of Rn and Ra A.

[15] E. Fermi and E. Amaldi, Ric. Scient. VI-II, 443 (1936).

6. ALBEDO

The measurements of normal activability as also the absorption measurements of which we have spoken up to now are made outside of the paraffin block. In this section we will study the properties of the slow neutrons inside the paraffin.

The detector (rhodium 10 g/28 cm², or silver (2.2 g/38.5 cm²) was placed in the center of the top of the normal paraffin block (1) and upon it was placed a second equal paraffin cylinder. The detector could be placed between appropriate filters.

In order to indicate rapidly the relative position of source, paraffin, detectors and absorbers, it is convenient to set up the following convention: We will indicate with the letter S the source, P the paraffin, R the detector, and with the symbols Cd and Ag the cadmium (0.27 g/cm²) and silver (0.057 g/cm²) absorbers. Thus S P Cd R Cd P means an experiment in which above the source (S) there are 3 cm of paraffin (P), followed by a layer of cadmium (Cd), the detector (R), a second cadmium layer (Cd), and finally the second paraffin cylinder (P).

In Table VII we give the activabilities of the two detectors of silver and rhodium in various experiments. If we compare the experiment S P R and S P R P we note the strong increase of the activity due to the superposition of the second block of paraffin. This large increase is due to the fact that neutrons, both fast and slow, which in the absence of the second block would escape, can now be reflected back from this block.

If we put the detector between appropriate absorbers, it is possible to analyze the radiation responsible for the activity into groups. Thus the comparison of experiments S P R P and S P Cd R Cd P shows that in the case of silver detectors the fraction $(417-66.5)/417=0.84$ of the activity is due to group C and in the case of rhodium detector, the fraction $(1025-140)/1025=0.86$ is

due to group C. It is to be noted that the ratio of group C to the other groups is much larger inside of the paraffin than outside; we will soon see the reason for this behavior. As a check of the correctness of the analysis into groups of the activity of a detector, also inside of the paraffin, we have doubled the thickness of the cadmium absorbers in the experiment $S\,P$ Cd R Cd P, and we have found only a very small further decrease in the activity. In the case of the silver detector, the addition of silver absorbers to those of cadmium causes a reduction of the activity to one-half (experiments $S\,P$ Cd R Cd P and $S\,P$ Cd Ag R Ag Cd P); this fact shows that also inside the paraffin it is possible to speak of a group A intensely absorbed by silver. In agreement with what is obtained outside the paraffin, the thin absorbers of silver added to those of cadmium do not produce a further reduction of the rhodium activity.

Let us now study the behavior of group C. Let us consider the results of the measurements $S\,P\,R\,P$, $S\,P$ Cd $R\,P$, $S\,P\,R$ Cd P, $S\,P$ Cd R Cd P; this last measurement indicates what part of the activity is not due to the group C, so that if we subtract this value from the results of the other three measurements, we will obtain the fraction of the activity due only to group C.

The difference between $S\,P$ Cd $R\,P$ and $S\,P\,R$ Cd P can easily be interpreted by taking into account the fact that the density of slow neutrons inside the paraffin decreases with the distance from the source in such a way that a sheet of cadmium which screens the detector on the side of the source stops more neutrons than an equal sheet on the other side. The mean value of these two experiments may be considered as the value which would be obtained in the case of a uniform density distribution of slow neutrons inside the paraffin, when the detector is screened on one side by cadmium.

Therefore we find for the silver detector, as activability due only to group C, $A_c=417-66.5=350.5$. The activability due only to group C when the silver is screened only on one side by a layer of cadmium is $B_c=(92.2+113.1)/2-66.5=36.1$.

The corresponding values for rhodium are $A_c=885$, $B_c=167.5$. The ratio A_c/B_c is for silver 9.7 and for rhodium 5.3.

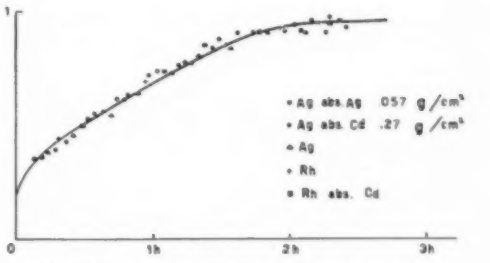

FIG. 5. Increase of activity as a function of time.

An elementary consideration allows us to understand the values of this ratio. We will call β the probability that a neutron that is incident on a flat surface which limits a very large paraffin block, comes out after having suffered several collisions in the paraffin.

We call this value β *albedo*, which corresponds to the coefficient of diffuse reflection of slow neutrons from a paraffin surface. Actually it depends upon the angle of incidence of the slow neutrons, and it is evidently smaller, the smaller the angle of incidence (see F, §5).

In this elementary consideration we will neglect this dependence.

We call ζ the probability that a neutron which traverses the detector is captured by it. Also for ζ we will neglect the dependence on the angle of incidence.

The method for the measurement of the albedo is based on the comparison of the activabilities A_c and B_c defined above.

Let N be the number of C neutrons which are incident on a detector of group C when it is screened on one side by a total absorber of C neutrons. The number of neutrons captured by the detector is $N\zeta$ and its activability B_c will be proportional to $N\zeta$.

TABLE VII. *Activabilities for various arrangements.* S=source, P=paraffin, Cd=cadmium, Ag=silver, R=detector.

Arrangement	Silver	Rhodium
$S\,P\,R$	66.1	282
$S\,P$ Cd R	32.2	80
$S\,P$ Cd Ag R	17.5	78
$S\,P\,R\,P$	417	1025
$S\,P$ Cd R Cd P	66.5	140
$S\,P$ Cd $R\,P$	92.2	244
$S\,P\,R$ Cd P	113.1	371
$S\,P$ Cd Ag R Ag Cd P	34.5	144
$S\,P$ Cd Ag R Cd P	45.6	–
$S\,P$ Cd R Ag Cd P	54.8	–

Let us now remove the absorber and let us calculate the increase of the activity of the detector.

First, we must take into account the fact that the neutrons can impinge on the detector on both sides; this gives rise to a factor 2.

But a much more important increase is due to the fact that when one places immediately behind the detector a sheet which absorbs all neutrons, a C neutron which impinges on the detector traverses it only once and therefore has the probability ζ of being captured; when the absorber is not present the neutron can traverse the detector many times.

Actually, the first time the neutron has the probability ζ to be captured and the probability $1-\zeta$ to go through; the probability that the neutron goes back to the detector is therefore $\beta(1-\zeta)$ and the probability that it is captured in the second passage is $\beta(1-\zeta)\zeta$ and so on. Thus we find that the probability of capture is

$$\zeta+\zeta\beta(1-\zeta)+\zeta\beta^2(1-\zeta)^2+\cdots = \frac{\zeta}{1-\beta(1-\zeta)}=\frac{\zeta}{1-\beta+\beta\zeta}.$$

The number of captured neutrons is

$$2N\zeta/(1-\beta+\beta\zeta)$$

and hence the ratio A_c/B_c is

$$A_c/B_c=2/(1-\beta+\beta\zeta). \tag{9}$$

If ζ is very small, i.e., in the case of very thin detector, this reduces to

$$A_c/B_c=2/(1-\beta). \tag{10}$$

Therefore the measurement of the ratio A_c/B_c allows us to determine the albedo β.

In the case of our silver detector, ζ is very small but not negligible. We can evaluate it from its thickness and absorption coefficient, also taking into account the obliquity of the neutrons. Thus we find $\zeta=0.03$ and therefore $\beta=0.82$.

The rhodium detector is much thicker; for it ζ is about 0.35; it is clear that a small error in this large value of ζ gives rise to a great error in the value of β. Therefore we cannot use the measurements with rhodium in order to determine β, but we can rather calculate for this detector the ratio A_c/B_c, using the value of the albedo found by silver measurements. We have $A_c/B_c=4.3$ in sufficient agreement with the experimental value 5.3.

We have observed that the concept of albedo, as we have introduced it, is not completely defined, since the percentage of neutrons reflected by a paraffin surface depends on the angular distribution of the incident neutrons. In order to give a more definite meaning to the concept of albedo, we can define β by means of Eq. (10), which holds in the case of an infinitely thin detector (experimental albedo; see *F*, §7).

The experimental albedo depends on the number N of free paths which a neutron C can traverse on the average before it is captured by protons in paraffin.

It is possible to show (*F*, formula 63) that the relation connecting these two values is

$$\beta=1-2/\sqrt{\mathrm{N}}. \tag{11}$$

This equation holds on the assumption that the energy of thermal agitation is negligible with respect to the quantum $h\nu$ of the elastic bond of hydrogen atom in paraffin; otherwise it is necessary to introduce a small correction (see §13).

From the value $\beta=0.82$, we find from Eq. (11) $\mathrm{N}=124$.

We have performed some experiments similar to those just described, in order to determine the albedo of the neutrons of group A, using a detector of silver of 0.010 g/cm², so that ζ for the A group is not too large.

The behavior of the group A is, in this respect, quite different from that of group C, as we found that the albedo of group A is practically zero. This fact must not be interpreted in the sense that the A neutrons are not at all reflected from paraffin, but it shows that when A neutrons are reflected they undergo such a change in velocity that they no longer belong to the A group.

Because of the low albedo of group A, the increase in activity produced by A neutrons when a second block of paraffin is placed on the detector is only of the order of 2. This increase is not due to the albedo but to the fact that the neutrons can enter the detector on both sides.

Groups B, D and I also have a negligible albedo. Hence it follows that for all the groups, except group C, the change in the velocity due to

one impact is normally sufficient to remove the neutron from the energy band corresponding to the group (see §12).

The high value of the albedo of the group C compared to the albedo of the other groups is responsible for the fact that inside the paraffin the percentages of the activations due to the C group are always much higher than outside the paraffin.

Similarly, one can interpret the experiments of Tillman[16] on the different behavior of various detectors lying on a block of paraffin, as a function of the thickness of a second superimposed layer of paraffin. A strong relative increase of the activity of a detector is to be expected, for detectors which are very sensitive to group C; naturally it is necessary to take into account in the interpretations of these experiments also the coefficient ζ of the detector according to relation (9).

7. Scattering of the Neutrons of a Single Group

From the results of the preceding paragraph we deduced that the C neutrons can traverse a large number of free paths. Their motion in paraffin is therefore analogous to a diffusion, provided that the destruction of the neutrons by proton capture is taken into account. Let N be the average number of free paths of a C neutron and λ its mean free paths; evidently the neutron will diffuse through a length of the order of magnitude of $\lambda\sqrt{N}$; therefore the diffusion experiments will enable us to measure this magnitude.[17] We shall call the expression

$$l=\lambda(N/3)^{\frac{1}{2}} \tag{12}$$

diffusion length; this magnitude can be obtained directly from the measurements we are going to describe.

Let us consider a C neutron inside a paraffin block limited by a plain surface and let x be the distance of the neutron from this surface.

It can be proved by the diffusion theory (see F, §3) that the probability $p(x)$ for the neutron to get out of the paraffin before it is captured is

$$p(x)=e^{-x/(D\tau)^{\frac{1}{2}}}, \tag{13}$$

where D is the diffusion coefficient for thermal neutrons in paraffin, and τ is their mean life for the capture process. In the case of thermal neutrons the kinetic energy is small compared to the quantum of the frequencies due to the elastic bond of the hydrogen in paraffin. We shall therefore make the assumption that the hydrogen atoms can be considered as fixed centers of isotropic diffusion, and that the mean free path λ is independent of the velocity (see F, §10, 11). These assumptions are not quite correct, as shall be discussed in detail in §13.

In the case of isotropic diffusion, the diffusion coefficient D is given by

$$D=\tfrac{1}{3}\lambda v, \tag{14}$$

v being the average velocity of the neutrons; we have furthermore

$$N=v\tau/\lambda; \tag{15}$$

hence

$$D\tau=\tfrac{1}{3}\lambda^2 N. \tag{16}$$

We find finally (see F, formula 34)

$$p(x)=e^{-x/(\lambda^2 N/3)^{\frac{1}{2}}}=e^{-x/l}. \tag{17}$$

By determining the probability $p(x)$ we shall be able to measure l and therefore also $\lambda^2 N$.

The principle on which the determination of $p(x)$ is based is the following: let R be a detector of the C group, large enough to cover all the plane surface of a large paraffin block from which C neutrons can emerge. We will assume that this detector absorbs all the outcoming thermal neutrons in a thickness small compared to the absorption of the β-rays. The activity of this detector is proportional to the number of neutrons emerging from the paraffin, and is independent of their angular distribution. If we now destroy Q thermal neutrons at a depth x below the paraffin surface, the activity of the detector shall decrease by an amount proportional to $Q\cdot p(x)$; in order to destroy these neutrons we can put an absorber of thermal neutrons at the depth x; we shall then be able to deduce Q from the activity induced in the absorber.

The experiment was performed by putting the detector on a cylinder of paraffin 24 cm in

[16] J. R. Tillman, Nature **137**, 107 (1936).
[17] T. Bjerge and C. H. Westcott, Proc. Roy. Soc. **A150**, 709 (1935); E. Fermi and E. Amaldi, Ric. Scient. **VI-II**, 443 (1935); **VII-I**, 56 (1936).

diameter and 15 cm high. The source was 3.5 cm below the center of the top face. The upper part of the cylinder was sectioned into slices so as to enable us to insert the absorber at the various depths. As detector we used a rhodium plate (10 g/28 cm²); as this plate covered only a small part of the upper paraffin surface, we took measurements placing the detector in nine different positions and adding the results.

As absorber of thermal neutrons, we used a plate of Cd−Sn alloy containing 0.019 g/cm² cadmium. As a small thickness of cadmium practically absorbs only the C neutrons, the decrease in activity of the detector is due to C neutrons only, as can be easily verified. Since the absorption of neutrons in cadmium does not activate this element we could not measure directly the number Q of the absorbed neutrons; therefore we measured the activity induced by C neutrons in a rhodium plate having for the C group the same absorption as our Cd absorber. We measured the activity on the two faces of this rhodium plate and added the results in order to take into account that the neutrons entered from both sides as explained in §11.

The absorber was put at the distances $x=0$, 1, 2, 3 cm. In Table VIII are collected the results of the measurements. Column one gives the depth of the absorber; column two gives the decrease in the activability of the detector due to the presence of the absorber; column three gives the sum of the activabilities of the rhodium plate equivalent to the absorber measured on both sides for the group C only; column four gives the ratio of column two to column three. In column five the values of these ratios are corrected in order to take into account the fact that our detector does not satisfy the condition of totally absorbing the C neutrons in a thickness small compared to the absorption of electrons (absorption coefficient for electrons 7.3 cm²/g in rhodium; absorption coefficient for neutrons 0.7 cm²/g; thickness 0.36 g/cm²). From this it follows that our detector is more sensitive to the neutrons of larger obliquity. The absorber, when in the position $x=0$, absorbs more intensely those neutrons that get out very obliquely; the decrease in activity of the detector is therefore in this case relatively larger than in the case when the absorber is placed deep inside the paraffin, since in this latter case there is no coherence between the direction of the emergent neutrons and the direction that they had when traversing the absorber. In order to take into account this factor we must reduce the value of the ratio for $x=0$ in order that it may be compared to the other ratios.

A quantitative calculation shows that the first ratio must be corrected by a factor 0.832.

The values of the corrected ratios given in the last column are proportional to $p(x)$; it can be seen that they depend with good approximation exponentially on x. The diffusion length is the inverse of the coefficient of this exponential; thus we find

$$l=2.1 \text{ cm}.$$

From this we obtain (12)

$$\lambda^2 N=13 \text{ cm}^2.$$

We performed similar experiments also for groups D and A. In the case of the D group, the source was 3.4 cm below the center of the upper face of a cylinder of paraffin similar to that used in the preceding experiments. In the case of group A the distance was 2.4 cm.

As detectors, we used, respectively, for the groups D and A indium (0.065 g/cm²) and silver (0.057 g/cm²), both screened with cadmium filters of about 0.5 g/cm². As absorbers we used for the D group rhodium (0.36 g/cm²) and for the A group silver (0.057 g/cm²).

In Table IX we have collected the results of these measurements; in column one we give the depth x of the absorber; columns two and five give for the groups D and A the decreases in activability of the detectors; column three is the sum of the activability measured at various depths on both faces of the rhodium absorber screened by cadmium so as to measure the activity due to the D group only; column six contains similar data for the silver absorbers of group A. Columns four and seven give the activabilities of the absorber measured on the lower face and due only to the neutrons of group D or A that enter the absorber from the lower face (for the method of performing this measurement see §11). The numbers in brackets of the last column have been interpolated using some results similar to those mentioned in §11.

TABLE VIII. *Data for the determination of the probability p(x).*

x (cm)	Decrease of Activability	Q	Ratio	Corrected Ratio
0	89	358	0.249	0.207
1	139	1135	0.123	0.123
2	128	1580	0.081	0.081
3	98	1950	0.050	0.050

From the low albedo of the groups D and A, we have already deduced in the preceding paragraph that the neutrons of these groups generally traverse as such only one free path. We cannot therefore apply to these groups the theory of diffusion. It is nevertheless illuminating to reduce the data of the measurements on the groups D and A by the same method that we used for the C group. For this, we examine, as a function of x, the ratios of the second to the third column, and the ratios of the fifth to the sixth column. One finds that both ratios decrease exponentially with a good approximation; in both cases the inverse coefficient of the exponential is 0.42 cm. We notice the analogous behavior of these two groups in contrast with the markedly different behavior of the C group.

It is more correct, however, to reduce the data of Table IX on the extreme assumption that the neutrons of groups D and A can traverse only one free path. Assuming this, we can deduce the mean free path of the neutrons of these two groups. If this assumption is not correct, the values that we shall obtain would represent only upper limits for the mean free path.

Let us compare the activities of the detector of group D with or without the absorber at a depth x. Both activities are the sum of two terms: (a) activity due to D neutrons that have not crossed the plane at depth x; (b) activity due to D neutrons that have crossed this plane.

From our assumption that the D neutrons can traverse only one free path, it follows that all the neutrons that contribute to the part (b) of the activity have traversed the plane x from below. The term (a) is not changed by the presence of the absorber in the position x, while the term (b) is decreased by the absorber. The total decrease in activity is hence equal to the decrease of the term (b) only. For simplicity we shall in this discussion denote as neutrons of class b the D neutrons that arrive on the plane x from below.

The decrease of the activity of the detector given in column two, Table IX, can thus be calculated by taking into account only the neutrons of class b. From our assumption, it follows that the layer of paraffin of thickness x that the neutrons of class b must traverse in order to reach the detector must be considered as an absorbing (and not as a scattering) layer, having absorption coefficient $1/\lambda_D$.

When there is no absorber, the activity of the detector due to the neutrons of class b only is thus proportional to

$$N_b c(x/\lambda_D),$$

where N_b is the number of the neutrons of class b, and c is the function defined by (6) (absorption curve taking into account the obliquity of the neutrons).

We have implicitly made the assumption that the angular distribution of the neutrons of class b is independent of the depth x; in reality this assumption is not quite correct, but we believe that it will not introduce an appreciable error.

Instead, when the absorber is in the plane x, the activity of the detector due only to the neutrons of class b is proportional to

$$N_b c\left(\frac{x}{\lambda_D}+K_D\delta\right),$$

where δ is the thickness of the absorber and K_D its absorption coefficient for the D neutrons.

Therefore the difference of the two activities is proportional to

$$N_b\left\{c\left(\frac{x}{\lambda_D}\right)-c\left(\frac{x}{\lambda_D}+K_D\delta\right)\right\}.$$

TABLE IX. *Data for D and A neutrons.* x = depth of absorber.

	Group D			Group A		
x	Decrease of Activity	Activity of Absorber	Lower Activity	Decrease of Activity	Activity of Absorber	Lower Activity
0	12.0	102	68	15.3	27.3	17.4
0.16	9.6	105	71	11.6	31.2	(18)
0.34	6.4	124	75	8.3	34.6	(19)
0.87	2.7	173	93	3.8	51.5	(22)
1.87	0.5	244	101	0.5	61.5	23.1

This expression corresponds to the data of column two, Table IX.

In column four is given the activability of the absorber due only to the neutrons of class b; this is evidently proportional to N_b (see §11). Therefore the ratios of the corresponding data of the second and fourth columns are proportional to

$$c\left(\frac{x}{\lambda_D}\right)-c\left(\frac{x}{\lambda_D}+K_D\delta\right). \qquad (18)$$

For our absorber of rhodium $K_D=1.8$ cm^2/g; $\delta=0.36$ g/cm^2 so that $K_D\delta=0.65$. Similar argument holds for group A ($K_A=20$ cm^2/g; $\delta=0.057$ g/cm^2).

In Fig. 6 are plotted the curves (18) for groups A and D, assuming their values equal to 100 for $x=0$; the points represent the experimental values of the ratio of columns two and four, Table IX. The abscissae were calculated assuming $\lambda_D=\lambda_A=1.1$ cm.

Therefore it seems that the neutrons of these two groups have the same mean free path which is a little larger than 1 cm. We have already noted that this method is based on the assumption that the neutrons of these groups traverse only one mean free path. Though this assumption is quite reliable for group A, it is more doubtful for group D (see §12). However, the fact that we have found approximately the same value for λ_D and λ_A can be considered an argument for the validity of this assumption.

8. Mean Free Path of Thermal Neutrons

In the preceding paragraphs, we have found the value of the mean free path of the groups D and A. The value found depends on the assumption that the neutrons of these groups traverse only one mean free path (see §12).

In order to check this assumption, one could measure directly the mean free path of these groups. Up to now, we have not been able to perform such a measurement because of feeble intensity. However, we were able to measure directly the mean free path λ of thermal neutrons in paraffin.

This result, plus the measured value of λ^2N of the preceding paragraph, allows one to calculate the average number N of mean free paths of a thermal neutron. We must remember that the albedo measurements also permit one to calculate the value of N (see §6).

The measurement of the mean free path λ can be made using a source and a detector of thermal neutrons placed at a distance as large as possible with respect to their dimensions, and interposing between them various thicknesses of paraffin, the dimensions of which are just sufficient to screen the detector from the source. In ideal geometric conditions, when the solid angles under which the detector is seen from the source, and the source from the detector, the activity of the detector would be proportional to $e^{-x/\lambda}$ where x is the thickness of the scatterer of paraffin.

In practice, in order not to get too small an intensity, we were very far from these ideal conditions, and therefore it is necessary to correct the results in order to take into account the imperfection of the geometry.

The disposition used was as follows:

Source

A paraffin cylinder of 12 cm diameter and 13 cm in height contained the source of Rn+Be, 2 cm below the center of the upper face. This cylinder was completely covered with the cadmium sheet of 0.5 g/cm^2; in the center of the upper face there was a window of 5×5.5 cm^2 in the cadmium, which could be opened or closed. If we measure the activity of a detector of slow neutrons, placed outside such a paraffin block, once with open window and once with closed window, and we take the difference of the two activities so measured, we will obtain the part of the activity due only to neutrons C coming out through the window. This difference is therefore equivalent to the activity that would be due to a source of only neutrons C having the same position and dimensions as the window. In this sense we will speak in following paragraphs of source of neutrons C, or simply source C.

Detector

In order to be able to have reasonably good geometrical conditions, and sufficient intensity, we have constructed[18] some small cylindrical

[18] E. Amaldi and E. Fermi, Ric. Scient. VII-I, 393 (1936).

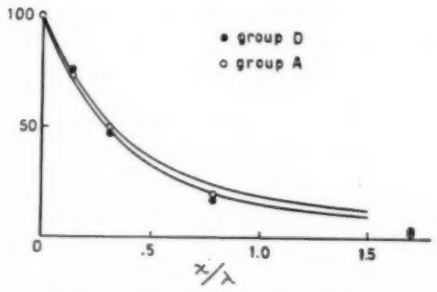

FIG. 6. Ratio of activities (Eq. 18). Dots are the experimental values. $\lambda_A = \lambda_D = 1.1$ cm.

ionization chambers of 3.5 cm inside diameter and 10 cm in length, full of oxygen at a pressure of 75 atmospheres. The element which must be irradiated (Rh 0.125 g/cm²) was placed, as a cylindrical sheet of 5 cm length and 3.5 cm diameter, inside the chamber, and was itself the electrode at high potential. The other electrode, connected to the electrometer, was a metal rod placed on the axis of the chamber. The wall of the chamber was of steel 4 mm in thickness and it practically absorbed none of the slow neutrons which, going through the wall of the chamber, could impinge on the detector.

This arrangement has the advantage, with respect to the methods we used up to now, that due to the high pressure, almost all the energy of the β-rays is spent inside the chamber; besides the electrode has a large useful surface and the geometrical conditions are very good. In fact, with this disposition it is possible to obtain almost the same sensitivity of observation as made with counters, and it has the advantage of the greater stability of the ionization chambers.

The chamber connected to the electrometer was irradiated for 2 minutes, and 15 seconds after having taken away the source we started the reading; i.e., we measured the number of scale divisions covered in 2 minutes.

We have performed two series of measurements: In the first one the distance of the source C from the axis of the ionization chamber was 20 cm; in the second one, 10 cm; in both series the paraffin scatterers were put at half distance between the source C and the detector. In order to avoid random diffusions, the ionization chamber and all the path between the source C and the detector was screened by a cadmium layer of 0.5 g/cm².

In Table X are given in arbitrary units the results of the two series of measures (each value is the average of three readings); the error is about one unit.

In the first column are given the thicknesses of the scatterers of paraffin (density 0.9) in centimeters. In columns two and three are given the measurements of activity at the distance of 20 cm, with the cadmium window of the source opened and closed. The activity due only to the neutrons C coming out from the window is, as we have said above, the difference of the values of these columns. Columns four and five are similar to columns two and three, for the case that the distance between the source and the detector is 10 cm.

In order to deduce from these measurements the value of the mean free path of the thermal neutrons, it is necessary to take into account the corrections due to the imperfections of the geometry, which are especially large in the measurements at 10 cm distance. Calculation of the corrections for thick scatterers are rather unreliable; instead, it is possible to obtain a fairly accurate evaluation of the correction for thin scatterers.

For the distance of 20 cm and a thin scatterer, the correction was calculated as follows: the cross section of the detector was 17.5 cm², and the area of the scatterer was 22.3 cm²; the neutrons that reach the detector are in part those that did not undergo collision in the scatterer, and in part those that had collided once in the scatterer (the case of multiple scattering can be neglected when the thickness x of the scatterer is small).

The first number of neutrons is evidently proportional to the area (17.5 cm²) of the detector, and to the probability $e^{-x/\lambda}$ that a neutron did not collide in the scatterer. For small x, the number of these neutrons is proportional to

$$17.5(1-x/\lambda).$$

The small effect due to the obliquity of the neutrons' path in the scatterer has been neglected.

On the other hand, the number of neutrons that strike the scatterer is proportional to 4

TABLE X. *Measurement of activity for different thicknesses (x) of paraffin with detector at 10 cm and 20 cm from the source.*

x	20 cm		10 cm	
	without Cd	with Cd	without Cd	with Cd
0	45.1	23.6	175	92.5
0.047	40.5	22.1	162	89.5
0.099	36.8	21.7	158	90
0.203	29.9	19.3	140.5	87
0.38	24.8	17.8	127	86
0.68	21.2	16.7	116.5	87

times its area, because its distance from the source is one-half the distance of the detector from the source. This number is hence proportional to

$$4 \cdot 22.3 = 89.2.$$

The fraction x/λ of these neutrons has a collision in the scatterer; assuming that the C neutrons are scattered isotropically by the paraffin hydrogens (see §13 and *F*, §§10 and 11), we find that the fraction of the scattered neutrons that impinge on the detector is equal to the ratio of the area of the detector to the area of a sphere with radius equal to the distance between the scatterer and the detector (10 cm).

The total number of scattered neutrons which hit the detector is hence proportional to

$$89.2 \cdot (x/\lambda) \cdot (17.5/4\pi 10^2).$$

Adding this number to the number of neutrons that hit the detector without being scattered by the scatterer, we obtain the total number of neutrons that impinge on the detector as a function of x. This number is proportional to

$$17.5(1 - 0.929(x/\lambda) + \cdots).$$

Therefore, assuming as 1 the activity for $x=0$, we find that the activity of the detector as a function of the thickness x of the scatterer is given by

$$1 - 0.929(x/\lambda) + \cdots.$$

From this relation we obtain that the tangent of the diffusion curve for $x=0$ cuts the abscissae axis at

$$x_1 = (\lambda/0.929) \text{ cm}.$$

From a graph of the experimental data we have found, by means of the method of the secants, the tangent for $x=0$; this cuts the axis of the abscissae at the point

$$x_1 = 0.29 \text{ cm}.$$

Thus we find

$$\lambda = 0.29 \cdot 0.929 = 0.27 \text{ cm}.$$

We have also verified that all the entire experimental diffusion curve could be brought to coincide, also for thick scatterer, with the calculated curve (calculation, of which we do not give details, is performed by means of the methods explained in *F*, §5).

A little more complicated is the calculation of the corrections for the experiments at 10 cm, because in this case one cannot neglect the obliquity of the neutrons.

The calculation was performed with a numerical procedure from which we have found as expression of the initial shape of the diffusion curve

$$1 - 0.84(x/\lambda) + \cdots.$$

From the experimental curve we have found, as above,

$$x_1 = 0.84 \text{ cm}$$

so that from this measurement we have

$$\lambda = 0.84 \cdot 0.4 = 0.34 \text{ cm}.$$

From these two combined measurements we can obtain, as the more probable value of the mean free path of thermal neutrons (see §13),

$$\lambda = 0.3 \text{ cm}.$$

9. GROUPS AS A FUNCTION OF THE DISTANCE FROM THE SOURCE; ENERGY RATIOS

In a preceding work[19] we have measured the activity of a rhodium detector in a water tank as a function of the distance from the source. The data given there correspond to a mixture of groups C and D, which are both efficient in activation of rhodium. It is evidently interesting to study, as a function of the distance from the source, the behavior of each single group.

The measurements were performed in a cylindrical water tank 95 cm deep and 90 cm in diameter. As detectors, we used:

[19] E. Amaldi, O. D'Agostino, E. Fermi, B. Pontecorvo, F. Rasetti and E. Segrè, Proc. Roy. Soc. **A149**, 522 (1935).

For groups C and D: rhodium (0.36 g/cm²), area 5×5.5 cm²): this detector, screened by 0.5 g/cm² of cadmium, is sensitive only to the D neutrons; instead the difference between the activities measured without and with cadmium gives the activity due only to group C. A detector of silver of 0.057 g/cm² and 5×5 cm² area, screened by cadmium, was used as a detector of groups $A+B$, which were not studied separately. Finally, for the group I we have used a detector of 0.068 g/cm² of PbI_2 screened by cadmium, the area of which was 5×5 cm².

The activities of the detectors were measured on both sides at various distances from the source; the sum of the two activities is proportional to the number of neutrons of the various groups which enter the detector (see §11).

In order to keep as small as possible the errors due to the finite dimensions of the tank, the measurements were performed, maintaining in the center of the water cylinder the mean point between the source and the detector.

The dimensions of our detectors, and also the bulb containing the Rn+Be, are not small enough that one can consider the distance between the centers of the source and the detectors equal to the distance between these two objects, especially for small distances. Therefore we have used average distances. The experimental results for groups C, D, $A+B$, and I are given in Tables XI, XII, XIII, XIV.

The numbers are the sum of the activities measured on both sides of the detectors. The data on groups C, D and $A+B$ are obtained as average values of three series of measurements on each side; for group I, we have made only one series of measurements on each side, since the period of iodine is long enough to get sufficiently accurate results.

In Fig. 7 the activations multiplied by r^2 (r=distance from the source) are plotted against r. The data are taken from Tables XI, XII, XIII, XIV; the units of the ordinates have been chosen so that each curve incloses the same area.

Although the differences among the curves D, $A+B$, and I are small, the accuracy of the measurements is sufficiently high to distinguish among them. By inspecting these curves, one can see that the activity due to the various groups decreases as a function of r according to different laws; the activity decreases more rapidly for groups in the following order: C, D, $A+B$, I. This fact enables us to dispose the groups in order of the increasing energy. We notice that neutrons of lower energy have, as an average, collided more times after they have been emitted, than neutrons of high energy; on the other hand, neutrons that have collided more times will as an average have diffused to a larger distance from the source. It follows that groups for which the intensity decreases more rapidly as a function of r, are those of greatest energy. The order of increasing energy is therefore, for the groups that we have investigated, the following:

$$C,\ D,\ A+B,\ I.$$

These considerations can be made quantitative, as follows: a convenient parameter, in order to characterize the rapidity of the decrement of the various groups as a function of the distance, is the mean value $(r^2)_{av}$ of the distances from the source for the neutrons of the various groups. $(r^2)_{av}$ was calculated for each group by

$$\int_0^\infty f(r)r^2dr \Big/ \int_0^\infty f(r)dr$$

where $f(r)$ is the curve of Fig. 7 referring to the group under consideration. The values of $(r^2)_{av}$ are given in Table XV.

Although the curves of the activities as a function of the distance have been measured very accurately, we were not able to measure the intensity of groups D, $A+B$, and I up to a long distance. In the calculation for $(r^2)_{av}$ we had therefore to extrapolate the intensities of these groups for great distances. These extrapolations are relatively reliable as for great distances the law of decrease becomes quite similar for all the groups so that the end part of the curves of Fig. 7 can be represented satisfactorily by exponential with coefficient 0.106 cm⁻¹.

Nevertheless, a considerable error might be due to this extrapolation.

It can be proved (see F, §2) that for groups of energy larger than the quantum $h\nu$ of the frequence of the elastic bond of hydrogen in paraffin (in practice, for groups of energy larger than 1 volt) the difference $(r'^2)_{av}-(r''^2)_{av}$ in the average square distances of two groups is con-

nected to the ratio W''/W' of the corresponding energies by the equation

$$\log \frac{W''}{W'} = \frac{(r'^2)_{av} - (r''^2)_{av}}{6\lambda_g^2}, \qquad (19)$$

λ_g being the mean free path of the neutrons of the two groups in paraffin. The assumption has been made that λ_g is equal for the two groups (see §7).

The preceding equation can easily be understood qualitatively, but for the numerical factor in the denominator; the left-hand side represents the average number of impacts necessary for the reduction of the energy from W'' to W'. On the other hand, the mean square of the displacement of a neutron in a free path is $2\lambda_g^2$ (the factor 2 is due to having performed mean square and not the square of the mean). If the orientations of successive free paths were incoherent, $(r^2)_{av}$ would then increase by $2\lambda_g^2$ for each impact, and then $\log W''/W'$ impacts would produce an increase by $2\lambda_g^2 \log W''/W'$; this assumption would then give a formula similar to (19) with a factor 2 instead of 6 in denominator. Factor 6 is obtained by taking into account the coherence of successive free paths, and also the fluctuations in the number of impacts necessary for reducing the energy from W'' to W'. We can use (19) in order to determine the energy ratio of two groups (except group C, for which this formula does not hold). This method is, however, very inaccurate, since small errors in λ_g and $(r^2)_{av}$ affect the ratio W''/W' considerably.

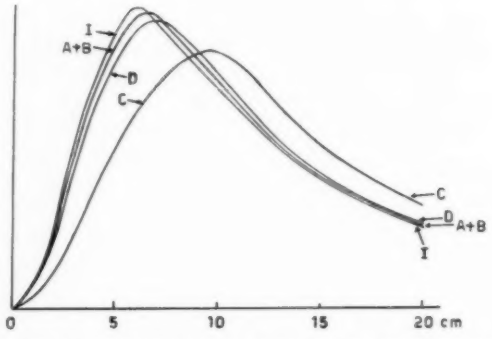

FIG. 7. Ordinates = activation $\times r^2$. Abscissae = r. The units of the ordinates are chosen so that each curve includes the same area.

As we measured $(r^2)_{av}$ in water, and not in paraffin, we shall have to put for λ_g the mean free path in water; we can deduce this from the value in paraffin (1.1 cm, for nonthermal neutrons, see §7) by assuming the mean free path to be inversely proportional to the concentration of hydrogen; we find then $\lambda_g = 1.27$ cm.

Assuming this value, we find from (19) that the difference in $(r^2)_{av}$ corresponding to a ratio e in the energies is $6\lambda_g^2 = 9.7$ cm^2.

From Table XV we obtain the following ratios of the energies for the groups I, $A+B$, and D:

$$W_I : W_{A+B} : W_D = 4.4 : 1.85 : 1.$$

It has been already mentioned that the error in these ratios can be very large.

It is perhaps more appropriate to deduce from (19) the values of the mean free path in water by assuming that the energies of the groups are inversely proportional to the square of their absorption coefficients in boron[20] (see also §13).

Taking the following absorption coefficients in boron

$$K_I = 1; \quad K_B = 2.3; \quad K_A = 3; \quad K_D = 4.7;$$
$$K_c = 38 \text{ cm}^2/\text{g}$$

TABLE XI. *Group C (difference of the activity of Rh detector without and with cadmium).*

r (cm)	2.5	3.6	5.4	7.3	10.2	15.1	20.1	25	30	35	40
Activity	2121	1898	1441	1006	523	167	58	23	9	3.3	1.7

TABLE XII. *Group D (Rh detector screened by cadmium).*

r (cm)	2.5	3.6	5.4	7.3	10.2	15.1	20.1
Activity	306	252	166	96	40	10.6	3.8

TABLE XIII. *Groups A+B (Ag detector screened by cadmium).*

r (cm)	2.5	3.6	5.4	7.3	10.2	15.1
Activity	144	119	73	39.6	15.7	4.3

TABLE XIV. *Group I (PbI_2 detector screened by cadmium).*

r (cm)	2.62	3.36	5.1	7.0	9.9
Activity	24.9	19.7	12.0	6.28	2.46

[20] O. R. Frisch and G. Placzek, Nature **137**, 357 (1936); D. F. Weekes, M. S. Livingston and H. A. Bethe, Phys. Rev. **49**, 471 (1936).

we obtain the following energy ratios:

$$W_I : W_B : W_A : W_D : W_c = 1440 : 270 : 160 : 65 : 1.$$

Assuming[21] $W_c = kT = 0.025$ volts we obtain

$$W_I = 36; \quad W_B = 7; \quad W_A = 4; \quad W_D = 1.6 \text{ volts}.$$

From these values and (19), we find the mean free path in water

$$\lambda_0 = 0.87 \text{ cm}$$

instead of 1.27 cm. The difference is within the limits of the experimental error.

We notice further that $(r^2)_{av}$ for the C group given in Table XV is considerably different from the values of $(r^2)_{av}$ for the other groups. For instance,

$$(r_C^2)_{av} - (r_D^2)_{av} = 50 \text{ cm}^2.$$

This difference is partly due to the large number of free paths of the neutrons when their energy is already reduced to the thermal energy; the amount due to this process of diffusion is (see §7)

$$2\lambda^2 N = 26 \text{ cm}^2.$$

The remaining 24 cm² correspond to the slowing down of the neutrons from the energy corresponding to the D group to the energy of thermal agitation. This process cannot be easily calculated, because it is complicated by the effect due to the chemical bond of hydrogen (see F, §19).

10. Passage of the Neutrons from One Group to Another

In the preceding section, we arranged the groups in order of decreasing energy. It is now obvious that a neutron of a group of high energy, after some impacts, will have a smaller energy, and may thus go over into a group of less energy.

Table XV. *Mean values of* r^2.

Group	$(r^2)_{av}$ (in cm²)
C	326.7
D	276.6
$A+B$	270.6
I	262.2

[21] H. H. Goldsmith and F. Rasetti, Phys. Rev. **50**, 328 (1936) show that it is more correct to use kT instead of $3kT/2$ as thermal energy in this calculation.

We must, to be more precise, expect that the neutrons of all the groups, after a certain number of impacts, become thermal neutrons.

We tried, therefore, to observe the transformation of D neutrons into C neutrons.[22]

The principle on which these experiments are based can be clearly understood if we assume that we have a detector R that can be activated only by C neutrons and an absorber A for the D neutrons only. We put the detector R on the center of the upper face of a paraffin cylinder, containing the source S; if the absorber is inserted between the upper face of the paraffin and the detector, no reduction of the activity of the detector will occur, since the C neutrons that came out of the paraffin are not absorbed by A. If we put the absorber A inside the paraffin, 1 or 2 cm below the upper face, it can happen that the absorber captures some of the D neutrons which could be transformed into C neutrons by impacts in the paraffin before reaching the detector.

If D neutrons can be really transformed into C neutrons, we must expect that the absorber A produces no effect when put between the paraffin and detector, but that it reduces the activity of A when put 1 or 2 cm inside the paraffin.

The experiment cannot be performed in this ideal way, because we have no detector of group C only, and no absorber of group D only. We have, therefore, used as detector a rhodium plate, 0.36 g/cm² thick; about 70 percent of its activity is due to the C group and the rest to the D group. In order to measure only the activity due to the C group, all measurements were performed without and with a cadmium absorber 0.54 g/cm² thick, that was put immediately below the rhodium plate. The difference in activities without and with cadmium gives the activity due to the C group only.

As absorber for the D group, we used an indium plate 1.83 g/28.5 cm²; the absorption coefficient of indium for the D group is 3.4 cm²/g, and for the C group 0.7 cm²/g. It follows that the absorption of C neutrons in our indium plate is far from negligible, the more so if we keep in mind the high numerosity and albedo of this group. In order to correct for this, we prepared a plate of Sn−Cd alloy that was

[22] E. Amaldi, E. Fermi, Ric. Scient. **VII-I**, 56 (1936).

equivalent to the indium plate as absorber for the C group, and practically did not absorb the D neutrons. Taking the difference of the activities produced by group C in the detector with the indium plate or the cadmium plate, we obtain the effect due only to the absorption of the D group by indium.

In Table XVI are collected the activities induced in the rhodium plate with different setups; the different arrangements are denoted by a notation similar to that used in §6; the number added in parentheses after the symbol P of paraffin, gives in centimeters the thickness of paraffin layers; since we used two different cadmium sheets, one of 0.54 g/cm² thickness for complete absorption of group C, and the other 0.0036 g/cm² thickness equivalent to the indium sheet as absorber in the C group, we denoted these two absorbers, respectively, with Cd and cd. The figures given in the table are averages of ten readings.

The first five measurements are performed in order to control the identity of the thin cadmium (Cd) and the indium (In) as absorbers of the C neutrons. Their result is that the absorption of the indium plate is probably slightly larger than the absorption of the cadmium sheet; the difference $280.4-68.7-(230.2-45.6)=27.1 \pm 1.2$ represents the activity of the rhodium detector due to group C that is absorbed by the indium plate; the difference $280.4-245.8=25.6 \pm 1$ is the analogous absorption of the thin cadmium sheet.

The next four measurements are performed with the absorber (Cd or In) 1 cm inside the paraffin. The difference $253.0-71.1=181.9\pm0.9$ is the activity of the detector due to the group C with the absorber Cd 1 cm inside the paraffin. The difference $241.5-64.9=176.6\pm0.9$ is the similar activity with the indium absorber. The difference between these two activities is 5.3 ± 1.2 and is considerably larger than the difference that we might expect from the small difference between the two absorbers when placed close to the detector.

The next four measurements are analogous to these last, with the only difference that the absorbers are 2 cm below the paraffin surface. Also in this set of measurements there is a difference analogous to that observed in the preceding set; this difference is now 4.0 ± 1.2.

TABLE XVI. *Activities induced in Rh plate under different arrangements.* S=source, P=paraffin (cm thick), R=detector.

$S\ P(3.5)\ R$	280.4 ± 0.7
$S\ P(3.5)$ In R	230.2 ± 0.7
$S\ P(3.5)$ In Cd R	45.6 ± 0.4
$S\ P(3.5)$ Cd R	68.7 ± 0.5
$S\ P(3.5)$ cd R	254.8 ± 0.7
$S\ P(2.5)$ cd $P(1)\ R$	253.0 ± 0.7
$S\ P(2.5)$ In $P(1)\ R$	241.5 ± 0.7
$S\ P(2.5)$ cd $P(1)$ Cd R	71.1 ± 0.5
$S\ P(2.5)$ In $P(1)$ Cd R	64.9 ± 0.5
$S\ P(1.5)$ cd $P(2)\ R$	254.0 ± 0.7
$S\ P(1.5)$ In $P(2)\ R$	248.9 ± 0.7
$S\ P(1.5)$ cd $P(2)$ Cd R	69.2 ± 0.5
$S\ P(1.5)$ In $P(2)$ Cd R	68.1 ± 0.5

By discussing together all these data, one might conclude that the observed effect has a sign corresponding to a transformation of D neutrons into C neutrons, and is 2.3 times larger than the quadratic error.

Although we have a serious presumption of a real effect in this sense, we cannot deduce from this experiment a final conclusion.

An evaluation of the effect that one must expect in this experiment shows that it is really of the order of magnitude of the observed effect; the evaluation was made as follows:

We have measured the induced activities in the indium sheet of the above experiment, placed inside the paraffin 2 cm below the upper face, separately in group C and D, and we have found, respectively, 257 and 47.5. These numbers are proportional to the numbers of neutrons of the two groups absorbed by our indium sheet.

Let p_1 be the probability that a neutron C which is in paraffin in the place of the indium absorber comes out from the upper face and is captured by the rhodium detector; similarly, let p_2 be the probability that a neutron D which is in the place of the indium sheet, comes out from the upper face transformed into a C neutron, and is captured by the rhodium.

The decrements of the activities of the rhodium sheet in group C, due, respectively, to the absorption by indium sheet of neutrons D and C are in the ratio $47.5\ p_2/257\ p_1$. Assuming p_1 and p_2 equal or at least of the same order of magnitude, we find that these decrements are about in the

ratio 47.5/257, and, since the decrement due to the absorption of C neutrons is 26.9 (see Table XVI), the effect which we must expect in the preceding experiment is equal to 5, and therefore of the same order of magnitude as the really observed effect.

Similar experiments were performed by Preiswerk and von Halban,[23] who found a genetic relation between groups I and A.

11. Behavior of the groups in the Neighborhood of the Surface of the Paraffin

In §9, we have studied the activity due to the various groups inside a water tank so large that we could neglect the disturbances due to the limitations of size. We will now study the behavior of the activity due to different groups close to the surface of the paraffin.

First, we shall consider the behavior of group C. From the theory of diffusion of thermal neutrons, it follows that, independently of the position of the source, the density of thermal neutrons close to the surface of the paraffin decreases toward the outside (see F, §6, formula 57); one can furthermore show that if we indicate with x the depth below the surface of the paraffin, the density $n(x)$ is, for small x, approximately proportional to

$$x+\lambda/\sqrt{(3)},$$

so that if we extrapolate the curve of $n(x)$ towards the outside of the paraffin ($x<0$), $n(x)$ is zero at a distance from the surface of the paraffin equal to

$$x_0=-\lambda/\sqrt{3}.$$

This is just the behavior of the density of thermal neutrons close to the surface which determines the law of angular distribution (5) of the outcoming C neutrons. If the density would be constant close to the surface of the paraffin, one would find the cosine law.

In order to measure $n(x)$, it is necessary to use a detector of group C thin enough not to disturb the neutrons' distribution. Its activity will then be proportional to the density $n(x)$ of thermal neutrons.

We have used two detectors which were obtained by electrolytic deposit of rhodium on a nickel plate (which served only as an inactive carrier) of 29 cm² area; the weights of rhodium deposited on the two detectors were respectively 0.087 and 0.169 g. Taking into account the absorption coefficient of rhodium for the C group (0.7 cm²/g) $K\delta$ for these two detectors is equal, respectively, to 0.002 and 0.004; to these values there corresponds a mean probability ζ for the capture of a thermal neutron which traverses the detector, of about 0.004 and 0.008, respectively (see §6). These probabilities are very small, and therefore the detectors used can be considered as thin.

The measurements have been performed using a paraffin cylinder 24 cm in diameter and 10 cm in height, containing the source 3.2 cm below the center of the upper face. The layer of paraffin of 3.2 cm thickness between the source and the upper surface was cut into sheets in order to be able to put the detector at various depths.

In order to find the activity due to the group C only, we have always made the difference between the activities of the detectors without and with two cadmium screens 0.44 g/cm² thick, between which could be placed the detectors.

In Fig. 8 the activity due only to the C group of our two detectors is plotted against the depth x. We give also the curve extrapolated towards negative values of x. The intersection, with the axis of the abscisse is close to the point

$$x_0=-0.18 \text{ cm}.$$

From this value we find

$$\lambda=0.31 \text{ cm}$$

in good agreement with the values obtained from the direct measurements (see §8).

We have already noticed that this experiment has a very simple interpretation, provided the detector is very thin. Instead, a thick detector disturbs strongly the density of thermal neutrons, so that the curve of the activity as a function of x is very different.

Thus, using a rhodium detector 0.36 g/cm² thick, and adding the activities due to C group measured on both sides, in order to get data comparable to that of the preceding experiment, we have found that the curve of the activity,

[23] Preiswerk and von Halban, Comptes rendus **202**, 840 (1936).

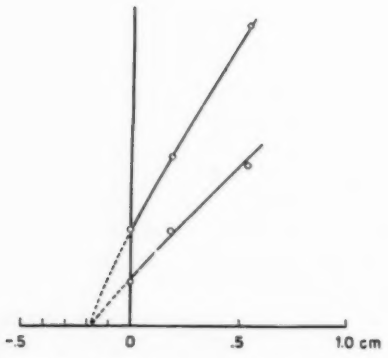

FIG. 8. Activity of C group plotted against the depth (x) in paraffin.

extrapolated toward negative values of x, cuts the x axis at

$$x_0 = -0.4 \text{ cm},$$

i.e., at a distance more than double than in the case of thin detectors.

In this experiment, we have added the activities measured on both sides of the detector, since this sum is proportional to the total number of thermal neutrons which entered the detector. Let N_1 and N_2 be the numbers of neutrons which enter the detector, respectively, through the face 1 and face 2; the activities measured on the faces 1 and 2 are, respectively, given by

$$\begin{aligned} A_1 &= N_1 a + N_2 b, \\ A_2 &= N_1 b + N_2 a, \end{aligned} \qquad (20)$$

where a and b are constants characteristic of the detector, which depend on its absorption coefficients for neutrons and electrons, and on its thickness. The ratio a/b can be obtained by measuring the ratio A_1/A_2 when the detector is placed outside the paraffin so that $N_2 = 0$.

For the rhodium detector, 0.36 g/cm² thick, $a/b = 4/3$ in the C group, and 2/1 in the D group. This difference depends on the larger absorption coefficient for D neutrons. For a thin detector, one would have $a = b$.

Summing up the two equations in (20), we find

$$A_1 + A_2 = (a+b)(N_1 + N_2),$$

and therefore the sum of the activities measured on both sides of a detector is always proportional to the total number $N_1 + N_2$ of neutrons which traverse the detector.

By (20) we find

$$N_1 = \frac{aA_1 - bA_2}{a^2 - b^2}; \quad N_2 = \frac{aA_2 - bA_1}{a^2 - b^2}. \qquad (21)$$

Therefore, measuring A_1 and A_2, and the ratio a/b, we can find values proportional to N_1 and N_2 (this method was used in §7 in order to measure separately N_1 and N_2). In Table XVII are given the values of N_1 and N_2 measured with our rhodium detector, 0.36 g/cm² thick for groups C and D separately. In order to be able to compare these two sets of data, we have taken as 1 in both groups the value of N_1 for $x = 0$. The source in these experiments was at $x = 2.4$ cm. The data on group C do not permit simple interpretation, since the detector cannot be considered as thin.

Instead, in group D the detector, although thick, does not disturb the distribution of the D neutrons, since the neutrons of this group traverse on the average only one mean free path (see §§6, 7, 12), and therefore each of them hits only once against the detector.

By extrapolation of the shape of the curve $N_1 + N_2$ for D group towards negative values of x, we find the intersection with the x axis at

$$x_0 = -0.9.$$

The fact that these intersections occur much farther from the surface of the paraffin than for group C ($x_0 = -0.18$ cm with thin detector), is due on one hand to the greater mean free paths (see §7), and on the other hand to the coherence of the orientation of successive free paths, which is very large for neutrons of energy larger than the quantum of the elastic bond of hydrogen in paraffin.

By comparing columns two and four, Table XVII, we notice that the shape of the curve N_1

TABLE XVII. *Number of neutrons that enter faces (1) and (2) of detectors.* x = thickness of paraffin.

	Group C		Group D	
x	N_1	N_2	N_1	N_2
0	1	0	1	0
0.16	1.10	0.28	1.07	0.07
0.34	1.15	0.63	1.17	0.14
0.53	1.28	0.91	1.25	0.28
0.87	1.60	1.19	1.31	0.45
1.87	2.19	2.00	1.35	1.00

close to the surface, for our detector, is not very different in groups C and D, instead, at greater depth the C group increases much more rapidly than group D. One can justify this behavior by taking into account the increase of the albedo of the layer of paraffin, superimposed on the detector, as a function of its thickness.

12. Width of the Energy Bands Corresponding to the Groups. Total Number of Neutrons

We shall discuss in this section a method for determining the width of the bands[24] of energy which correspond to the various groups; more precisely, the ratio W_{max}/W_{min} of the maximum to the minimum energy which limits a band. In the calculation the bands were assumed to be sharply defined. It would be possible to perform a similar calculation, assuming for the band a resonance form; however, this seems scarcely worth while, owing to the small accuracy of the experimental data.

In the last part of this section we will give an evaluation of the total number of neutrons emitted by the source of Rn+Be.

The method for determining the width of the band which corresponds to a group g of energy larger than 1 volt, is based on the comparison of the two following values: the activability A_g of a detector due to the neutrons of the considered group g, and the activability B_c of the same detector due to the thermal neutrons and obtained by screening the detector on one side with a cadmium sheet thick enough to absorb completely the thermal neutrons hitting on it. B_c can naturally be obtained as the difference of the activabilities of our detector with a cadmium sheet on one face only or on both sides.

If the distribution of the fast neutrons inside a large block of paraffin were uniform, it is clear that A_g and B_c would have values independent of the position and orientation of the detector. However, the source of fast neutrons is small and therefore we must compare the mean values of A_g and B_c averaged for all positions and orientations inside the paraffin; i.e., we must compare

$$\int \bar{A}_g d\tau; \quad \int \bar{B}_c d\tau,$$

where the integrands $\bar{A}_g$ and $\bar{B}_c$ are the mean values of the activabilities of the detector measured with the two opposite orientations; these mean values are practically identical with the average taken over all directions. By using the said integrals we eliminate all the complication arising from the nonuniform distribution of the neutrons.

We suppose now that in the paraffin around our detector, q fast neutrons are produced per cubic centimeter and per second. These neutrons are slowed down in such a way that we shall have in the neighborhood of our detector neutrons of all velocities.

It can be shown (see F, §1) that for energies larger than 1 volt, the number of neutrons having velocity between v and $v+dv$ is

$$(2q\lambda(v)/v^2)dv. \tag{22}$$

From this we can easily calculate the activity A_g as a function of the energy W_{min} and W_{max} limiting the energy band g, of the mean free path λ_g and the absorption coefficient K_g of the detector for the group g and of the surface s and thickness δ of the detector. We find (see F, §8)

$$A_g = \eta s q \lambda_g K_g \log \frac{W_{max}}{W_{min}}$$

$$\times \int_0^\delta b(K_g x) e^{-\mu x} dx + \int_0^\delta b(K_g x) e^{-\mu(\delta - x)} dx \Big/ 2, \tag{23}$$

where μ is the absorption coefficient of the β-rays of the detector in the detector itself and $b(K_g x)$ is the function (4); η is the efficiency of the ionization chamber for the β rays of the detector. The last factor in (23) represents the effect of the absorption of the neutrons and of the β-rays in the detector. This factor would be equal to δ for a very thin detector.

Also the activity B_c due to the thermal neutrons can be calculated in terms of the diffusion length $(D\tau)^{\frac{1}{2}} = (\lambda^2 N/3)^{\frac{1}{2}}$ (see §7), of the ab-

[24] E. Amaldi and E. Fermi, Ric. Scient. VII-I, 310 (1936).

sorption coefficient K_c of the detector; taking into account the angular distribution (5) of the neutrons impinging on the detector, we find

$$B_c=\eta sq\lambda(\mathrm{N})^{\frac{1}{2}}K_c\int_0^\delta c(K_cx)e^{-\mu x}dx, \qquad (24)$$

where $c(K_cx)$ is the function (6). We have disregarded the variation of the absorption coefficient of our detector for thermal neutrons of different velocities. For a very thin detector, the integral is equal to δ.

We must now integrate (23) and (24), as already mentioned, and we obtain

$$\int A_g d\tau=\eta sQK_g\lambda_g\log\frac{W_{\max}}{W_{\min}}$$
$$\times\int_0^\delta b(K_gx)e^{-\mu x}dx+\int_0^\delta b(K_gx)e^{-\mu(\delta-x)}dx\Big/2, \qquad (25)$$
$$\int B_c d\tau=\eta sQK_c\lambda(\mathrm{N})^{\frac{1}{2}}\int_0^\delta c(K_cx)e^{-\mu x}dx,$$

where $Q=\int qd\tau$ is the total number of neutrons emitted by the source per second. From (25) we obtain

$$\log\frac{W_{\max}}{W_{\min}}=\frac{K_c}{K_g}\frac{\lambda(\mathrm{N})^{\frac{1}{2}}}{\lambda_g}\frac{\int A_g d\tau}{\int B_c d\tau}$$
$$\times\frac{2\int_0^\delta c(K_cx)e^{-\mu x}dx}{\int_0^\delta b(K_gx)e^{-\mu x}dx+\int_0^\delta b(K_gx)e^{-\mu(\delta-x)}dx}. \qquad (26)$$

We performed the experiments on the groups D, A, and I. For D group we used a rhodium detector (0.36 g/cm²); for the group A a silver detector (0.057 g/cm²); and for group I a lead iodide detector (0.76 g/cm²); since the small absorption coefficient of iodine in the C group is not too well known, we used the rhodium data also in the calculation of B_c for the I group, assuming equal efficiency of the chamber for β-rays of rhodium and iodine. In order to calculate the integrals

$$\int \bar{A}_g d\tau, \quad \int \bar{B}_c d\tau$$

we determined $\bar{A}_g$ and $\bar{B}_c$ for a fixed distance, and deduced the values for all the distances by using the curves of Fig. 7.

In the following equations, the numerical values are written in the same order in which the various magnitudes appear in formula (26)

Group D
$$\log\frac{W_{\max}}{W_{\min}}=\frac{0.7}{1.8}\frac{\sqrt{(13)}}{1.1}\frac{4.58\cdot10^5}{1.5\cdot10^6}\frac{2\cdot0.108}{0.087+0.052}=0.60,$$

Group A
$$\log\frac{W_{\max}}{W_{\min}}=\frac{0.25}{20}\frac{\sqrt{(13)}}{1.1}\frac{7.8\cdot10^4}{2.04\cdot10^5}\frac{2\cdot0.048}{0.021+0.019}=0.038,$$

Group I
$$\log\frac{W_{\max}}{W_{\min}}=\frac{0.7}{0.38}\frac{\sqrt{(13)}}{1.1}\frac{4.16\cdot10^4}{1.5\cdot10^6}\frac{2\cdot0.108}{0.085+0.049}=0.27.$$

From these values we may derive the ratios $W_{\max}/W_{\min}$ for each group; we shall call the magnitude $\log W_{\max}/W_{\min}$ logarithmic width; this magnitude has a simple physical meaning because it represents the average number of impacts of a neutron while it belongs to a given group. For example, group A that has a logarithmic width 0.04 is such a narrow energy band that only 4 percent of the neutrons pass through it during the process of slowing down. In the case of group A, the detector used cannot be considered as thin with respect to the absorption of the neutrons; if one would take into account the resonance form of the band, one would find, by a simple numerical evaluation, that the logarithmic width of group A as calculated from (26) is too large by a factor of about 2. For the other detectors, this correction is much smaller.

The logarithmic width of group I, and even more of group D, is considerably larger, as shown

also by the larger numerosity (see §5) of these groups. Even for group D, the probability that a neutron belongs to the group for more than one free path is relatively small and amounts to 0.27. These facts explain our results that the albedo of all nonthermal groups is practically zero.

Instead, one might expect a small difference in the behavior of groups D and A with respect to the diffusion experiments described in §7. The fact that we failed to find any such difference might, however, be explained by inaccuracy of our measurements, as the expected difference is fairly small.

If we assume that the energy of the groups are those deduced in §9 by the boron method, we obtain for the width of group D, A and I:

$$1; \qquad 0.15; \qquad 10 \text{ volts}.$$

Finally, we can use the second of (25) in order to calculate the total number Q of the neutrons emitted from the source. In (25), B_c is the initial activity of the detector used. In order to get the activability (3), it is necessary to multiply B_c given in (25) by the factor

$$1000/I \cdot U = 1000/I \cdot 840\eta_U.$$

So that we find

$$\frac{Q}{I} = 0.84 \frac{\eta_U}{\eta} \frac{\int B_c d\tau}{s\lambda(\mathrm{N})^{\frac{1}{2}} K_c \int_0^\delta c(K,x) e^{-\mu x} dx}. \qquad (27)$$

In this formula, the same elements enter which we have used in the calculation of the logarithmic width. Using, for instance, the data on the activation of the rhodium, we find

$$Q/I = 160{,}000(\eta_U/\eta).$$

Assuming $\eta = \eta_U$ we have that one of our neutronic units corresponds to 160,000 neutrons per second, and taking into account that 1 neutronic unit corresponds to about 6 mc of Rh+Be we have finally

27,000 neutrons per sec. and per mc.

This value is considerably larger than the values found with different methods;[25] this fact can be only partially accounted for by a difference between η and η_U.

13. Summary and Discussion

From the results we have explained, it seems that one must conclude that in elements which are sensitive to slow neutrons, the capture cross section is often an irregular function of the energy of slow neutrons, with sharp maxima representing some sort of absorption bands.

The analysis of the absorption curve of the various elements with several detectors enables us to identify several absorption bands (groups A, B, C, D, I).

There are several reasons for believing that group C (radiation strongly absorbed by cadmium) corresponds, at least for its largest part, to neutrons having a velocity of thermal agitation, while the other groups correspond to larger velocities.

The most direct proof of this statement is the experiment with a velocity selector of cadmium[26] (so as to observe just group C) that enabled a direct measurement of the velocity of the C neutrons that was found equal to the thermal velocity.

The same result can be derived from the experiments by Preiswerk and von Halban and others,[27] who found that the radiation filtered by cadmium is not sensitive to temperature variations; this shows that the neutrons not belonging to group C have energy larger than thermal agitation energy.

Finally, our albedo measurements (see §6) show that only the C neutrons can traverse many free paths while belonging to this group. This fact can be easily understood on the assumption that the C group consists of neutrons in thermal equilibrium, since then successive impacts do not alter the average energy; instead, a neutron belonging to an energy band $\gg kT$, has a high

[25] Cf., e.g., R. Jaeckel, Zeits. f. Physik **91**, 493 (1934); F. A. Paneth and H. Loleit, Nature **136**, 950 (1935).

[26] J. R. Dunning, G. B. Pegram, G. A. Fink, D. P. Mitchell and E. Segrè, Phys. Rev. **48**, 704 (1935); Lincei Rend. **23**, 340 (1936).

[27] P. Preiswerk and H. von Halban, Nature **136**, 1027 (1935); F. Rasetti and G. Fink, Phys. Rev. **49**, 642 (1936).

probability of getting out of the band after one impact.

In all the cases investigated by us, a large percentage of the activity (in most cases larger than 50 percent) is due to thermal neutrons; this does not mean, however, that the absorption coefficient for thermal neutrons is, as a rule, larger than the absorption coefficient for neutrons having an energy of some volts. This fact can be explained to some extent by the large number of thermal neutrons that get out of a paraffin block containing the source (see Table VI).

The problem of determining the energy bands corresponding to the known thermal groups can be attacked by the following method, first used by Frisch and Plazcek and by Weekes, Livingston and Bethe. They assumed that the capture cross section of a slow neutron in boron is inversely proportional to the velocity v of the neutron. Assuming this, we obtained from our measurements the following energies:

Group	C	D	A	B	I
Volts	0.037	1.6	4	7	36.

The error in this type of measurements can be, however, fairly large.

A quite independent determination of the energy order of the groups, and also an estimate of the energy ratio (this last only for nonthermal groups) was given by us in §9 by considerations based on the behavior of the intensity of the various groups as a function of the distance from the source. The energy order found by us coincides with the one deduced from the boron absorption, and the values of the energy ratios found by us, although smaller than the ratios obtained by the boron method, are not inconsistent because of the fairly large error involved in these determinations.

Our method, although very inaccurate, has the advantage of being very direct.

We were also able to derive, by analogous methods, the width of the energy bands (more exactly, the relative width $\Delta W/W$) for the nonthermal groups; we found that the narrowest band is group A (radiation strongly absorbed by silver), for which $\Delta W/W = 0.04$. The other groups (see §12) are somewhat wider; nevertheless, the probability that a neutron remains in the same group after one free path is fairly low.

Connected to the width of the absorption bands, is the numerosity of the various groups, which corresponds essentially to the number of neutrons coming out per second from the surface of a paraffin block containing the source (see §5). The most numerous group of all is the thermal one (numerosity 40), while the least numerous is group A) (numerosity 0.5), which, as we have seen, is the narrowest.

These facts are qualitatively in agreement with the consideration of Bohr and Breit and Wigner.

Some further information on the properties of these absorption bands can be obtained by comparing the behavior of two periods of the same element, both sensitive to slow neutrons. We were able to investigate in this respect only silver, rhodium, indium and bromine. Only in the case of silver we found a different behavior for the two periods of this element. In all the other cases, no difference was found within the limits of our accuracy. It may be noticed that rhodium, indium and bromine are the three cases for which the number of observed periods produced by slow neutrons is larger than the number of known isotopes.

Sections 6 to 11 are devoted to a study of the diffusion properties of slow neutrons in hydrogenated substances. The diffusion process can be analyzed in two successive phases. First (slowing-down phase), the neutron loses energy by means of successive impacts until it reaches the energy of thermal agitation; afterwards (diffusion phase), the energy does not decrease further on the average and the neutron is scattered until it is captured by the protons or other nuclei.

During the phase of slowing down, the mean free path decreases very soon to a value of the order 1 cm, afterwards it remains approximately constant until the energy of the neutron is comparable with the quantum $h\nu$ of the frequencies of the elastic bond of the hydrogen atom in paraffin.

We can say that all the studied groups except the thermal one, belong to the interval of energy where the mean free path λ_s in paraffin is about 1 cm.

From the theory of the impact of slow neutrons and hydrogen atoms, taking into account the chemical bond of these last (see *F*, §§10 and 11), one finds that when the energy of the slow neu-

trons passes from values larger than $h\nu$ to values smaller, the mean free path decreases and tends to a limit equal to $\lambda_g/4$. This variation of the mean free path is connected also to a different angular distribution of the neutrons after an impact; when $W \gg h\nu$ the angle between the directions of the motion of the neutrons before and after the impact is always sharp, while for $W \ll h\nu$ the angular distribution after an impact tends to become isotropic.

In agreement with this theoretical result, one observes a really remarkable decrease of the mean free path in going from the nonthermal to the thermal group.

For this last, one can take $W/h\nu$ equal to about 1/10; although this value is pretty small, one cannot consider the thermal neutrons as neutrons of energy practically zero. Thus one finds (see *F*, formula 102) that for $W/h\nu = 1/10$ the mean free path is

$$\lambda = \lambda_g/3.3 \qquad (28)$$

while at the limit for $W=0$, one would have $\lambda = \lambda_g/4$.

We can also evaluate how much the coherence is conserved between the directions of the motion of a thermal neutron before and after an impact. As a quantititative expression of the coherence, we can take $(\cos\theta)_{av}$, i.e., the mean value of the cosine of the diffusion angle of the neutrons after an impact; $(\cos\theta)_{av}=1$ means complete coherence, while for an isotropic diffusion, $(\cos\theta)_{av}=0$. For the neutrons of energy larger than 1 volt, we find $(\cos\theta)_{av}=2/3=0.67$; for the thermal neutrons, assuming $W/h\nu=1/10$, we deduce (see *F*, formula 103) $(\cos\theta)_{av}=0.067$, i.e., one-tenth of the preceding value.

These results justify the approximations that were made sometimes in this work, in considering the diffusion of thermal neutrons as isotropic. We must, however, notice that in such a way we have introduced a small error which is in the sense that the diffusion length, given by (12), is too small, while the albedo, given by (11), is too large. It would also be possible to calculate these corrections, if one knew the value of $(\cos\theta)_{av}$; this value is, however, subordinate to the knowledge of $W/h\nu$ of which we can give only the order of magnitude.

In §§6–11 five different magnitudes have been measured, which can be expressed by means of only two, using the relations obtained from the theory of the diffusion of the neutrons (see *F*).

These five magnitudes are: the mean free paths λ and λ_g of thermal neutrons (see §8) and of neutrons of groups *D* and *A* (see §7); the albedo β of thermal neutrons (see §6); the diffusion length l of thermal neutrons (see §7); and the length $|x_0|$ relative to the thermal neutrons, considered in Section 11, which is bound to λ by the relation

$$|x_0| = \lambda/\sqrt{(3)}.$$

By means of (28), (11), (12), and (29), the five above-mentioned magnitudes can be expressed as functions of λ and N (number of mean free paths traversed on the average by thermal neutrons).

In Table XVIII we compare the measured values of these five magnitudes with the values calculated by means of the above-mentioned formulae, assuming

$$\lambda = 1.0 \text{ cm}; \quad N = 140.$$

As we see, the agreement is good.

From these values of λ and N, we find the following values for thermal neutrons in paraffin:

elastic cross section with hydrogen	$\sigma_e = 43 \cdot 10^{-24}$ cm^2
capture cross section	$\sigma_c = 0.31 \cdot 10^{-24}$ cm^2
mean life	$\tau = 1.7 \cdot 10^{-4}$ sec.

This last value is in very good agreement with the measure of τ performed with a mechanical set-up[28] and with the theoretical value deduced from the theory given in *F*, §12, based on the assumption that the capture of slow neutrons by protons is due to the emission of a γ-quantum by magnetic dipole radiation.[29] It is shown there that ac-

TABLE XVIII. *Comparison of measured and calculated values.* λ and λ_g = mean free paths of thermal neutrons and of group *D* and *A*, respectively. β = albedo for thermal neutrons, l = diffusion length, $(x_0) = \lambda/\sqrt{(3)}$.

λ	0.3	0.30
λ_g	1.1	1.0
β	0.82	0.83
l	2.1	2.05
$\lvert x_0\rvert$	0.18	0.174

[28] E. Amaldi, O. D'Agostino, E. Fermi, B. Pontecorvo and E. Segrè, Ric. Scient. **VI-I**, 581 (1935).

[29] A preliminary account of this theory has been given by E. Fermi, Phys. Rev. **48**, 570 (1935).

cording to whether the ^1S state of the deuteron ($\pm 120{,}000$ volts) is assumed to be real or virtual the theoretical value of τ is 6.5×10^{-4} or 2.6×10^{-4}. The satisfactory agreement of this last value with the experimental result, seems to indicate that the ^1S state is virtual.

We express our warmest gratitude to the Istituto di Sanita-Pubblica of Rome and in particular to Professor G. C. Trabacchi for having supplied us with the radon sources used in this research. Our thanks are also due to the Consiglio Nazionale delle Ricerche of Italy for a grant.

NOVEMBER 15, 1936 PHYSICAL REVIEW VOLUME 50

Characteristics of the Compton Modified Band

PAUL KIRKPATRICK, P. A. ROSS AND H. O. RITLAND, *Department of Physics, Stanford University, California*

(Received August 31, 1936)

The shapes of Compton modified bands have been calculated for all scattering elements from hydrogen to argon. These shapes vary periodically with atomic number, atoms with one-valence electron being characterized by sharp, narrow lines while atoms with completed electron shells produce broadly rounded bands. Experimental results, though incomplete, confirm these variations except as to absolute breadth. Breadths of observed modified bands exceed calculated breadths on the average by 75 percent for carbon scatterers and 140 percent for beryllium. Variation of scattering angle has only a second-order effect upon the observational breadth of wide modified bands. To an accuracy of about 10 percent the intensity ratio of modified to unmodified radiation from carbon (graphite) scatterers is found to agree with predictions based upon the Wentzel-Waller theory of scattering by bound electrons for wave-lengths in the range 435 X.U. to 710 X.U. and scattering angles between 27 and 139°. Though previous measurements showed the magnitude of the wave-length shift of the maximum in the modified band to be less than that given by the Compton equation it is now argued that present theory predicts a still smaller shift.

Energy Distribution in the Modified Band

JAUNCEY'S[1] suggestion that the distribution of energy with wave-length in Compton modified radiation is a direct result of the distribution of momenta among the electrons of the scatterer has been confirmed and greatly extended by others.[2–4] This hypothesis has been used for the theoretical prediction of the shapes of shifted bands (or lines) upon bases of atomic theory, and while Jauncey's specific predictions are not now acceptable, being derived from Bohr orbits, DuMond[2, 4] has shown that line shapes may be deduced from any given electron momentum distribution, and has illustrated the method by theoretical shapes pertaining to scattering by carbon and beryllium atoms with electron momenta distributed as required by modern atom models.

Bloch[5] gave special attention to the modified radiations scattered by carbon and by beryllium and developed formulae for the calculation of the intensity distributions upon the basis of Wentzel's[6] theory of the Compton scattering by bound electrons. Hydrogen scattering has recently been treated by Schnaidt[7] and neon by Burkhardt,[8] intensity (or energy) distributions being obtained in both cases. The interest of the present writers has been not only in the form of the distribution for a specific element but also in the nature of the variations of this form with change of the atomic number of the scatterer, and for investigating this matter the method of DuMond,[4] utilizing the general momentum distribution formula of Podolsky and Pauling,[9] is most appropriate, notwithstanding its restriction to atoms which may be regarded as hydrogen-like and which are free from the entangling alliances of the crystal state.

[1] G. E. M. Jauncey, Phys. Rev. **25**, 314 and 723 (1925).
[2] J. W. M. DuMond, Phys. Rev. **33**, 643 (1929).
[3] J. W. M. DuMond and H. A. Kirkpatrick, Phys. Rev. **37**, 136 (1931); S. Chandrasekhar, Proc. Roy. Soc. **A125**, 231 (1929); J. W. M. DuMond and H. A. Kirkpatrick, Phys. Rev. **38**, 1094 (1936).
[4] J. W. M. DuMond, Rev. Mod. Phys. **5**, 1 (1933).
[5] F. Bloch, Phys. Rev. **46**, 674 (1934).
[6] G. Wentzel, Zeits. f. Physik **43**, 1 (1927).
[7] F. Schnaidt, Ann. d. Physik **21**, 89 (1934).
[8] G. Burkhardt, Ann. d. Physik **26**, 567 (1935).
[9] B. Podolsky and L. Pauling, Phys. Rev. **34**, 109 (1929)

Using screening data from Slater[10] we have calculated the energy distributions in modified bands from scattering atoms with atomic numbers from 1 through 18. This method of calculation ignores all higher order effects productive of line asymmetry and it therefore suffices to plot half of each line only, as has been done in Fig. 1. Theories[2, 5, 6] of the structure of the modified band agree in predicting line profiles whose functional forms to a good approximation depend only upon the nature of the scattering atom, being independent of wave-length λ or angle of scattering φ. These variables affect only the wave-length scale, that is, the breadth of the line. Since it is further indicated that line breadths should be practically proportional to $\lambda(1-\cos\varphi)$[1] the curves of Fig. 1, though furnished with an abscissa scale correct for a particular wave-length and scattering angle, may be adjusted to represent theoretical expectations for any desired angle and for any wave-length within the usual observational range for the Compton effect.

The computed curves show how the modified line reflects the process of atom building by the addition of successive electrons. Generally speaking, a wide line or a line which is in part wide denotes the existence of electrons of large momentum, while a steep, narrow maximum is evidence of the presence of relatively slow electrons. The helium curve is broader than that of hydrogen since increase of nuclear charge causes the momentum per electron to increase. The lithium line exhibits a helium-like base with a narrow superposed spectrum due to scattering by the slower, single L electron. With the binding of additional electrons the scattered line loses its sharply peaked character since the L electrons are increasing in both individual momentum and numerical importance. At neon the contribution of the K electrons is inappreciable except at the wings of the curve, the profile as a whole being of the helium type. The next electron, however, produces, in sodium, a narrow maximum like that of lithium, after which the smoothing and broadening process ensues and at argon there recurs a smooth, broad line resembling those of the other rare gases.

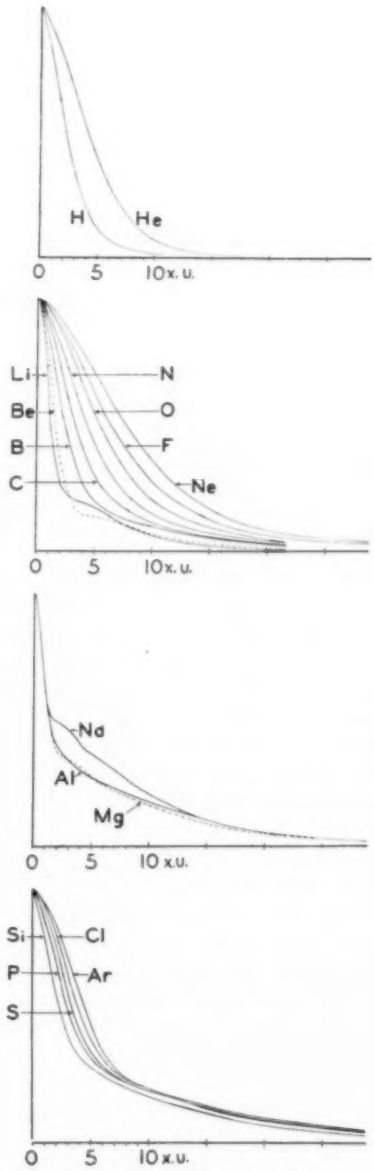

FIG. 1. Theoretical half-profiles of Compton modified bands from free atoms with consecutive atomic numbers from 1 to 18. Angle of scattering: 90°. Wave-length: 500 X.U. Abscissa scale is the same for all curves. Ordinate scales are arbitrarily selected to make curves coincide at maxima. Profiles for other wave-lengths and scattering angles may be obtained by simple alterations of the abscissa scale.

Experimental data are not now available for checking these curves in all particulars. All de-

[10] J. C. Slater, Phys. Rev. **36**, 57 (1930).

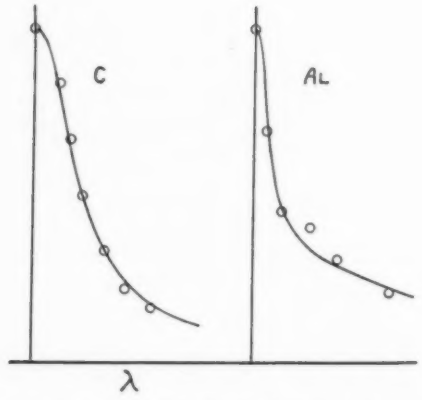

FIG. 2. Theoretical line shapes from Fig. 1 shown in comparison with corresponding spectrometer observations. The comparison is significant as to shape but not as to width since the experimental curves have been arbitrarily narrowed to fit the theoretical curves at half-maximum height.

tails of shape were missed by Woo[11] in his pioneer survey of scattered spectra from fifteen elements, since it suited his purposes to sacrifice resolving power for intensity. In general other observers have made the same choice. Kappeler,[12] however, has observed the scattering of Mo $K\alpha$ by gaseous neon under conditions favorable to the study of line form, and his results agree most satisfactorily in shape and width with their theoretical counterpart in Fig. 1.

When solid scatterers are used we find as did DuMond[2] that observed modified lines are broader than those predicted from theories of the free atom. This matter will come up in a later paragraph but it is relevant to note here that in spite of this broadening the modified lines from solid scatterers of differing atomic number, when observed with good resolving power, exhibit conspicuously differences in form such as appear in Fig. 1. In Fig. 2 the carbon and aluminum curves from Fig. 1 are repeated in conjunction with a few observed points for each case. The wave-length scales of the observations have been contracted relatively to that of the theoretical curves in order to make the comparative shapes more conspicuous. The carbon and aluminum theoretical curves are quite different in type and cannot be made to coincide by any linear manipulation of their abscissa scales, and the observed lines from carbon and aluminum evidently differ similarly. The degree of agreement between the points and the curves is a little surprising in view of the fact that the observations were not corrected for the broadening and presumably somewhat distorting instrumental effects referred to in the next section. We were first impressed by the difference between the sharply peaked aluminum lines and the more broadly rounded lines from carbon upon discovering that the $K\alpha$ doublet of molybdenum, which always appears as a single, broad line in the modified radiation from graphite, may readily be resolved into two sharp and well separated maxima in the modified scattering from aluminum.

It may be concluded that differences in the form of the Compton band characteristic of different scattering elements are not only theoretically predicted but are also experimentally observable with solid scatterers, and that comparisons of predictions with observations may be expected to yield information about the momenta of electrons in conducting and nonconducting solids.

BREADTHS OF MODIFIED LINES

Upon examining line breadths at half the maximum height in Fig. 1 it is seen that this quantity varies periodically with atomic number, attaining maxima at the rare gases and decreasing abruptly thereafter with increasing Z. This behavior is in general agreement with Kappeler's[12] wide neon line and with spectra from solid scatterers of beryllium, carbon, sulfur and aluminum, obtained in this laboratory, but has not been precisely confirmed as yet throughout a wide range of atomic numbers.

Using the ring-target x-ray source[13] and a double spectrometer[14] we have secured some fifty spectrum curves representing three different wave-lengths, two angles of scattering, and two scattering elements, carbon (graphite) and beryl-

[11] Y. H. Woo, Phys. Rev. **27**, 119 (1926).

[12] In Burkhardt's paper (reference 8) Kappeler's experimental line is compared with three theoretical shapes, one of which is equivalent to the neon curve in our Fig. 1. A full account of Kappeler's work on gaseous and solid scatterers has recently appeared in Ann. d. Physik **27**, 129 (1936).

[13] P. Kirkpatrick and P. A. Ross, Rev. Sci. Inst. **4**, 645 (1933).

[14] P. A. Ross, Rev. Sci. Inst. **3**, 253 (1932).

lium. These spectra were previously[15] discussed in another connection but we have found them suitable for breadth measurement and are presenting the results in figures and Table I. In addition to the modified line broadening which distinguishes crystalline scatterers from those composed of free atoms there are in practice breadth increments produced by the wave-length breadth of the incident radiation, the finite resolving power of the spectrographic or spectrometric apparatus, and the range of scattering angles simultaneously effective.

The first of these additional effects is entirely negligible in the present connection. The second produces a small effect whose magnitude depends upon what may be called the spectrometer transmission pattern, that is, the curve of transmitted intensity of monochromatic radiation *vs.* dihedral angle between the spectrometer crystals. The actual shape of this curve is not known for any spectrometer, but with the limited resolution afforded by our polished crystals it was permissible to take as its width the angular width of unmodified lines, which was 1.6′. Following Ehrenberg and Mark[16] we assume that both the spectrometer transmission pattern and the modified line may be approximated by Gaussian curves, in which case, as these authors show, the square of the width of the observed line equals the sum of the squares of the corrected width and the width of the spectrometer transmission pattern. Upon this basis corrections for spectrometer effects have been made in Table I. Since the corrections are well within the probable errors of observation the approximations mentioned above are deemed unobjectionable.

Line broadening because of variation of scattering angle may sometimes be rendered negligible by a proper choice and restriction of the angle, but in the general case special consideration is necessary. The Compton equation shows that a variation of scattering angle, $d\varphi$, causes the theoretical position of the center of the shifted line to occur simultaneously over a wave-length range

$$d\lambda = (h/mc) \sin \varphi d\varphi. \qquad (1)$$

Analysis shows that the effect on the observed line is to increase its half-maximum width *not* by $d\lambda$ but by a smaller amount which depends upon the true shape which the line would possess for a single-valued scattering angle. In order to correct observed lines for excess width from this cause it is then necessary to have some knowledge or assumption about the real shape of modified lines when freed from these experimental effects. Since only the approximate line form is required it has been assumed that the real line may be represented by $y = a/(1+(x/b)^2)$, a convenient function[17] which happens to fit the carbon curve of Fig. 1 rather well. In this expression a and b are constants and x is the wave-length variable, with origin at the center of the line. The ordinate of a modified line resulting from a variable scattering angle will then be represented by the integral of ydx over a range of x sufficiently wide to correspond to $d\varphi$. The equation of the resultant curve which is obtained upon integrating is found to possess a half-maximum breadth significantly greater than the breadth of the elementary (integrand) curves *only* when the latter breadth is small compared to $d\lambda$. In other words, the breadths of modified curves as observed are almost independent of variability of scattering angle so long as real line width is large compared to the wave-length range (Eq. (1)) introduced by the variability. As a special example, if the wave-length range due to variation of scattering angle is one-third the observed line width then it is found that a three percent correction is required to reduce the observed line width to the width for constant scattering angle.

It is not suggested that this analysis renders correction unnecessary but rather that the smallness of the correction makes unnecessary the frequently impracticable task of determining the range of scattering angles with high precision. We have calculated and applied the correction in all cases to follow in this section.

Line ordinates for locating the half-maximum height were measured from a somewhat indefinite background level whose determination probably constituted the most important source of error in our breadth measurements. The result of the various corrections is shown in Table I. Corrected breadths are thought to be good to one or two X units. These results are shown in comparison to

[15] P. A. Ross and P. Kirkpatrick, Phys. Rev. **46**, 668 (1934).
[16] W. Ehrenberg and H. Mark, Zeits. f. Physik **42**, 807 (1927).
[17] A. Hoyt, Phys. Rev. **40**, 477 (1932).

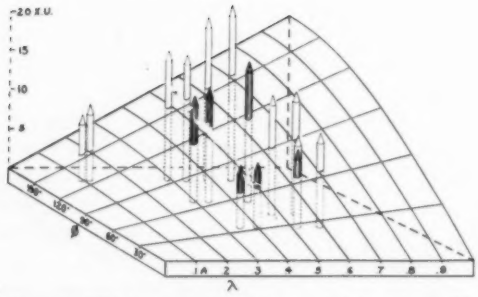

FIG. 3. Widths at half-maximum height of modified bands scattered by carbon, shown as a function of wave-length and angle of scattering. The cross-ruled surface gives theoretical widths for free carbon atoms (except that the assumptions underlying the theory are not well fulfilled for very short wave-lengths) while the vertical columns show measured widths obtained with graphite scatterers. Shaded columns represent the new measurements, corrected for instrumental broadening, while unshaded ones are from uncorrected measurements of DuMond and H. A. Kirkpatrick.

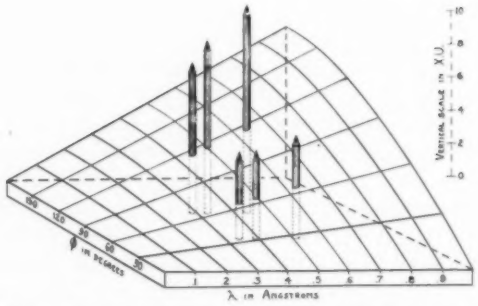

FIG. 4. Theoretical and observed modified band widths for beryllium scatterers, represented as in Fig. 3 (though with a different vertical scale).

theoretical breadths in Figs. 3 and 4. Fig. 3 also includes uncorrected breadth measurements by DuMond and H. A. Kirkpatrick.[3, 18]

It is evident that our experimental breadths with graphite and beryllium agree with free atom theory in respect to the linear variation of breadth with wave-length, and that they disagree but slightly in the functional variation of breadth with angle of scattering. As to absolute breadths the measured lines are found to be broader than those of theory by an average value of 75 percent with carbon and 140 percent in beryllium, the discrepancies for the two substances standing, perhaps significantly, in the order of their conductivities.

These results support and extend those which DuMond and H. A. Kirkpatrick[13] obtained by very dissimilar experimental means. Since Mo $K\beta$ was one of the radiations used in both investigations it is possible for this case to compare the two sets of results on one graph, as in Fig. 5. This agreement is of some interest since experimenters have heretofore obtained very discordant results in the measurement of modified line breadths. Bearden[19] and Gingrich[20] have reported modified lines from graphite which are very much too narrow to be at all consistent with the theoretical surface of Fig. 4, not to mention the associated experimental data. Gingrich obtained clear reso-

[18] These quoted data are not in need of significant correction for variation of the scattering angle since this angular range was kept small. Small corrections for spectrograph characteristics, comparable to those which we have used in Table I, might appropriately have been applied, though they would have been somewhat smaller than what we judge to be the observational probable errors.

[19] J. A. Bearden, Phys. Rev. **36**, 791 (1930).
[20] N. S. Gingrich, Phys. Rev. **36**, 1050 (1930).

TABLE I. *Observed and corrected widths of the Compton modified bands for various lines and scatterers.*

Radiation	Scatterer	Mean Angle of Scattering	Observed Width	Corrected for Spectrometer Effects		Corrected for range of angle of scattering
Sn $K\beta$	Be	64°	8.4 min.	8.2 min.	7.2 X.U.	5.2 X.U.
Sn $K\beta$	Be	116°	11.8	11.7	10.3	9.0
Ag $K\beta$	Be	64°	8.5	8.3	7.3	5.3
Ag $K\beta$	Be	116°	13.3	13.2	11.6	10.3
Mo $K\beta$	Be	64°	9.2	9.1	8.0	6.2
Mo $K\beta$	Be	116°	15.4	15.3	13.5	12.4
Sn $K\beta$	C	64°	11.0	10.9	9.6	8.1
Sn $K\beta$	C	116°	16.6	16.5	14.5	13.5
Ag $K\beta$	C	64°	11.3	11.2	9.9	8.5
Ag $K\beta$	C	116°	17.7	17.6	15.5	14.6
Mo $K\beta$	C	64°	12.8	12.7	11.2	10.0
Mo $K\beta$	C	116°	21.3	21.2	18.6	17.9

lution of the Mo $K\alpha$ doublet in the modified band upon scattering from graphite at about 165° 25′. The theoretical width of each component of this modified doublet, assuming perfect spectrometer resolving power, no variability of scattering angle and free carbon atoms, is 13 X.U. at half-maximum. Since the spectral separation is only 4.3 X.U. no resolution is to be expected even with these unrealizable ideal conditions.

Intensities of Modified Lines

Theories of the Compton process provide many predictions about modified line intensity which are as yet untested by experiment. The areas of the spectrum curves just discussed were determined by planimeter measurement for the purpose of obtaining the relative intensities of modified radiation scattered at the available supplementary angles 64° and 116°. According to the Wentzel[6]-Waller[21] theory (for free atoms) this ratio is not sensitive to wave-length variation and remains in the neighborhood of unity for the three wave-lengths and two scattering materials used in this work. Our data when corrected for absorption in the scatterer give, for all six cases, ratios equal to unity plus or minus five or six percent but do not permit more decisive checking chiefly because of the difficulty of locating the base lines of the curves.

The relative intensity of modified to unmodified radiation has been determined for a graphite scatterer and a variety of wave-lengths and angles, using some of the data already described and many additional spectra. As in the measurements of the previous paragraph, the shifted and unshifted lines obtained from spectrometer observations were plotted and the ratio of the areas of the lines was taken as the ratio of emitted intensities. Two slight systematic errors in this practice, due to differential absorption of the shifted and unshifted lines in the scatterer and to variation of spectrometer sensitivity with wave-length, are both smaller than the accidental observational errors, and since they are furthermore opposed as to sign we have applied no corrections for them.

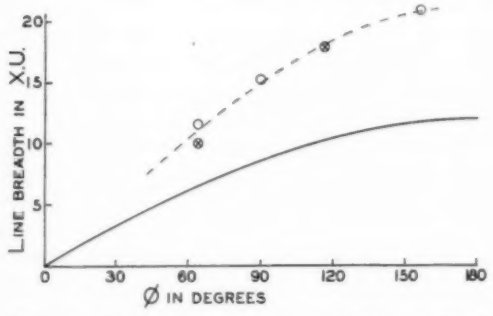

Fig. 5. Breadth at half-maximum height of Mo $K\beta$ (λ=631 X.U.) modified by scattering from graphite, showing relation between present work (crosses) and previous measurements by DuMond and Kirkpatrick (open circles), who used very dissimilar experimental methods. A smooth curve is fitted to the points. The curve lying below the observed points presents theoretical expectations for a scatterer of free carbon atoms.

[21] I. Waller, Phil. Mag. **4**, 1228 (1927).

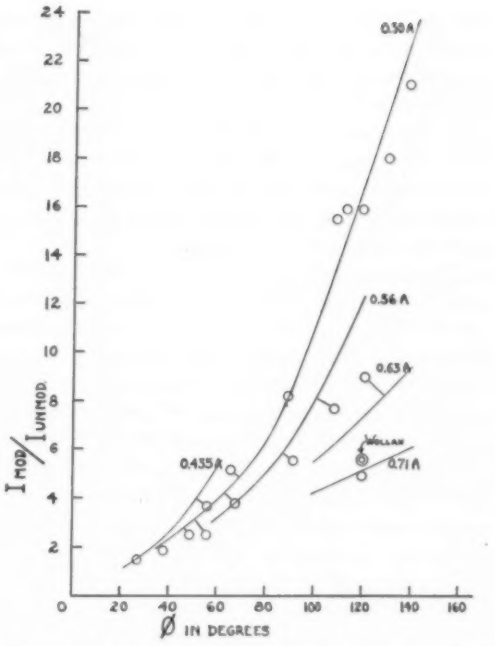

Fig. 6. Relative intensities of modified and unmodified scattering from carbon as a function of incident wave-length and angle of scattering. The curves show the predictions of the Wentzel-Waller theory of scattering while circles indicate observations with graphite scatterers.

For a wave-length λ scattered at the angle φ from atoms of atomic number Z, Wentzel's theory of scattering as extended by Waller furnishes the expression

$$I_{\text{mod}}/I_{\text{unmod}} = (Z - \Sigma f_n^2)/(1 + (h/mc\lambda) \text{ vers } \varphi)^2 F^2.$$

Here F is the structure factor of the atom as a whole and Σf_n^2 is a summation of the squares of

the individual structure factors of the atomic electrons, taken over the Z electrons present. The expression given omits a term, negligible here, which Waller deduced from the Pauli principle. Values of this modified to unmodified ratio have been computed, using carbon structure factor data from James and Brindley,[22] with results which are plotted in Fig. 6 with the experimentally determined ratios.

Though a few individual points show striking percentage discrepancies the agreement between theory and experiment is on the whole as complete as the experimental and theoretical uncertainties could permit. For large scattering angles or small wave-lengths theoretical predictions may be in error by ten percent or more because of uncertainty as to F, and the scatter of the observed points in Fig. 6 suggests that the probable error of experiment may be of similar magnitude. Although a majority of the observations fall *below* the theoretical curves there is no definite systematic discrepancy here such as one finds in comparing observed and theoretical *widths* in Figs. 3 and 4. Since we are not in fact dealing with the free atoms of theory but with a crystal lattice, such a discrepancy might not cause surprise. However, it is to be realized that for the angles and wave-lengths represented here the unmodified scattering is mostly by the undisturbed K electrons while the intensity of modified scattering is not very responsive to electronic rearrangement. The *widths* of modified lines on the other hand are almost entirely controlled by L electron scattering and should indeed be sensitive to the alteration of momentum which accompanies this change of physical state.

Prior measurements of the ratio of modified to unmodified intensity have been made by Ross,[23] Defoe,[24] Woo,[11, 25] Jauncey and Boyd,[26] Albrecht,[27] Wollan,[28] and Backhurst.[29] Though these data disclose no exception to the rule that the intensity ratio increases with angle and decreases with wave-length they are extremely discrepant as to numerical values. For carbon scatterers within the wave-length range of Fig. 6 published ratios are quite generally distinctly lower than the Wentzel-Waller values. Ross and Woo, using, respectively, photographic and ionization single-crystal spectrometers, obtained ratios less than half as large as those required by the theory. We are unable to account for the low results of these early experiments but cannot agree with Wollan that they are a reasonable consequence of the differing widths of the two lines. Defoe and Jauncey and Boyd used a single filter method in which unfortunately the errors of observation become enormously amplified in the modified-unmodified ratio as this ratio becomes large in comparison to unity. Where this difficulty does not apply their results (at least for carbon) are found to be below those of theory. Albrecht used the short wave-length 0.21A exclusively and his results are therefore not comparable with those of the present report. Wollan, using an extension of Ross'[30] balanced filter method, determined the carbon modified-unmodified ratio for a single wave-length and angle, obtaining a value in good agreement with theory and with the corresponding determination of this work. Backhurst's method was a refinement of that of Defoe and is subject to the same criticism for large values of the ratio. His single datum relevant to the range of this investigation (0.395A, scattered by carbon at 150°) gives a ratio of 12.5 which is obviously much too small to conform to either the observations or the theoretical curves of Fig. 6. Backhurst's neglect of the real breadth of the modified band has the effect of depressing his ratios to some slight extent.

We have also made a number of measurements of the intensity ratio for scatterers of Al, Mg and S, but these relatively poor scatterers present special difficulties which have restricted present conclusions to the statements that the modified-unmodified ratios for these elements are several times smaller than for carbon; that the ratios for Al and Mg are identical within a few percent (with $\lambda = 0.5$A), and that the sulfur ratio is still lower.

Although present results are in agreement with Wollan in promoting confidence in the Wentzel-

[22] R. W. James and G. W. Brindley, Phil. Mag. **12**, 81 (1931).
[23] P. A. Ross, Proc. Nat. Acad. Sci. **11**, 569 (1925).
[24] O. K. Defoe, Phys. Rev. **27**, 675 (1926).
[25] Y. H. Woo, Phys. Rev. **28**, 426 (1926).
[26] G. E. M. Jauncey and R. A. Boyd, Phys. Rev. **28**, 620 (1926).
[27] E. Albrecht, Zeits. f. Physik **57**, 326 (1929).
[28] E. O. Wollan, Phys. Rev. **43**, 955 (1933).
[29] I. Backhurst, Phil. Mag. **17**, 321 (1934).
[30] P. A. Ross, Phys. Rev. **28**, 425 (1926).

Waller theory as applied the relative intensities of modified and unmodified scattering it cannot be claimed that the experimental evidence is as yet either complete or satisfactorily concurrent.

Wave-Length of the Modified Band

Previously published measurements[15] of the magnitude of the Compton shift showed that the wave-length of maximum intensity is separated from the unmodified line by a wave-length interval slightly less than that given by the Compton formula,[21] the difference being found proportional to the square of the wave-length of the incident radiation. This shift defect was ascribed to the binding energy of atomic electrons[22] and Bloch[5] found it possible, upon certain approximately fulfilled assumptions, to calculate its magnitude. The defect has also been theoretically justified by Burkhardt.[8]

The quantitative agreement between theory and the observations, however, is now somewhat less satisfactory than it appeared to be in 1934, for the following reasons: (1) Errors in calculation have been discovered which when corrected increase the theoretical defects by some 10 percent. (2) The choice of numerical values of binding energies for use in the theoretical calculations has been questioned. Any alteration of the values used must be in such a sense as to increase further the theoretical defects. (3) Burkhardt has called attention to a neglected source of shift defect associated with the sign of the electron momentum, which requires a further increase in the theoretical value of the defect.

It is not certain that this widening gap between predicted and observed shift defects can be explained by the fact that the scatterers have actually been solids whereas theories have been concerned with free atoms. Precise shift measurements using monatomic gaseous scatterers are expected to clarify this point.

[21] In a summary of evidence on the question of the correctness of the original Compton shift formula Compton and Allison (*X-Rays in Theory and Experiment*, p. 210) assigned chief weight to the results obtained by Gingrich (see reference 20). It is suggested here that consideration discussed above (p. 933) weaken the force of this evidence.

[22] P. A. Ross and P. Kirkpatrick, Phys. Rev. **45**, 223 (1934).

NOVEMBER 15, 1936 PHYSICAL REVIEW VOLUME 50

Columnar Ionization

W. R. Kanne and J. A. Bearden, *The Johns Hopkins University, Baltimore, Maryland*

(Received September 5, 1936)

The ionization collected from single alpha-particles has been measured as a function of the angle between the path of the particle and the direction of the electric field. Data obtained for electric field strengths of 8, 100 and 500 volts per cm and for air pressures of one and two atmospheres are given. These results have been compared with curves based on the theory given by Jaffé. The agreement between theory and experiment is satisfactory and shows clearly that for low field strengths the loss of ions by recombination is appreciable even for large angles between particle path and electric field. In contrast with values of the recombination coefficient given by Jaffé, it is indicated in the present work that previously accepted values for this quantity are correct. A description of the FP-54 Pliotron circuit which has been used for this work is given.

THE theory for the fraction of ions collected from a strongly ionized column of gas by an electric field has been developed by Jaffé.[1, 2] In this theory it is assumed that the electric field separates the intensely ionized column into two parts, one of positive ions and the other of negative ions. During separation these columns broaden by diffusion, and, wherever they overlap, there is a loss of ions by recombination to the extent given by the recombination coefficient.

The expressions given by Jaffé for the ratio of the ions collected to those formed are as follows:

[1] Jaffé, Ann. d. Physik **42**, 303 (1913).
[2] Jaffé, Physik. Zeits. **30**, 849 (1929).

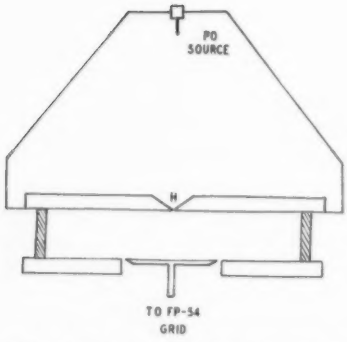

FIG. 1. Ionization chamber used to measure the number of ions collected from alpha-particles making angles from 0° to 45° with the electric field. The separation of the plates is 1 cm.

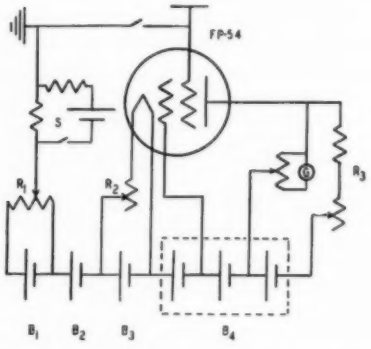

FIG. 2. FP-54 circuit. B_1 and B_2 are 1.5-volt dry cells, B_3 is a 2.5-volt Eveready Air Cell and B_4 is a 6-volt radio storage battery. R_1 is a 4000Ω potentiometer, R_2 is a variable resistance of 10Ω to 12Ω, and R_3 is a variable resistance of 250,000Ω. S serves to check the sensitivity of the tube.

(1) When the path of the particle and the electric field are parallel,

$$i/i_\infty = (pe^{-p}/z)(li\ e^{p+\ln\ (1+z)} - li\ e^{p}), \qquad (1)$$

where $z = 2dD/ub^2x$ and $p = 8\pi D/\alpha N_0$.

(2) When the path of the particle is at an angle φ with the electric field, provided that φ is not too small,

$$i/i_\infty = 1/(1+(1/p)(\pi/z')^{\frac{1}{2}}S(z')), \qquad (2)$$

where $z' = u^2b^2x^2 \sin^2\varphi/2D^2$, u is the average mobility[3] of the positive and negative ions, D is the diffusion coefficient, α is the recombination coefficient, N_0 is the number of ion pairs per cm length of path, d is the length of the path, x is the field strength, $b = r_0(4/\pi)^{\frac{1}{2}}$, and r_0 is the mean distance of the ions from the center of the column at the time of formation. For air at one atmosphere Jaffé found $b^2 = 3.2\times10^{-6}$ cm^2 by fitting the theoretical curves of Eqs. (1) and (2) to experimental data. The integral logarithm of p is $li\ e^p$.

$$S(z') = \frac{1}{(\pi)^{\frac{1}{2}}}\int_0^\infty \frac{e^{-s}ds}{(s(1+s/z'))^{\frac{1}{2}}}.$$

$S(z')$ may be evaluated from the expression[1]

$$S(z')(\pi/z')^{\frac{1}{2}}e^{z'/2} = (i\pi/2)H_0^{(1)}(iz'/2),$$

where H_0^1 is the Hankel function of zero order, and may be found, together with the integral logarithms, in Jahnke-Emde, *Tables of Functions* (Leipzig, 1933). A curve for the ratio of the ionization collected to that actually formed, as a function of the angle, is obtained by joining the one point for $\varphi = 0$ (Eq. (1)) with the valid portion of the curve given by (Eq. (2)).

The present experiment is concerned with the determination of i/i_∞ as a function of angle φ, field strength x, gas pressure, and with the comparison with theory.

EXPERIMENT

In Fig. 1 is shown the parallel plate ionization chamber with a guard ring to assure a parallel electric field. The polonium alpha-particle source was mounted above the chamber and arranged so that the distance to the conical defining hole H could be varied. The source could be rotated about an axis lying in the lower surface of the upper plate and passing through the apex of H. The spread in φ was determined from the diameter of the hole and its distance from the source of alpha-particles. This amounted to ±30 minutes of arc for the observations at one atmosphere and ±2° for those at two atmospheres. The distance of the source was adjusted so that in both cases the range of the alpha-particles was 6 mm after passing through the hole into the chamber. Thus, under no condition was it possible for the particles to strike the lower plate, nor for any of the ions formed to be collected by the guard ring. The gas in the chamber was dry air.

[3] For air at one atmosphere, $u = 1.65$ cm sec.$^{-1}$ volts^{-1}, $D = 3.7\times10^{-2}$ cm^2 sec.$^{-1}$, and $\alpha = 1.60\times10^{-6}$ cm^3 sec.$^{-1}$. For air at two atmospheres, $u = 0.825$, $D = 1.85\times10^{-2}$, and $\alpha = 1.88\times10^{-6}$.

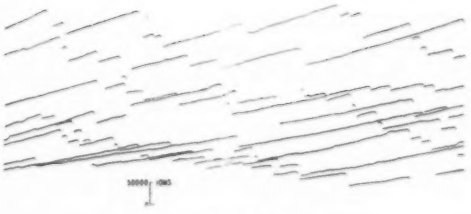

FIG. 3. Sample record.

The number of ions collected from single alpha-particles was measured by an FP–54 vacuum tube mounted in an evacuated metal container which eliminated fluctuations of the zero base line due to ions formed near the control grid terminal. The electrical circuit was the simple non-balancing type shown in Fig. 2. An Eveready Air Cell B_3 for the filament supply has been shown to give an exceedingly constant voltage when operated in a circuit of this type,[4] provided its temperature is held constant. A radio storage battery B_4 was used as the plate supply, and dry cells B_1 and B_2 were used across the grid bias potentiometer. With continuous operation it was necessary to recharge the storage battery and replace the dry cells about every four or five months. The air cell lasts about eighteen months.

Observations were made with the control grid "floating." By grounding the circuit through the potentiometer R_1 the potential of the grid could be made the same as that of the grounded guard ring. It is obvious that this was necessary if a parallel field was to be maintained in the ionization chamber.

[4] D. Lyford, Thesis, The Johns Hopkins University (1934).

The changes in plate current were measured with a Leeds & Northrup 2500 R galvanometer (sensitivity 5×10^{-11} amperes per mm) whose deflections were recorded by photographic paper on a rotating drum. When the filament of the tube was operated at the normal 2.5 volts, the sensitivity was about 180,000 mm per volt. A sensitivity of 25,000 mm per volt was found ample for recording the present deflections. Instead of using a galvanometer shunt for reducing the sensitivity, the filament voltage was reduced to 2.0 volts, and the plate resistance increased to 225,000 ohms. The latter method gave the smoother base line. Fig. 3 shows a sample record.

The curves given in Figs. 4 and 5 show the efficiency of ion collection as a function of angle φ. About 100 deflections were measured and averaged for each point on the curves. To determine the saturation current at one atmosphere, the ionization was measured with a field of 1000 volts per cm for an angle of 45°, as is indicated in Fig. 4 by a triangle. At two atmospheres pressure the saturation current could not be reached with the present apparatus, but was determined as follows: For any angle the value of i/i_∞ was calculated from theory and the value of i obtained experimentally. A curve was plotted between i and i/i_∞ for various values of φ and the resulting straight line extrapolated to $i/i_\infty=1$. This, then, gave the saturation value of i. The curve at two atmospheres shows how difficult it is to obtain even partial saturation for air and suggests the use of lower pressures if a large fraction of the ions formed is to be collected. This purpose may also be achieved by choosing a gas for which $D/\alpha N_0$ is large. Such are, for

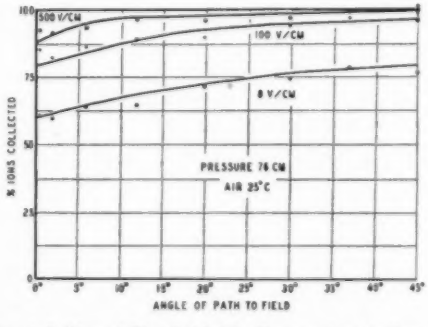

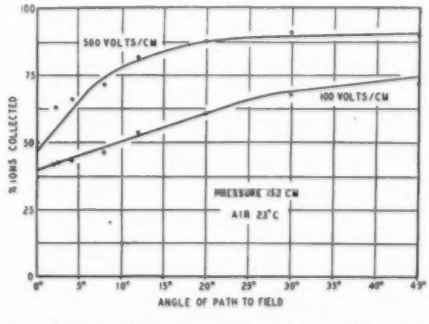

FIG. 4 (left) and Fig. 5 (right). Percent ions collected as a function of the angle between the alpha-particle path and the electric field. The points indicated are experimental and the solid line is an evaluation of Jaffé's theory.

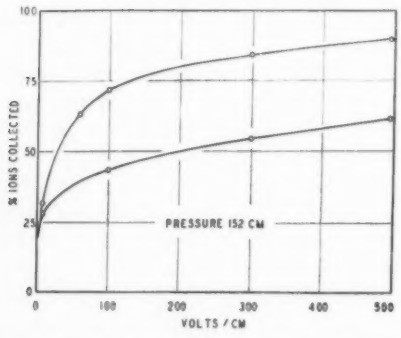

FIG. 6. Saturation curves for air at two atmospheres pressure. The upper curve is for an angle of 45° between the alpha-particle path and the electric field, and the lower curve is for path and field parallel.

example, the noble gases, which have very small electron affinities and thus do not easily form negative ions. For these gases α is then small, for there is very little recombination between free electrons and positive ions.

Computations based on data presented in Figs. 4 and 6 are in satisfying agreement with observations on columnar ionization by Lyford and Bearden.[5] They used a hemispherical ionization chamber of 2 cm radius with an electrode of 0.8 mm radius, the top of which contained a point source of polonium. The ion columns were then always parallel to the electric field. Using nitrogen at one-half atmosphere pressure they reached saturation at about 100 volts. With one atmosphere pressure and a chamber potential of 350 volts they collected 77 percent of the ions, and with two atmospheres they collected 40 percent of the ions. Rough calculations based upon the present results show that, under similar conditions of potential but with air in the chamber, 74 percent of the ions at one atmosphere and 40 percent at two atmospheres should be collected. These comparisons are not exact, since small sections of the ionized column were considered to be in an average field strength, and the fraction of ions which should be collected from these sections taken directly from our curves without considering the length of path d, which enters Eq. (1).

Jaffé[2] has obtained saturation curves for several gases at pressures from one to six atmospheres under conditions approaching parallelism of path and field. Due to the fact that he used a less sensitive electrometer which recorded the integrated effect of large numbers of alpha-particles, his conditions of collimation were not as good as ours—the spread in angle was $\pm 4°$. He found agreement between the experimentally measured ionization and the predictions of Eq. (2) by using his data to calculate recombination coefficients at the various pressures. Eq. (2), however, drops sharply at small angles and deviates considerably at 4° from the curves which combine Eqs. (1) and (2). His values for the recombination coefficient α decrease continually as the pressure is increased from one to six atmospheres instead of reaching a maximum at about two atmospheres.[3, 6] He finds $\alpha = 1.32 \times 10^{-6}$ cm^3 sec.$^{-1}$ for two atmospheres of air. Upon comparing our data at two atmospheres with theory, it is found that the relationship of the four quantities—Eqs. (1) and (2) evaluated for each of the two field strengths—requires that α be considerably greater. Satisfactory agreement is obtained if $\alpha = 1.88 \times 10^{-6}$, as has been given by Langevin.[6]

In conclusion, the columnar effect on the loss of ions by recombination within the parent ion column is appreciable over large angles between the path of the alpha-particle and the electric field, and is correctly predicted by Jaffé's theory under the various conditions of pressure and field strength used in these experiments.

[5] Lyford and Bearden, Phys. Rev. **45**, 743 (1934).

[6] Langevin in Thomson, *Conduction of Electricity through Gases* (Cambridge, 1928), p. 35.

Line Intensity Variations in the Hydrogen High Frequency Glow Discharge

G. W. Fox and C. H. Bachman, *Iowa State College, Ames, Iowa*

(Received June 25, 1936)

Intensity variations in the lines of the Balmer series as excited in a high frequency "glow" discharge in hydrogen for a wave-length range of 5.1 to 32.5 meters and pressure range of 5 to 300 microns have been studied spectroscopically in conjunction with a logarithmic sector disk. The results of the investigation indicate that a distinct variation in intensity ratios with excitation frequency exists. A region of excitation frequencies is found which produces minimum excitation of each term with respect to H_α and further, this region depends on the pressure and the term under consideration. Ionization efficiency and intensities of the higher series terms vary more or less directly with each other if cumulative ionization is negligible. The intensities of the higher terms increase with decreasing pressure down to about 10 microns below which H_β and H_γ continue to increase in intensity while the higher terms decrease. If a value $e^{-0.1(f/10^7)^2}$ be chosen for $\phi(f)$ in J. Thomson's equation for the striking voltage for this type of discharge, curves can be calculated in good general agreement with the experimental results.

Introduction

HIGH frequency electrical discharges in gases are known as glow or ring discharges, depending on whether the type of excitation is electrostatic or electromagnetic.

The theory of the glow discharge as developed by J. Thomson[1] may be summed up by the equation

$$P=\phi(f)[Vd/L+2\pi^2f^2Ld/e/m] \qquad (1)$$

in which P is the peak potential between the electrodes and d is the electrode separation. V is the ionizing potential of the gas, and f is the frequency of potential alternation. L is proportional to the mean free path, e/m is the ratio of charge to mass of the electron, and $\phi(f)$ accounts for diffusion losses. Thomson[1] suggests that these losses may increase with increasing electron oscillation amplitude and, since this amplitude varies inversely with the square of the frequency of oscillation, $\phi(f)$ should be some function of $1/f^2$.

Experimental Procedure

In this investigation, high frequency discharges were excited in hydrogen by voltages applied through external electrodes, thus insuring an electrostatic or "glow" type of discharge. The spectrum of the discharge was studied as a function of the applied frequency for a series of pressures. In particular, the relative intensities of certain lines in the Balmer series were measured for a number of frequencies and pressures.

The applied potential difference was that developed across the output circuit of a push-pull oscillator powered with type 852 tubes. This potential was so adjusted that a calculated peak of 1600 volts was maintained across 30 cm of gas for a series of wave-lengths between 5.1 and 32.5 meters. The high frequency current in the plate tank circuit was measured with a 0–10 ampere thermocouple ammeter especially constructed for high frequency use. The hydrogen, generated electrolytically, was dried over phosphorus pentoxide and was admitted to the discharge tube by diffusion through palladium. Oil diffusion pumps were used and a Pirani gauge, previously calibrated for hydrogen, measured the pressures. The whole vacuum system was of Pyrex glass except for a Corex window sealed to the end of the discharge tube and all joints up to the stopcock at the pumps were glass sealed. The discharge tube was 4.8 cm in diameter and 75 cm long. It was separated from the pumps by a trap cooled with solid CO_2 and acetone.

The relative intensities of the Balmer lines were determined by means of a logarithmic sector disk similar to that described by Twyman and Simeon.[2] The disk was constructed to the equation $-\log\theta=0.2L$ and differed from theirs in having two symmetrically placed spirals rather than one. The value of θ represents the circumferential aperture at a distance L measured inwards radially from the outermost part of the disk. This device produces wedge shaped spectra in which the length of a line is propor-

[1] John Thomson, Phil. Mag. **10**, 280 (1930).

[2] F. Twyman and F. Simeon, Trans. Opt. Soc. London **31**, 169 (1929–30).

tional to its intensity. Ratios of intensity are obtained by measuring the lengths of two lines and calculating from the equation:

$$\log I_2 - \log I_1 = 0.2p(L_2 - L_1). \qquad (2)$$

The value of p, the Schwarzschild constant was of no interest in this investigation since only variations of intensity ratios were studied.

The accuracy of the sector disk as a device for making intensity measurements has been established by Webb,[3] Twyman and Harvey,[4] and others, who have proved it to be a very convenient and accurate instrument when properly used and rotated at sufficiently high speeds. The disk was driven at 3000 r.p.m. and was used in conjunction with a Bausch and Lomb medium quartz spectrograph. Line lengths were measured consistently to 0.1 mm. *W* and *W* panchromatic plates of the same emulsion batch were used.

Although a pure spectrum of hydrogen was easily obtained in the visible region, the removal of the 3085A water vapor band was impossible in spite of a protracted period of pumping and baking. This band may well arise, as suggested by Wood,[5] from the combination of hydrogen with oxygen released from the glass by dissociation of SiO_2 due to electron bombardment. The 2882A and 2899A CO_2 bands also persistently appeared at pressures less than a few microns, though no other bands from the well-known spectra of this molecule were detected. These bands may have arisen from a small diffusion of oil vapor into the tube from the oil pumps.

A series of spectrograms of the discharge were obtained over the range of excitation wave-lengths mentioned, while the pressure and applied potential difference were held constant. Data for six pressures of from 5 to 300 microns were obtained and the intensity ratios for these cases are plotted in Figs. 1 to 6, inclusive.

Discussion

In attempting to explain conflicting data for some intensity ratios in the Balmer series obtained by a number of workers under widely different experimental conditions, Herzberg[6] concluded that the ratios were affected by tube dimensions, pressure and the portion of the discharge viewed. The pressure variation is well illustrated in this experiment and to the above list should also be added the factor, frequency of excitation.

In order to facilitate comparison with other similar work, let us assume that excitation of the higher terms of the series is most probable when there is maximum ionizing efficiency of the discharge. The six sets of curves then indicate that the most favorable pressure is between 30 and 5 microns. Brasefield[7] has found maximum conductivity for 20 meter excitation to be between 10 and 20 microns. He also showed that, for pressures in the region 30 to 10 microns, the discharge efficiency decreases as the h.f. excitation changes from 30 to 25 meters. It then increases to a maximum at 20 meters and again decreases rapidly as the wave-length approaches 15 meters, the shortest wave-length he used.

If the relative heights of the curves are used as criteria for discharge efficiencies, those of Figs. 3 and 4 show the efficiency decreasing from 32.5 meters to between 20 and 25 meters, then reaching a maximum at 10 to 15 meters with a very inefficient discharge indicated at 5 meters and shorter wave-lengths. At pressures above and below the range 10 to 30 microns, this inefficiency at the very short wave-lengths does not seem indicated.

Now, if high ionization efficiency in the discharge is favorable to the excitation of the higher series terms, it would seem that Eq. (1) should yield information as to the efficiency of the discharge for different pressures and excitation frequencies when subjected to a constant field.

Curves of the field required for initiation of the discharge *vs.* excitation wave-length calculated from Eq. (1) for various pressures are shown in Fig. 7. As has been suggested by Thomson,[1] the function $\phi(f)$ in this equation is to account for a decrease in electron loss by diffusion, which loss may increase with increasing amplitude of vibration of a free electron. Since this amplitude will vary inversely with the square

[3] J. H., Webb, J. Opt. Soc. Am. **23**, 157 (1933).
[4] F. Twyman and A. Harvey, Trans. Opt. Soc. London **33**, 1 (1931–32).
[5] R. W. Wood, Phil. Mag. **8**, 207 (1929).
[6] Gerhard Herzberg, Ann. d. Physik **84**, 565 (1927).
[7] C. J. Brasefield, Phys. Rev. **35**, 1073 (1930).

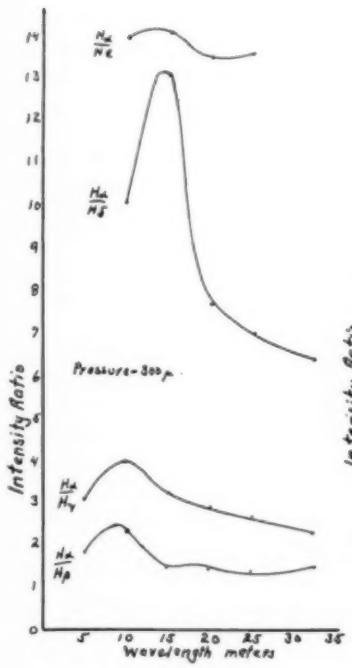

FIG. 1.

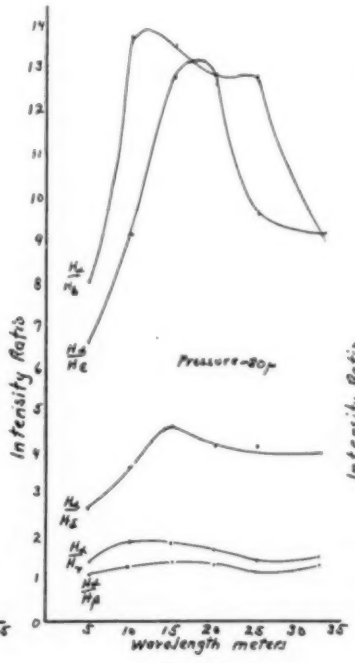

FIG. 2.

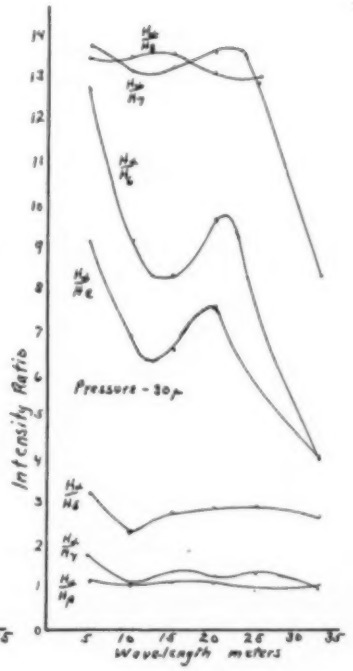

FIG. 3.

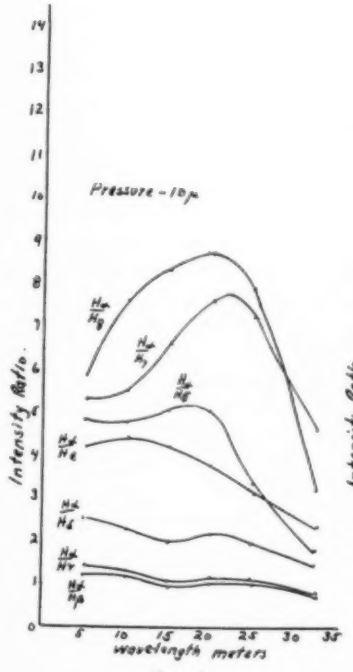

FIG. 4.

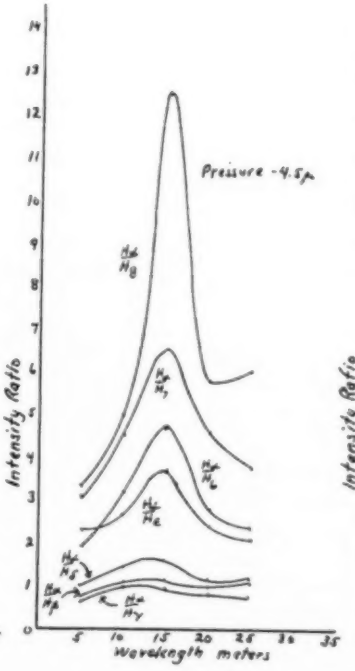

FIG. 5.

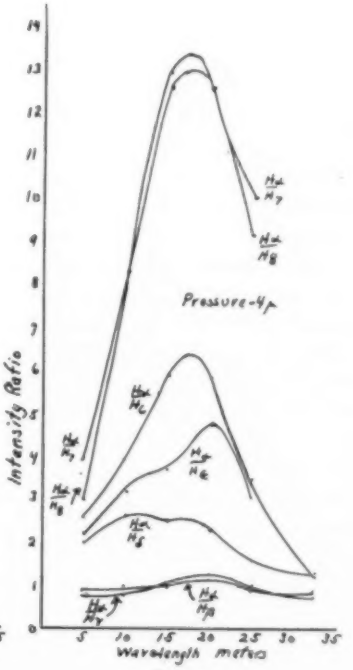

FIG. 6.

FIGS. 1–6. Plots of intensity ratios *vs.* wave-length for various pressures.

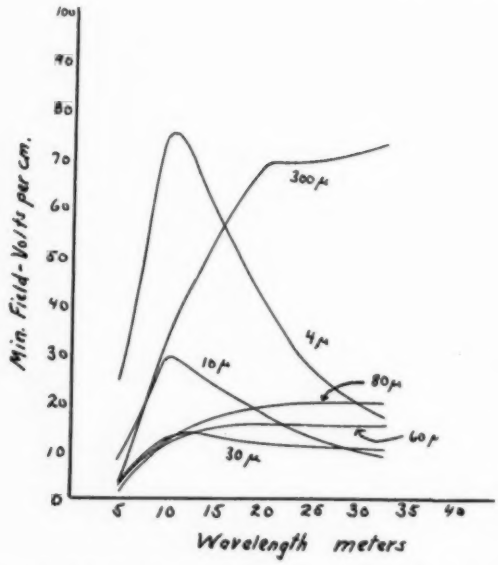

FIG. 7. Calculated curves of minimum field for discharge at constant pressure.

of the frequency, $\phi(f)$ should be some inverse square function of f.

A function $\phi(f)=e^{-0.1(f/10^7)^2}$ was found by trial to give the curves shown in Fig. 7. The heights of the calculated curves indicate the efficiencies of the discharge since low values of minimum field denote greater efficiencies. The curves of Fig. 7 show conditions to be most favorable as the pressure decreases from 300 microns through 30 microns and then the efficiency decreases (field increases) sharply for further lowering of pressure. This general trend appears in the experimental curves as has been mentioned.

The relative heights and shapes of these curves for different pressures are in general agreement with the experimental curves, though with data over a wider range of frequencies and pressures, it would be possible to determine a more accurate and probably more complicated value of $\phi(f)$. It should be kept in mind that the calculated curves represent values of field at minimum striking potential, whereas the experimental data are for a discharge already started. For this reason, some differences due to cumulative ionization in the discharge already in operation may well occur between the calculated and experimental curves. Possibly this idea explains the double maxima of Figs. 3 and 4, for, in the pressure region there shown, for high frequencies of excitation, some of the higher terms of the series may be diminished, on account of collisions of the second kind in which the excited atoms would aid ionization rather than their respective line intensities. Such a process might well affect the diminished diffusion loss $\phi(f)$ and would bring about an upward trend of the curves as shown in Figs. 3 and 4. In this event, however, the general height of the curves would no longer indicate ionization efficiency in the same way as has been assumed.

The variation in maxima of different term ratios for a given pressure might also occur because of cumulative ionization. Another factor which could affect the shape of the curves is the charge taken up by the glass walls which probably changes with both pressure and frequency.

The steady increase in intensities of H_β and H_γ and H_δ with respect to H_α at lowered pressures indicates that the population of these higher states becomes greater with decreased pressure. That pressure is not the only factor is indicated by the curves of Figs. 5 and 6 in which H_α, H_β, H_γ assume a different order as to intensity depending upon the frequency. This variation with frequency is noticeable, however, only at low pressures.

Intensities in the $^3\Pi$, $^3\Sigma$ Band of PH

PHILIP NOLAN* AND F. A. JENKINS, *Department of Physics, University of California, Berkeley, California*

(Received September 3, 1936)

Measurements of the relative intensities of the lines in the 0,0 band of PH at λ3400 are given. The band was excited by a high voltage discharge through hydrogen and phosphorus vapor. The distribution of molecules in the initial states is evaluated by using the sum rule, and is found to correspond to thermal equilibrium at 696°K, not only for the various rotational levels of a given electronic state, but also for the three components of the $^3\Pi$ multiplet. The intensity factors i are tabulated and compared with their theoretical values for $^3\Pi$ (case *a*), $^3\Sigma$ and for $^3\Pi$ (case *b*), $^3\Sigma$. These theoretical factors are given for the first time in explicit form. The observed i factors are in qualitative agreement with theory. For the main branches, they are linear functions of J', with relative values close to those expected for case *b* at all except the lowest J values. For the satellite branches, they increase nearly linearly at low J, but soon reach a maximum and fall off, due to the uncoupling of the spin by the rotation. From the experimental i factors, the sum rule is also verified for the lower states.

VERY few experimental data on the intensities of the rotational structure in multiplet bands have thus far appeared, in spite of the existence of a fairly complete theory of the intensity distribution in such bands. Of the band systems showing an appreciable electronic multiplet separation, only the $^3\Pi$, $^3\Pi$ bands[1] of N_2 and the $^2\Pi$, $^2\Sigma$ bands[2] of HgH have been investigated quantitatively. The $^3\Pi$, $^3\Sigma$ system of PH analyzed by Pearse[3] presents a favorable case for accurate intensity measurements, since the 0,0 band at λ3400, which is the only one of any intensity, has an open structure free from overlapping by other bands. Pearse showed that the $^3\Pi$ state is inverted, with separations $^3\Pi_0-{}^3\Pi_1=121$ cm^{-1} and $^3\Pi_1-{}^3\Pi_2=111$ cm^{-1}. All of the 27 branches predicted for a coupling in the $^3\Pi$ state intermediate between case *a* and case *b* were identified. Theoretical intensity factors have not been derived for the intermediate case, although they are available for the two limiting cases $^3\Pi$ (case *a*), $^3\Sigma$ and $^3\Pi$ (case *b*), $^3\Sigma$, between which the actual case lies. For this reason, only a qualitative comparison of the experimental i factors with theory can be made, but it will be shown that the principal features of these are well accounted for. In addition, application of the intensity sum rules has made possible the determination of the distribution of molecules in the initial states under the conditions of excitation used.

Experimental Procedure

The discharge tube was similar to that described by Pearse.[3] Phosphorus is continuously vaporized into a stream of hydrogen flowing through the capillary of an ordinary end-on tube. The hydrogen pressure was 1.5 to 2.0 mm on the high pressure side of the 2 mm capillary, and a discharge current of 45 m amp. was maintained by a 25 kv transformer. The spectrum was photographed in the first three orders of the 21-foot concave grating, which has a dispersion of 1.29A/mm at λ3400 in the second order. It was necessary to use a slit as narrow as 0.025 mm, in order to suppress as far as possible the continuous spectrum of hydrogen, which always accompanied the PH spectrum. Plates were developed $4\frac{1}{2}$ minutes in 1 : 20 Rodinal at 18°C, and the standard precautions for uniform development were taken.

Each plate carried a set of intensity calibrations, produced by a platinum-on-quartz step-weakener having seven steps 1.5 mm wide and 27 mm long. The step-weakener was placed 1.5 cm in front of the plate, normal to the incident light, so that each spectrum line produced calibration marks of the same width and character as the lines of the direct spectrum. The transmissions of the steps for the wave-length used were measured by a photographic method, in which the blackenings produced by the continuous H_2 spectrum photographed through the step-weakener in the above position were compared with those produced on the same plate by three different neutral methods of intensity reduction: neutral screens, the step-slit (used in

* Now at the Institute of Paper Chemistry, Appleton Wisconsin.

[1] W. R. van Wijk, Zeits. f. Physik **59**, 313 (1930).

[2] W. Kapuscinski and J. G. Eymers, Zeits. f. Physik **54**, 246 (1929); J. G. Eymers, Zeits. f. Physik **63**, 396 (1930).

[3] R. W. B. Pearse, Proc. Roy. Soc. **A129**, 328 (1930).

TABLE I. *Intensities and i factors in the 0,0 band of PH at λ3400.*

	P_1		Q_1		R_1		P_2		Q_2		R_2		P_3		Q_3		R_3	
J'	I	i	I	i	I	i	I	i	I	i	I	i	I	i	I	i	I	i
0													8	18	8	22		
1									28	$R_{23}(2)$			15	43	19	54	12	$P_{31}(1)$
2	18	33	58	$Q_{23}(5)$	105	$Q_1(4)$	5	12	11	26	79	$R_2(2)$	23	69	31	92	15	$P_{31}(2)$
3	35	$R_{13}(4)$	130	270	78	153	11	31	21	56	66	$R_1(9)$	36	121	51	171	26	$P_{31}(3)$
4	59	$P_3(8)$	105	$R_1(1)$	79	173			36	110	16	49	85	$Q_2(10)$	63	243	26	100
		$P_1(4)$												$Q_{23}(2)$				
5	46	117	133	342	92	232	86	$R_{12}(2)$	47	168	22	79	53	255	75	350	60	$R_{21}(5)$
6	56	173	140	412	86	266	28	123	61	265	64	$R_1(12)$	42	250	76	445	33	190
7	61	232	144	520	88	329	29	165	65	358	31	166	39	298	71	530	33	244
8	59	280	144	660	79	$R_2(2)$	30	216	65	$P_3(11)$	30	210	52	$R_{13}(4)$	63	630	28	280
9	50	320	123	745	67	$R_2(3)$	26	248	59	554	30	275	42	$P_{23}(4)$	54	745	24	330
10	49	420	96	790	53	440	22	300	85	$Q_{23}(2)$	22	285			42	840	19	381
11	32	400	74	890	43	514	20	$R_{13}(10)$	36	670	41	$Q_{32}(1)$	35	$P_{12}(4)$	28	800	14	400
12	24	440			67	$R_2(6)$	12	340	72	$Q_{23}(3)$			21	$R_{12}(5)$			24	$R_{21}(6)$
13	21	550	41	1120	23	620	9	400	12	$P_{23}(1)$								
14			26	1130	14	600												
15			18	1200	34	$Q_{21}(8)$												
16			12	1280														

	${}^{Q}P_{21}$		${}^{R}Q_{21}$		${}^{S}R_{21}$		${}^{Q}P_{32}$		${}^{R}Q_{32}$		${}^{S}R_{32}$		${}^{R}P_{13}$		${}^{S}Q_{31}$		${}^{T}R_{13}$	
J'	I	i	I	i	I	i	I	i	I	i	I	i	I	i	I	i	I	i
0							18	50										
1			31	67			28	79	42	$R_2(11)$					13	$P_{31}(5)$		
2	41	97	50	117	22	52	31	92	40	120	10	30			17	$Q_{32}(10)$		
3	70	$R_{23}(3)$	61	157	28	73	33	111	45	151	12	40			10	30		
4	55	$R_{23}(4)$	64	188	27	80	32	126	48	184	13	50	12	46	8	30	2	
5	35	125	55	192	58	$R_3(5)$	29	134	41	191	12	56			5	22		
6	28	122	52	221	24	$R_3(12)$	21	123	33	192	11	60			9	$R_{21}(9)$		
7	92	$R_1(5)$	41	222	17	93	21	157	25	184	9	66			3	22		
8	40	$Q_{23}(1)$	34	$R_1(15)$	13	76	16	$R_{23}(1)$	19	188	5	50						
9	11	106	23	$R_1(18)$	9	86	11	156	14	191								
10	9	123	13	169	6	82			11	$Q_{31}(2)$								
11	5	99	15	269	3	57			6	170								
12									12	?								

	${}^{O}P_{12}$		${}^{P}Q_{12}$		${}^{Q}R_{12}$		${}^{O}P_{23}$		${}^{P}Q_{23}$		${}^{Q}R_{23}$		${}^{N}P_{13}$		${}^{O}Q_{13}$		${}^{P}R_{13}$	
J'	I	i	I	i	I	i	I	i	I	i	I	i	I	i	I	i	I	i
0																		
1							14	32										
2	9	16	40	72	91	$P_3(5)$	17	41			29	$Q_2(1)$			11	19	9	16
3	61	$Q_{12}(9)$	66	128	82	160	22	59	73	$Q_{12}(12)$	70	$P_{21}(3)$				$R_{13}(9)$	35	$P_1(4)$
4	33	$P_3(10)$	79	174	74	162	46	$P_3(8)$			55	$P_{21}(4)$			10	23	59	$P_1(5)$
																		$P_3(8)$
5	20	$P_3(11)$	79	203	81	210	17	62	57	$Q_1(2)$	40	143			9	24	16	41
6			74	228	61	190	15	66	47	208	33	141			8	24		
7	19	73	63	240	47	$R_{12}(8)$			37	208	34	186			5	19	19	73
8			56	$P_{12}(3)$	47	$R_{12}(7)$	11	$P_{13}(4)$	27	190	21	149					14	67
9			33	210	96	$Q_{23}(4)$			21	204	13	123						
10			23	198	43				13	176	23	?						
11			14	175	16	180					6	122						
12			11	190					6	160								
13									4	180								

a prism spectrograph) and rotating sectors used centrally in a collimated beam.

The plates were photometered on the Zeiss recording microphotometer, and a separate calibration curve constructed for each plate. It was assumed that the plate characteristics, as well as the step-weakener transmissions, did not vary over the wave-length range of 80A covered by the band. The calibration curves drawn from several different lines were closely parallel, and the final curve was obtained by parallel displacement of these curves along the log I axis to obtain the best average coincidence. To obtain the intensity of a line, the intensity of the continuous background was subtracted from the peak intensity. In reducing the microphotometer curves, the mechanical ratiometer described by Langstroth[4] for drawing the density curves and reading intensities directly by settings on the projected image of the microphotometer trace was found convenient.

Table I gives the observed relative intensities I of all measurable lines, together with the resulting intensity factors i obtained in a manner explained below. The intensities given represent average values from three second-order plates and one third-order plate. In the case of known blends the intensity given is the total, measured value, and the designation of the blended line or lines appears in place of the i factor. The errors of measurement should not exceed about 3 percent for lines which are clearly resolved.

Interpretation of The Results

The intensity of any band line may be conveniently written[5]

$$I = k\nu^4 i R', \tag{1}$$

in which k may be considered as constant for the lines of any one band. The intensity factor i is a function of the rotational quantum number, and is independent of the excitation conditions, while R' is the number of molecules in the initial state divided by the statistical weight of that state. In most cases of electrical excitation, the function R' is experimentally found to have the form $e^{-E'_r/kT}$ corresponding to the distribution among the rotational levels required for thermal equilibrium at the temperature T. The distribution between the vibrational levels, and between the components of wide electronic multiplet levels, on the other hand, has not been found to correspond even approximately to thermal equilibrium at this temperature.[5] Hence for the present we may write

$$I = g'\nu^4 i e^{-E_r/kT}, \tag{2}$$

leaving open the equation of the relative values of g' in the three sub-bands $^3\Pi_0 \rightarrow {}^3\Sigma$, $^3\Pi_1 \rightarrow {}^3\Sigma$ and $^3\Pi_2 \rightarrow {}^3\Sigma$.

Distribution of molecules in the initial state

The existence of an effective temperature for rotation may be directly tested from the data, without any knowledge of the i factors, by applying the sum rules:

$$\sum_{J''} i = \text{const. } (2J'+1), \tag{3}$$

$$\sum_{J'} i = \text{const. } (2J''+1). \tag{4}$$

From Eq. (2):

$$\sum_{J''} I = g'\nu^4 e^{-E_r/kT} \sum_{J''} i, \tag{5}$$

neglecting the variation of ν^4 over the band. Hence by Eq. (3),

$$\sum_{J''} I = \text{const. } (2J'+1)e^{-E_r/kT}, \tag{6}$$

and $$\log \left(\sum_{J''} I/2J'+1\right) = -E_r/kT + \text{const.} \tag{7}$$

These summations have been carried out for the various initial states J' of the three sub-bands. Intensities of all blended lines of appreciable intensity were interpolated on graphs of the intensities of the various branches against J'. The results are given in Fig. 1a, where the ordinate is $F(J')$, the rotational term values in the upper states taken from Pearse's analysis, and the abscissa $\log R' = \log \left(\sum_{J''} I/2J'+1\right)$. Three lines are obtained for the three sub-bands $^3\Pi_0 \rightarrow {}^3\Sigma$, $^3\Pi_1 \rightarrow {}^3\Sigma$ and $^3\Pi_2 \rightarrow {}^3\Sigma$, respectively, from left to right, the lines being straight and parallel within the experimental error. The temperatures derived by least squares from the slopes, $-1/kT$,

[4] G. O. Langstroth, Rev. Sci. Inst. **5**, 255 (1934).
[5] R. S. Mulliken, Rev. Mod. Phys. **3**, 100 (1931).

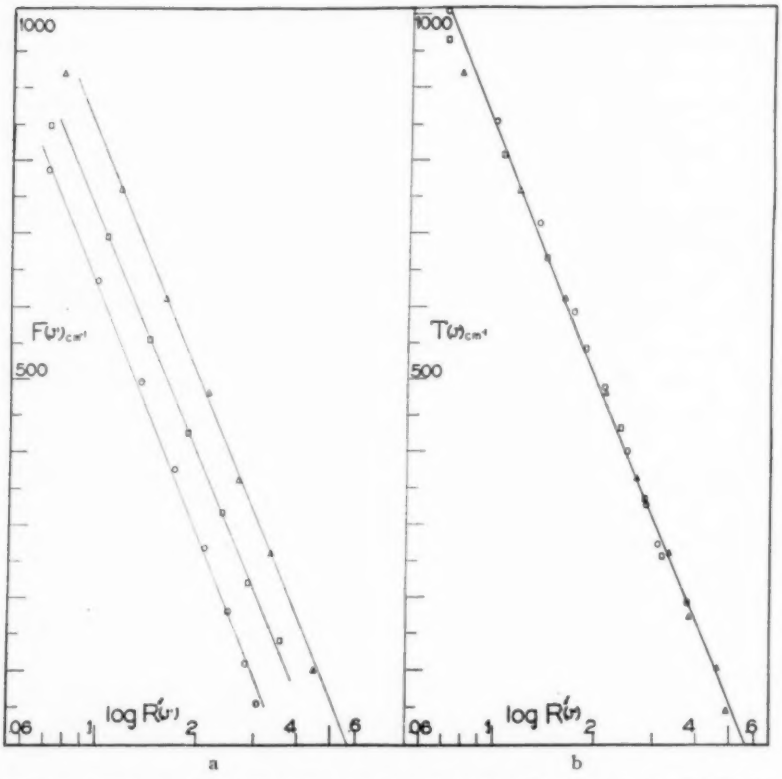

FIG. 1 (a). The rotational term values as a function of log R' where $R'=(\sum_{J''} I/2J'+1)$; (b) Total term value of upper state as a function of log R'.

of the three curves are 700°K, 694°K and 689°K, respectively.

It is seen that the band originating on the lowest level, $^3\Pi_2$, is relatively the strongest, as would be the case if thermal equilibrium determined the relative numbers of molecules in the multiplet components. Hence the results were replotted, as in Fig. 1b, against the total term value of the upper state $T(J')=F(J')+A\Lambda\Sigma$, where $A\Lambda\Sigma$ represents the electronic coupling energy. The fact that the three lines now become coincident shows not only the distribution of molecules between the electronic multiplet components corresponds to temperature equilibrium, but that the same temperature is effective for both electronic and rotational energy. This result is in marked contrast to that for HgH,[2] where, however, the multiplet separation is an order of magnitude greater. The difference shows definitely that with the small multiplet separation existing in PH, it is possible for the molecules to be redistributed by thermal impacts while in the excited state. In HgH, under the conditions used other processes evidently determined the relative numbers of molecules in the multiplet components. Besides the pressure, the ratio of the mean translational kinetic energy to the energy intervals involved play an important part.[6] The ratio of the spin coupling energy to kT is 5 to 1 for HgH, while it is only 1 to 5 for PH.

The intensity factors

No explicit i factors for $^3\Pi$, $^3\Sigma$ transitions could be found in the literature, although in principle they are contained in the general equations of Hill and Van Vleck.[7] The derivation of closed

[6] L. S. Ornstein and H. Brinkman, Physica **1**, 797 (1934).
[7] E. L. Hill and J. H. Van Vleck, Phys. Rev. **32**, 250 (1928).

TABLE II. *i factors for* $^3\Pi$, $^2\Sigma$ *transitions with ideal coupling.*

$^3\Pi$ (*case a*), $^2\Sigma$			$^3\Pi$ (*case b*), $^2\Sigma$		
$^3\Pi_2$, $^3\Sigma$					
P_1: $\frac{(J-1)J(J+2)}{(J+1)(2J+3)}$	$^OP_{12}$: $\frac{(J-1)J}{J+1}$	$^NP_{13}$: $\frac{(J-1)J}{2J+3}$	P_1: $\frac{(2J-3)(J-1)}{2J-1}$	$^OP_{13}$: 0	$^NP_{13}$: 0
Q_1: $\frac{(J-1)(J+2)}{J}$	$^PQ_{12}$: $\frac{(J-1)(J+2)(2J+1)}{J(J+1)}$	$^OQ_{13}$: $\frac{(J-1)(J+2)}{J+1}$	Q_1: $\frac{(J-3)(J-1)(2J+1)}{J^2}$	$^PQ_{13}$: $\frac{J-1}{J^2}$	$^OQ_{13}$: 0
R_1: $\frac{(J+1)(J+2)}{2J-1}$	$^QR_{12}$: $\frac{(J+1)(J+2)}{J}$	$^PR_{13}$: $\frac{(J-1)(J+1)(J+2)}{J(2J-1)}$	R_1: $\frac{J(2J+1)}{2J-1}$	$^QR_{13}$: $\frac{2J+1}{J^2}$	$^PR_{13}$: $\frac{J-1}{(2J-1)J^2(2J+1)}$
$^3\Pi_1$, $^2\Sigma$					
$^QP_{12}$: $\frac{2J(J+1)}{2J+3}$	P_2: 0	$^OP_{12}$: $\frac{2J(J+2)}{2J+3}$	$^QP_{12}$: $\frac{2J-1}{J^2}$	P_2: $\frac{(J+2)J^2}{(J+1)^2}$	$^OP_{12}$: 0
$^RQ_{12}$: $2J$	Q_2: 0	$^PQ_{12}$: $2(J+1)$	$^RQ_{12}$: $\frac{J+1}{J^2}$	Q_2: $\frac{(J^2+J-1)^2(2J+1)}{J^2(J+1)^2}$	$^PQ_{12}$: $\frac{J}{(J+1)^2}$
$^SR_{12}$: $\frac{2(J-1)(J+1)}{2J-1}$	R_2: 0	$^QR_{12}$: $\frac{2J(J+1)}{2J-1}$	$^SR_{12}$: 0	R_2: $\frac{(J^2-1)(J+1)}{J^2}$	$^QR_{12}$: $\frac{2J+3}{(J+1)^2}$
$^3\Pi_0$, $^3\Sigma$					
$^RP_{11}$: $\frac{(J+2)^2}{2J+3}$	$^QP_{11}$: $J+2$	P_3: $\frac{(J+1)(J+2)}{2J+3}$	$^RP_{11}$: $\frac{1}{4J(J+1)^2}$	$^QP_{11}$: $\frac{2J+1}{(J+1)^2}$	P_3: $\frac{(2J+1)(2J+7)}{2J+5}$
$^SQ_{11}$: $J+1$	$^RQ_{11}$: $2J+1$	Q_3: J	$^SQ_{11}$: 0	$^RQ_{11}$: $\frac{J+2}{(J+1)^2}$	Q_3: $\frac{J(2J+1)(J+2)}{(J+1)^2}$
$^TR_{11}$: $\frac{(J-1)J}{2J-1}$	$^SR_{11}$: $J-1$	R_3: $\frac{(J-1)^2}{2J-1}$	$^TR_{11}$: 0	$^SR_{11}$: 0	R_3: $\frac{(2J-1)(J+2)}{2J+1}$

Note: J represents the J value of the upper state in all cases.

formulas to cover all intermediate types of coupling in the $^3\Pi$ state, as was done for $^2\Pi$, $^2\Sigma$, is probably not possible here, but they can be obtained for the limiting conditions $^3\Pi$ (case *b*), $^2\Sigma$ and $^3\Pi$ (case *a*), $^3\Sigma$. Table II gives these factors, which are here given explicitly for the first time. The case *a* factors were kindly communicated to us by Professor Van Vleck as the results of some unpublished work. They were derived by a modification of the intensity formulas for the intercombination bands $^1\Sigma$, $^3\Pi$ as given by Schlapp.[8] The case *b* factors were calculated for us by Dr. Melba Phillips in this laboratory, using a method suggested by Mulliken.[9] They are given by the relation

$$i(\text{case } b) = i(\text{case } a) \cdot i(\text{atomic}) \cdot N(\Delta K)$$

$$K \rightarrow J \qquad \Delta J,\ s \rightarrow s$$
$$\Lambda \rightarrow \Omega \qquad \Delta K,\ K \rightarrow l,$$

where the arrows represent the replacement of one quantum number by another. $N(\Delta K)$ is a normalizing factor such that

$$\sum_{\Delta J} i(\text{atomic}) \cdot N(\Delta K) = 1.$$

The band in question represents a stage of coupling intermediate between case *a* and case *b*, the spin coupling parameter A/B being -14.8. We expect a tendency toward case *a* for very small rotational quantum numbers, but with increasing rotation the i factors should approach those of case *b* rapidly. The i factors may be determined from the measured intensities, once the distribution function R' is known, since, from Eqs. (1)

$$i = \text{const.} \times (I/R') = \text{const.} \times I e^{T'/kT},$$

where T' is the value of the total initial term, electronic+rotational, and T the temperature, 696°K. These experimental i factors are given in Table I, following the observed intensities. In Fig. 2a they are compared, for the main branches ($\Delta J = \Delta K$) with the theoretical curves for case *a* (dotted lines) and case *b* (full lines). In this comparison, the slopes of the experimental and

[8] R. Schlapp, Phys. Rev. **39**, 806 (1932).
[9] R. S. Mulliken, Phys. Rev. **30**, 785 (1927).

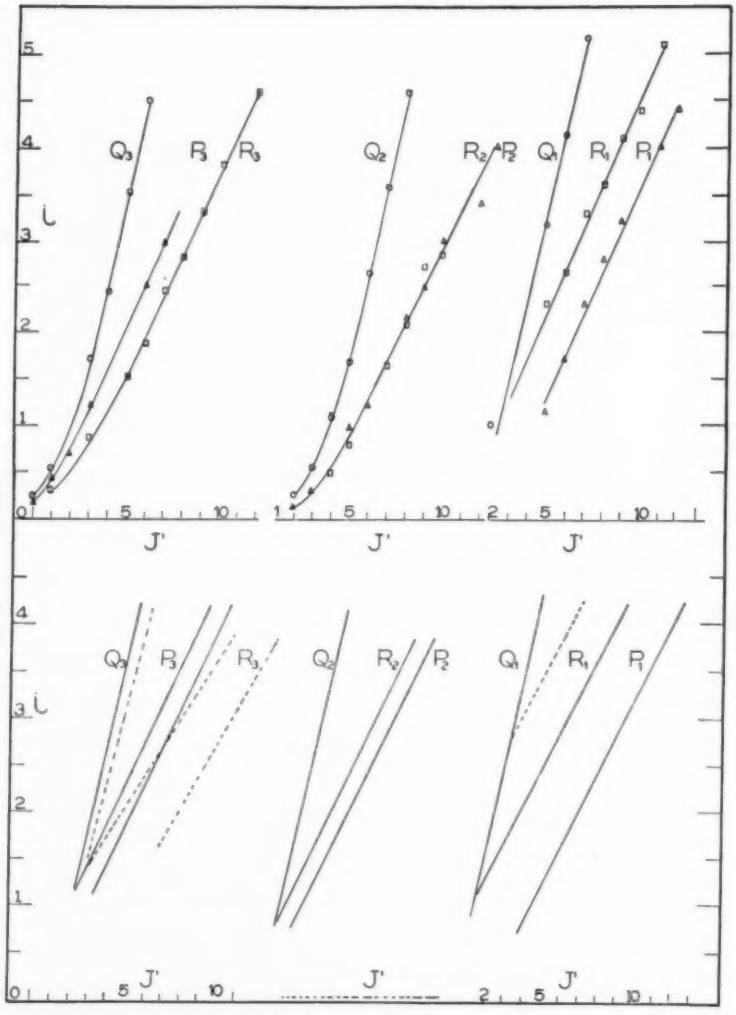

FIG. 2 (a). Comparison of the observed i factors with theoretical curves for case a (dotted lines) and case b (full lines).

theoretical curves for the Q_1 branch have arbitrarily been made equal. It will be seen that for the main branches, the experimental i factors increase linearly with J' for $J'>5$, and that the relative intensities of the branches agree closely with those from the case b formulas. An exception appears in the R_2 and P_2 branches, which are too nearly equal. The theoretical vanishing of the Q_2, R_2 and P_2 branches for pure case a is in agreement with the low observed intensities of these branches at the start.

The intensities of the satellite branches ($\Delta J \neq \Delta K$) shown in Fig. 2b are more sensitive to the type of coupling than are those of the main branches. In the lower part of the figure, the straight lines are the theoretical values for case a, and the hyperbolic curves of very low intensity are those for case b. The scale of the theoretical curves has been reduced throughout by a factor of 2 to render them comparable with the experimental values. Therefore it is apparent that the observed satellite branches are much

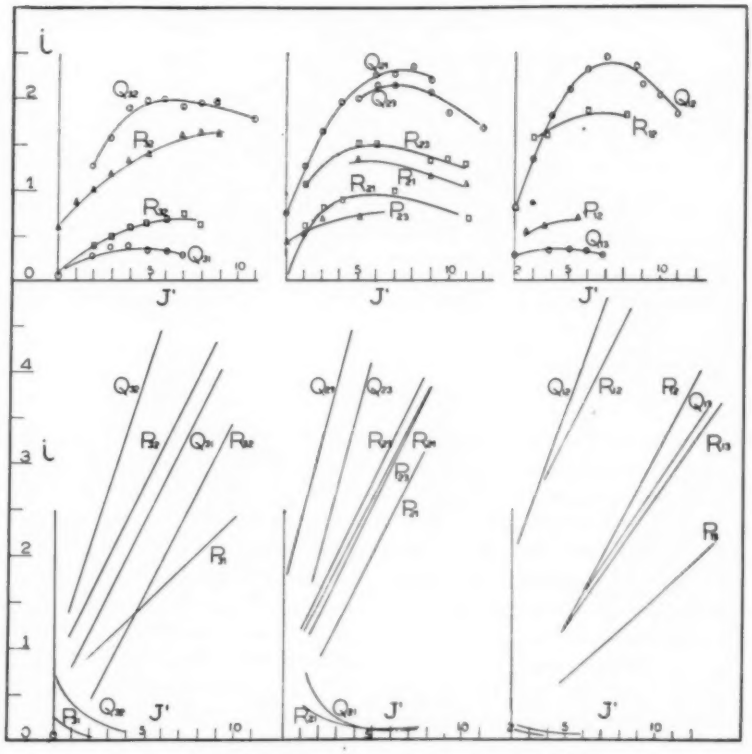

FIG. 2 (b). Intensities of satellite branches ($\Delta J \neq \Delta K$).

weaker than predicted for pure case a, becoming more so at higher values of J'. The relative order of intensity of the branches appears on the whole to be in fair agreement with theory, the outstanding discrepancies being an undue faintness of the Q_{31}, P_{23} and Q_{13} branches.

In conclusion, we have tested the validity of our experimental i factors by applying the sum rule for the final states. From Eq. (4), the sum of the i factors for all transitions to a given final state should be proportional to the weight of that level, $2J''+1$, so that

$$\sum_{J'} i/(2J''+1) = \text{const.}$$

This requirement was found to be accurately fulfilled, the average values of the constant obtained for the F_1, F_2 and F_3 levels being 1.02 ± 0.02, 1.01 ± 0.005 and 1.04 ± 0.02, respectively.

Absolute Values of the Electron Drift Velocity in Nitrogen, Helium, Neon and Argon

RUSSELL A. NIELSEN,* *Stanford University, California*

(Received September 12, 1936)

The electrical shutter method for measuring electron mobility has been employed for measurements of the electron drift velocity in nitrogen, helium, neon and argon. The values obtained experimentally as a function of X/p are compared with those computed by theoretical equations and a discrepancy is shown to exist. In every case the deviation of the experimental from the calculated curves is explained by the hypothesis that the distribution of electron velocities is such that occasional inelastic collisions occur. Under such circumstances the energy losses are greater than those calculated, and the experimental values of the electron drift velocity are thus greater than predicted by theory. It is shown, in all cases studied, that electrons of sufficient energy are present to produce the postulated excitations. Assuming such inelastic collisions, a value for the probability of excitation of electronic levels in helium, neon, and argon is calculated. The probabilities so obtained agree in order of magnitude with those given by other experiments.

AN electrical shutter method for measuring the drift velocities of electrons in gases and its application to hydrogen gas have been described in a previous paper.[1] In this method, the shutters take the form of two fine wire grids, alternate wires of which are connected to a high frequency potential. Electrons pass through the grids only when the potential between adjacent grid wires is zero, and only electrons which cross the space in one-half cycle are received at the collecting electrode. This results in a sharp maximum in the electrometer current when the drift velocity of the electrons multiplied by the time of one-half cycle is equal to the distance between the grids.

In the present paper, measurements are reported on nitrogen and the rare gases. To facilitate the taking of data on the rare gases, the constant potential but varying frequency method of obtaining measurements was employed. The oscillator was so arranged that it would develop a nearly constant voltage over a wide range of frequency. The tube potential was then set at some fixed value and the frequency adjusted until a current maximum at the electrometer was observed. Various maxima at different frequencies, corresponding to electron groups taking one-half, one, or three halves, of a cycle to traverse the distance between the grids, appeared as in the previous method. Measurements of a few values over a wide range of X/p in hydrogen gave the same values for the drift velocity as those previously obtained, thereby justifying the method of correction used with the constant frequency method.

In the rare gases at high X/p, the grid efficiency became so low (due to the high random electron energy) that the maxima became too broad and flat for accurate measurement. In order to reach higher values of X/p, a new tube was therefore constructed. The principal changes in the second tube were: first, smaller size in order to require less gas for filling; second, a thermionic source of electrons consisting of a plane grid of tungsten filaments carefully outgassed; and finally, a reduction in grid wire spacing by fifty percent. These and minor improvements made it possible to reach values of X/p more than twice those obtainable with the first tube.

In helium and argon where values were obtained from each of the tubes, the overlapping points showed that within experimental error the two tubes gave the same values for the electron drift velocity. The gas pressure in the tube was measured at room temperature (20°C) when the filaments were cold. The heating of the gas by the filaments was investigated by a thermocouple mounted between the grids. The correction was found small enough to neglect.

Nitrogen was obtained from a commercial tank of the gas and purified by passing over finely divided hot copper and through a series of traps immersed in liquid air. The rare gases were obtained in glass flasks and stated to be of greater than 99.8 percent purity, the impurity being largely helium. These gases were in conse-

* Charles A. Coffin Fellow.

[1] Bradbury and Nielsen, Phys. Rev. **49**, 388 (1936).

quence merely passed through liquid-air traps before using.

Theory

In deriving the Compton equation for the drift velocity of electrons, a Maxwellian distribution for the electron velocities is assumed. This is an assumption which is valid only when the electrons are in thermal equilibrium with the gas molecules through which they move. However, the energy of the electrons in a gas in which there is an electric field, is very much greater than the energy of the gas molecules; and increases with the strength of the applied field. Assuming that the average electronic energy is such that the electrons lose no energy by inelastic collisions, Morse, Allis and Lamar[2] have derived expressions for the electron drift velocity, and for the velocity distribution function. For constant electron-molecular collision cross section, the equation obtained reduces directly to the Compton equation with a small difference in the numerical constant. In the Morse derivation, the collision cross section enters the integral equation in such a way that it is justifiable to remove it from under the integral sign before integrating. After performing the integration, varying values of the cross section, found experimentally by Ramsauer, Normand, and others, may be substituted into the expression. The effect of the changing cross section on the velocity distribution function and on the drift velocity may then be seen. A small cross section tends to flatten the distribution curve moving its maximum to higher values. A molecular cross section increasing with increasing electron energy, tends to sharpen the distribution curve by decreasing the number of both fast and slow electrons, resulting in an increase of the number of electrons in the region of the most probable energy. Similarly, a cross section decreasing with increasing electron energy tends to flatten the distribution curve, thus extending the allowed energy of the electrons to higher values. The magnitude of these effects depends of course upon the rapidity of the variation of cross section with the electron energy. For the case of constant collision cross section, the Morse equation for the distribution of electron velocities is symmetrical about its maximum. The velocities extend from zero to approximately twice the value at the maximum. Electron energies for the fastest electrons of which appreciable numbers exist, are therefore about four times the most probable electron energy.

[2] Morse, Allis and Lamar, Phys. Rev. **48**, 412 (1935).

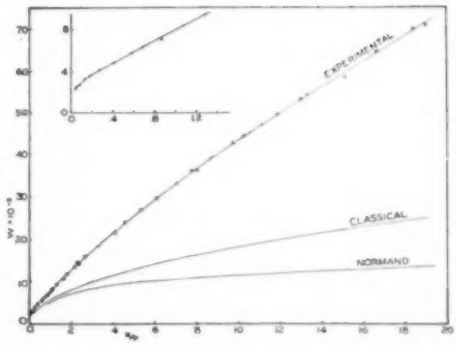

FIG. 1. Drift velocity of electrons in nitrogen as a function of X/p. Theoretical curves are shown for comparison.

Inelastic collisions, if they occur, will affect both the energy distribution function and the drift velocity of the electrons. The inelastic impacts will increase w, the drift velocity by increasing f, the average fraction of its energy which an electron loses at a collision, since w is proportional to $f^{\frac{1}{2}}$. Qualitatively this is due to the fact that inelastic collisions reduce the random energy of the electrons, thus permitting the applied electric field to be more effective.

Experimental Results

Nitrogen

In Fig. 1 is presented a summary of the experimental values for the electron drift velocity in nitrogen as a function of X/p obtained by using the same method and technique as employed in making the measurements on hydrogen.[1] A comparison between theory and experiment is also shown. The curve marked "classical" is obtained by substituting into the Compton equation the ordinary kinetic theory value of the molecular cross section. If, instead of this cross section one uses the Ramsauer cross section for each value of X/p, as obtained from the experiments of Townsend[3] and of Normand,[4] the curve marked "Normand" is obtained. The

[3] J. S. Townsend, J. Frank. Inst. **200**, 563 (1925).
[4] C. E. Normand, Phys. Rev. **35**, 1217 (1930).

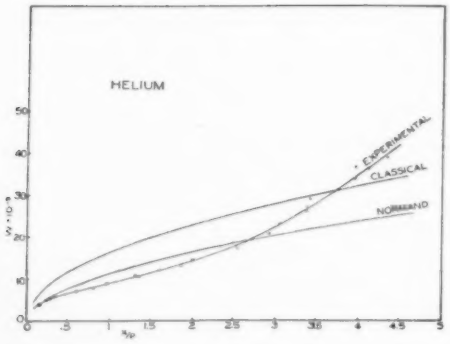

FIG. 2. Drift velocity of electrons in helium as a function of X/p. Theoretical curves are shown for comparison.

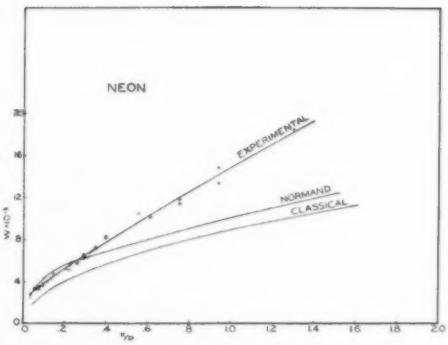

FIG. 3. Drift velocity of electrons in neon as a function of X/p. Theoretical curves are shown for comparison.

experimental curve is seen to lie above the calculated curves throughout the range of the experiment. This departure, as in the case of hydrogen[1] is ascribed to the energy losses of the electron in exciting the first level of the nitrogen molecule. At an X/p of 0.25, Townsend gives the average value of the electron energy as 0.29 volt, which is the energy of the first vibrational level in nitrogen. The experimental curve therefore should rise above the calculated ones at values of X/p greater than 0.25 due to the electronic energy losses caused by excitation of the first vibrational level in nitrogen. This is seen to be the case.

In hydrogen at an X/p of 19, where the electron energy is approximately five times the energy of the first vibrational level, the experimental drift velocity is greater than that calculated from the Ramsauer cross sections by a factor of 2.1. In nitrogen at an X/p of 4.0 where the electron energy is again five times the energy of the first vibrational level, the experimental value of the drift velocity is greater than that calculated from the Ramsauer cross sections by a factor 2.3. The correlation is good and indicates that the same process is responsible in both cases for the rise of the experimental curves above the calculated ones. At an X/p of 20 in nitrogen, the average electron energy is 2.2 volts. At this X/p, the fastest electrons in the velocity distribution may have energies greater than the excitation energy of the first electronic level of the nitrogen molecule at 6.14 volts. Energy losses from electronic excitations may therefore be a contributing factor in raising the experimental curve above the calculated ones at the high values of X/p.

To justify the assumption that the deviation of the experimental curve from the one calculated from the Ramsauer cross sections is due to the excitation of vibrational levels in the molecules, experiments were undertaken upon the rare gases where vibrational levels do not exist. Under these circumstances it is to be expected that the experimental curves will follow the calculated ones as long as energy losses do not occur as a result of the excitation of electronic levels in these gases. Since the electron is able to lose only the classical momentum transfer amount of energy at a collision, it will continue to gain energy from the field until the average energy loss per collision equals the average energy gain from the field in a mean free path. Thus, for the same X/p, the electron energy will be very much greater in the monatomic than in the diatomic gases since in the latter the electron energy is kept at low values by the inelastic collisions which excite vibrational levels.

Helium

In Fig. 2 are shown the experimentally determined values for the electron drift velocity in helium as a function of X/p. These values were obtained by the constant potential method. A comparison between theory and experiment is also given. The experimental curve is seen to follow the theoretical curve, obtained from Normand's values for the cross section, up to an X/p of 2.25 at which point it deviates markedly. The electron energy at this X/p is given by

Townsend as 4.25 volts. For constant cross section, according to the distribution function of electron velocities given by Morse, Allis and Lamar, the value of the energy of the fastest electrons is 16 or 17 volts. However, the cross section for helium[4, 5] in this range of X/p is decreasing with increasing electron energy. Therefore the distribution function will be flattened and elongated on the high energy side. Thus it may be assumed that the fastest electrons have energies of 19 or 20 volts which makes them energetically able to excite the first electronic level of helium at 19.77 volts. The rise of the curve at higher X/p is then due to the increasing number of electrons having suitable energy for such excitations.

Neon

In Fig. 3 the experimentally determined values for the electron drift velocity in neon are shown together with a comparison between theory and experiment. The experimental curve departs almost at once from the calculated curves and again this departure is ascribed to excitation. At an X/p of only 0.4 Townsend gives the electronic energy as 4.3 volts. The cross section of neon in this range of electron energy is slowly rising and leveling off at higher energies. One would therefore expect the fast electrons to have energies of the order of 16 volts. However, 16.58 volts is the first excitation potential of neon, so at this X/p inelastic collisions should begin to occur. At slightly higher X/p where the electron energy as given by Townsend rapidly increases, excitation will become much more probable. Thus the experimental curve lies increasingly above the calculated ones at values of X/p greater than 0.4.

Argon

In Fig. 4 the experimentally determined values for the electron drift velocity in argon are shown together with a comparison between theory and experiment. In the energy range of this experiment, the collision cross section of argon rapidly increases with increasing electron energy. This results in a distribution of electrons with energy very nearly that of the most probable value. The argon experimental curve follows the "Normand" curve quite well up to an X/p of about 1.75 at which it changes its trend by bending upward. Townsend gives the energy of the electrons at this X/p as 11.1 volts, which is nearly the excitation potential of argon (11.57 volts). At this X/p inelastic collisions should occur and produce the bending up of the experimental curve as is observed.

[5] R. B. Brode, Rev. Mod. Phys. **5**, 257 (1933).

Discussion

From the above data it is seen that the experimental curves agree well with those calculated from the Ramsauer values for the molecular and atomic cross sections. Where deviations occur, they may in all cases be associated with electron energy losses greater than those given by classical momentum transfer. In every case studied it is shown that sufficient energy is available for inelastic collisions. These collisions produce excitations of the vibrational levels in the case of hydrogen and nitrogen, and excitation of the electronic levels in the case of the monatomic gases, helium, neon, and argon.

Loeb[6] and Wahlin[7] have measured electron mobilities in helium and nitrogen at $X/p=0.5$ using high pressures and the Rutherford alternating current method. These results are in good agreement with the data reported here over the narrow range where comparison is possible. Townsend[3] and his students have measured the random velocity of electrons by diffusion methods, simultaneously measuring the electron drift velocity by deflecting the moving electrons in a magnetic field. The apparatus of Townsend

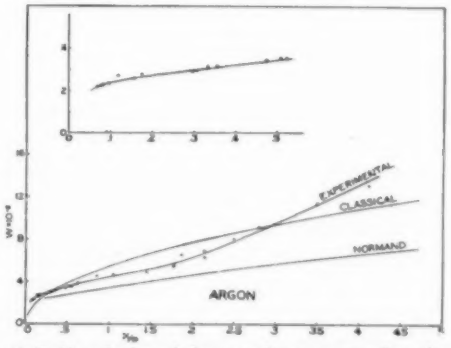

FIG. 4. Drift velocity of electrons in argon as a function of X/p. Theoretical curves are shown for comparison.

[6] L. B. Loeb, Phys. Rev. **19**, 24 (1922).
[7] H. B. Wahlin, Phys. Rev. **23**, 169 (1924).

and Bailey[8] could be evacuated only to a pressure of approximately 0.01 mm of mercury. This permits the presence in the gas of a considerable amount of impurity, small traces of which can produce effects greatly out of proportion to their concentration. Townsend's values for the electron drift velocity agree reasonably well with those here presented. Greater discrepancies exist in the case of the rare gases which may presumably be ascribed to the presence of impurity in their gas, inasmuch as Townsend and Bailey observed that the values which they obtained for the electron drift velocity in argon were strongly dependent upon the length of time of purification.

The only available experimental values of the random electron energy as a function of X/p are those of Townsend. These have been used in the above comparison of theory with experiment. It may be noted in justification of this procedure that first, Townsend's values for the electron energy agree reasonably well with those calculated where inelastic collisions do not occur; secondly, where inelastic collisions do occur, as in argon, the electron energy given by Townsend increases rapidly with X/p and then flattens off. The magnitude of the energy at this turning point is closely that of the first excitation potential of argon. Finally it may be noted that the collision cross section in many cases over these energy ranges is not strongly energy dependent.

Few measurements have been made upon the probability of electronic excitation at a collision.[9, 10] Various values have been obtained which give only the order of magnitude of the probability; in helium experimental values ranging from 0.03 to 0.001 are given. An order of magnitude value for the excitation probability in helium, neon and argon can be obtained from the measurements here presented. At an X/p of 1.2 in neon, the energy of the electrons is 8.75 volts, and f, the average fraction of its energy which an electron loses at a collision, as obtained from the curves in Fig. 3 is 5.7 $(2m/M)$. The classical value of the energy loss per collision is $2m/M$ times the average energy or for neon, about 4.8×10^{-4} volt. Inelastic collisions must therefore account for about 4.7 times this much energy loss or 22.6×10^{-4} volt. At an inelastic collision an electron must lose at least 16.58 volts. Let k be the fraction of the electrons having over 16.58 volts energy, and p be the probability for excitation at a collision; then $16.58\ kp=22.6\times10^{-4}$. Using the velocity distribution function of electrons as given by Morse, Allis and Lamar, it is seen that for the maximum of the distribution function at an energy of 8.75 volts, 0.11 of the electrons will have energy greater than 16.58 volts. This gives $p\sim0.001$. This calculation assumes a constant cross section for neon which is not greatly in error. If a slightly increasing cross section is used, the change in the percentage of electrons over 16.58 volts is small but will tend to increase p slightly. Performing a similar calculation in the case of helium for an X/p of 4.5 where the average electron energy is 6.1 volts and f is $7.35(2m/M)$, one obtains $p=5.47\times10^{-4}/k$. For constant cross section k is about 0.003 resulting in $p\sim0.2$. Actually the distribution curve flattens and extends to higher energies for cross sections decreasing with increasing electron energy (as in helium). More high energy electrons are thus available than given by the Morse, Allis and Lamar distribution function. At an X/p of 4.5 only a very small percentage of the electrons have an energy of more than 19.77 volts. Hence any change in the distribution function of the electrons greatly changes the percentage of electrons in excess of this value, and increases k accordingly. Therefore the above value of p is an upper limit, and more probably has a value ~0.01. Performing a similar calculation in the case of argon for an X/p of 4 where the average electron energy is 11.5 volts and f is $16(2m/M)$, one obtains $p=0.0004/k$. In argon at this X/p, k is ~0.5. Therefore $p\sim0.001$. It is to be noted that the p here considered is not the probability of excitation of only the first resonance level but is an integrated effect over all the levels that may be excited and over a comparatively narrow range of electron energy.

The experiments are being continued in other gases in some of which dissociation processes and negative ion formation are possible. The author desires to thank Professor N. E. Bradbury for his help throughout this research, and the Faculty Research Committee of Stanford University for a grant-in-aid.

[8] Townsend and Bailey, Phil. Mag. **42**, 873 (1921); **44**, 1033 (1922).
[9] G. Hertz, Zeits. f. Physik **32**, 298 (1925).
[10] E. G. Dymond, Proc. Roy. Soc. **A107**, 291 (1925).

The Complete Equation of State of One, Two and Three-Dimensional Gases of Hard Elastic Spheres

LEWI TONKS, *Research Laboratory, General Electric Company, Schenectady, N. Y.*

(Received August 3, 1936)

Equations of state have been derived for one, two and three-dimensional gases of hard elastic spheres of finite size. *For the linear gas* the phase integral is directly integrable, and by using the virial the equation was found to be $fl=NkT/(1-\theta)$, f being the force of the gas, l the length of the gas, N the total number of atoms, and θ the fraction of the gas length occupied by the atoms themselves. By two tests a *linear gas consisting of a single atom was found on a time average basis to obey statistical laws*, the first showing that the equation of state is unchanged if l be subdivided into N equal compartments with an atom in each; and the second showing that the length of the single atom gas consisting of one atom bounded by its two neighbors obeys the Boltzmann equation. This is significant for the Debye-Hückel theory of electrolytes. *For the plane gas,* Boltzmann's method of correcting the virial is used for low θ, the fraction of the surface which would be covered in close triangular packing, giving $\tau a=NkT(1+1.814\,\theta+2.573\,\theta^2+\cdots)$, where τ is the surface tension and a the area of the gas. For θ near unity, a combination treatment involving both the virial and an extension of the concepts developed for one dimension leads to $\tau a=NkT/(1-\theta^1)$. The adsorption isotherm of the plane gas is derived from the equation of state and is compared with those for films in which the adatoms occupy fixed positions on the surface. *In three dimensions* the same methods give $pv=NkT(1+2.962\theta+5.483\theta^2+\cdots)$ and $pv=NkT/(1-\theta^1)$, respectively. Expressions which match these near $\theta=0$ and $\theta=1$ but cover the complete range are given.

THE exhaustive investigations carried on in this laboratory concerning the behavior of monatomic films of caesium on tungsten[1] have led to the need of deriving the equation of state of a two-dimensional gas. The nature of the forces between the particles themselves and between the particles and the underlying solid surface is important for the actual cases, but it is of value to know what can be expected in the simplest case, that of the classical hard elastic spheres. Equations of state are derived on this basis in the present paper, not only for low concentrations of the gas but for concentrations approaching the maximum possible; that is, close packing of the particles. For that condition it was necessary to employ ideas based on an analysis of the one-dimensional case. These ideas also made an extension of the analysis to three dimensions possible.

Aside from the specific results which formed the objective of the inquiry, two others of special interest have been developed; first, an actual integration in generalized positional space of a simple one-dimensional case with excluded regions, and second, a theoretical justification for the application of certain statistical concepts on a time-average basis to a gas containing only a single atom.

[1] J. B. Taylor and I. Langmuir, Phys. Rev. **44**, 423 (1935).

1. The Equation of State of a Two-Dimensional Gas for Low Concentrations

By using the virial of Clausius the equation of state of a three-dimensional gas can be written[2]

$$pv=NkT+\tfrac{1}{3}\sum r\varphi(r), \qquad (1)$$

where $\varphi(r)$ is the repulsive force between two atoms at a distance r and the summation extends over all pairs of atoms. A similar derivation in two dimensions yields[3]

$$\tau a=NkT+\tfrac{1}{2}\sum r\varphi(r), \qquad (2)$$

τ being the surface tension and a the area of the two-dimensional gas.

Since the centers of two hard spherical atoms of diameter σ cannot approach closer than σ to each other, it is as if each center were surrounded by a sphere of radius σ which is impervious to the center of all other atoms. Such an imaginary sphere will be called an exclusion sphere. In two dimensions it becomes an exclusion circle and in one dimension an exclusion length. It is convenient for analytical purposes to replace the gas of finite atoms by the corresponding gas of point masses each carrying its exclusion figure.

For the three-dimensional case Jeans gives a

[2] Jeans, *Dynamical Theory of Gases*, 4th edition, §164.

[3] This equation was originally stated by I. Langmuir, J. Am. Chem. Soc. **54**, 2798 (1932), Eq. (56).

derivation of the expression

$$\sum r\varphi(r) = 2\pi N^2(1+\beta)\sigma^3/2hv, \qquad (3)$$

where $2h = 1/kT$ and β is a density correction.

Although some such correction as indicated by β is necessary, the explanation which Jeans gives of its origin is misleading. It is not possible, as he implies, that a decrease in density over a finite volume due to repulsive forces should result in a finite increase in density throughout an infinite volume. Nor is this interpretation borne out by his reference to Boltzmann.[4] With $\beta = 0$, Eq. (3) is a first-order approximation for small N/v. The second order involves corrections to both numerator and denominator. β will, therefore, be dropped, and these corrections will be calculated separately.

The derivation of Eq. (3) will not be reproduced here. It depends upon the assumption that $\varphi(r)$ is zero beyond a distance $\sigma + d\sigma$ and is so great within the infinitesimal zone between σ and $\sigma + d\sigma$ that no atoms approach each other within the distance σ. Analysis of the derivation shows that the expression for $\sum r\varphi(r)$ can be broken down into the independently significant factors,

$$\sigma N(\tfrac{1}{2})(4\pi N\sigma^2 d\sigma/v)(kT)(d\sigma)^{-1}. \qquad (4)$$

The meaning of most of the factors is self-evident: σ, the particle diameter, N the total number of particles, $\frac{1}{2}$ to eliminate duplication in enumerating colliding pairs, kT the thermal energy factor, $d\sigma^{-1}$ the collision zone thickness, which cancels out. The fourth factor gives the probability that a particular particle A will be found in the collision zone of some (meaning "any") other atom, neglecting the repulsive force operating there. Its numerator is the total volume of collision zones; its denominator is the whole volume in which the center of A may lie.

The first-order corrections to each of these was made by Boltzmann[4] for the three-dimensional gas, and Fowler[5] gives the method for any degree of approximation. Here we shall adapt what is essentially Boltzmann's method to two dimensions. The reasoning, although different in detail, is fundamentally the same and leads to the same results. Exclusion circles replace exclusion spheres, the collision zone of an atom is $2\pi\sigma d\sigma$ instead of $4\pi\sigma^2 d\sigma$, and a replaces v, so that

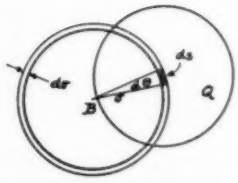

FIG. 1. Calculation of collision probability.

$$\sum r\varphi(r) = \tfrac{1}{2}\sigma N(2\pi N\sigma d\sigma/a)kTd\sigma^{-1}. \qquad (5)$$

The probability that the particular atom A lies with its center in an element $ds = \sigma d\theta d\sigma$ of the collision zone of a particular atom B, as shown in Fig. 1, is ds/a to a first approximation. To the next approximation the probability is higher than this because to a certain extent B shields ds from the presence of other atoms whose exclusion circles might cover it. When ds is so covered, the probability of a ds collision is zero. When it is not so covered, the probability is ds/a' where

$$a' = a - \pi N\sigma^2$$

is the total nonexcluded area. Now ds lies in an exclusion circle if some other atom is centered within the circle Q of radius σ about ds as center. But of this circle only the portion of the area lying outside of B's exclusion circle, amounting to $\sigma^2(\pi/3 + 3^{\frac{1}{2}}/2)$ is free to be occupied by a possible collision-preventing atom, so that the probability that ds is covered by an exclusion circle is

$$(\pi/3 + 3^{\frac{1}{2}}/2)N\sigma^2/a,$$

and the probability that it is free for the A collision is

$$1 - (\tfrac{1}{3} + 3^{\frac{1}{2}}/2\pi)\pi N\sigma^2/a.$$

Multiplying by ds/a', the collision probability, and by N, the number of atoms which can fill the role of B, and integrating over-all values of θ from zero to 2π, the probability-of-impact factor of Eq. (5) becomes

$$\frac{2\pi N\sigma d\sigma}{a}\,\frac{[1 - (\frac{1}{3}) + 3^{\frac{1}{2}}/2\pi)\pi N\sigma^2/a]}{1 - \pi N\sigma^2/a}.$$

The introduction of $\psi = \pi N\sigma^2/a$ and simplifica-

[4] *Vorlesungen über Gas Theorie*, V. 2, §51.
[5] R. H. Fowler, *Statistical Mechanics*, §8–31.

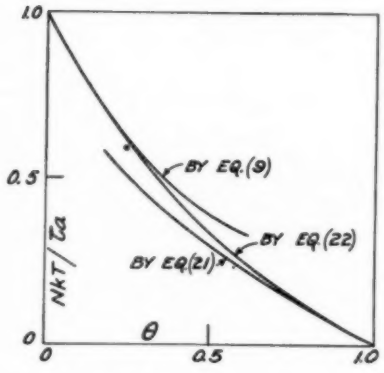

FIG. 2. Equation of state of two-dimensional gas.

tion converts this to

$$(2\psi d\sigma/\sigma)[1+(\tfrac{2}{3}-3^{\frac{1}{2}}/2\pi)\psi]$$

and $\frac{1}{2}\sum r\varphi(r)=(\psi/2)NkT[1+\frac{2}{3}-3^{\frac{1}{2}}/2\pi)\psi]$. (6)

If the N atoms were arranged in triangular close packing, they would occupy a minimum area, $3^{\frac{1}{2}}N\sigma^2/2$ in extent. The fraction of the surface covered, expressed by θ, is defined as the ratio of this area to the actual area a.

$$\theta=3^{\frac{1}{2}}N\sigma^2/2a. \tag{7}$$

Accordingly, $\psi=2\pi\theta/3^{\frac{1}{2}}=3.628\theta$. (8)

For the equation of state we therefore have from Eqs. (6) and (2)

$$\begin{aligned}\tau a &= NkT[1+\pi 3^{-1}\theta+(4\pi^2/9-3^{-1}\pi)\theta^2] \\ &= NkT(1+1.814\theta+2.573\theta^2).\end{aligned} \tag{9}$$

The parenthesis gives the departure from the perfect gas law. Its reciprocal is plotted against θ in Fig. 2.

Successive coefficients of the power-series multiplier of NkT could undoubtedly be evaluated according to the method given by Fowler, but the task would become increasingly complicated and, in any case, since we recognize that $\tau=\infty$ at $\theta=1$, the series would fail to converge. The problem must be faced from the other direction.

Near $\theta=1$ it is readily perceived that the atoms form an approximate triangular lattice in which each atom center finds itself hemmed in by a hexagonal boundary formed by short arcs of the exclusion circles of its six neighbors. It is evident that, except for rare extreme motions of a large number of adjacent atoms, these hexagons are equiangular to a first approximation, but that they are not equilateral; that, in fact, it will frequently happen that one or more sides will momentarily shrink to zero. Only rarely will a particular hexagon expand sufficiently to allow the imprisoned atom to escape to a new position, another taking its place; and this will happen the less frequently the closer θ approaches unity. It is therefore allowable to ignore this contingency and consider that any particular atom A is continuously confined to its hexagonal space.

The probability that A is in collision with one of its neighbors is $qd\sigma/S$, q being the perimeter and S the area of A's hexagon; but knowledge of what average values to use for S and q is lacking because of the constant variation of both which accompanies the atom motions. Some progress could be made by introducing an arbitrary scale factor now, but this will be postponed until a new fundamental idea has been developed by a statistical analysis of a linear gas.

2. Statistical Analysis of a Linear Gas

Consider a set of N atoms, $A_1, A_2, \cdots A_n$, of diameter σ constrained to move along a line between two fixed boundaries at a distance l apart. Let the position of A_k be x_k. Since the velocity coordinates are independent of the positional, and since we are interested only in the latter, we can leave the velocities out of consideration. Now the possible values of x_k are restricted, both by the boundaries and by the finite size of the other atoms. The conditions imposed on the atom positions are

$$\sigma/2\leqq x_k\leqq l-\sigma/2, \quad |x_k-x_j|\geqq\sigma. \tag{10}$$

If the phase of the system be represented by a point in N dimensional space, these conditions mark off regions from which the representative point is excluded.

It is evident that whatever sequence the atoms are in remains fixed for all time; but all sequences, $N!$ in number, are possible *a priori*. In terms of the N-dimensional space, the excluded regions form partitions which divide the N-dimensional cube defined by (10) into $N!$

completely separated compartments. As we are interested in the behavior of a given system in the course of time, we shall without loss of generality number the atoms from 1 to N in the order that they actually occur, thereby establishing the more restricted conditions

$$\sigma/2<x_1, \quad x_1<x_2-\sigma, \quad x_2<x_3-\sigma, \quad \cdots x_N<l-\sigma/2 \quad (11)$$

which leave only one of the former $N!$ compartments as a permitted region.

In general, the statistical theory of equilibrium in the absence of external fields is based on the condition that the representative points of a large number of identical systems chosen at random at some instant are uniformly distributed throughout the permitted portions of the generalized positional space. As for one of these systems, in the course of time its representative point moves continuously through this space. Its motion may be such that its sequence of positions taken at equal short time intervals has a nonuniform distribution in the space. We assume that this is true only of a negligible fraction of the systems, and that the successive positions of all the rest differ only infinitesimally from a random distribution.[6]

With reference to the particular case under discussion, such an assumption can only apply within the single permitted region established in the next to the last paragraph, for with a number of unconnected permitted regions, a representative point would in the course of time give a distribution confined to only one compartment.

Various combinations of the conditions restricting the coordinates can be made; those that are useful will depend upon the way integrations are carried out. For instance, the successive elimination of x_1, x_2, x_3, etc., to give

$$\sigma/2<x_1, \quad 3\sigma/2<x_2, \quad 5\sigma/2<x_3, \quad \cdots (2N-1)\sigma/2<x_N$$

together with Eq. (11) will be employed in the first integration below.

Let the uniform density of a very large number of successive positions of the representative point be ρ. The total number of point positions is

$$M_N=\rho\int_{(2N-1)\sigma/2}^{l-\sigma/2}\cdots\int_{3\sigma/2}^{x_3-\sigma}\int_{\sigma/2}^{x_2-\sigma}dx_1dx_2\cdots dx_N. \quad (11.5)$$

The multiple space integral is readily evaluated as an N-dimensional volume and

$$M_N=\rho(l-N\sigma)^N/N!.$$

The distribution of point positions, $\rho_{N-1}dx_N$, relative to x_N is found by stopping short of the last integration:

$$\rho_{N-1}dx_N=\rho dx_N\int_{(2N-3)\sigma/2}^{x_N-\sigma}\cdots\int_{\sigma/2}^{x_2-\sigma}dx_1dx_2\cdots dx_{N-1}$$
$$=\rho dx_N[x_N-(N-\tfrac{1}{2})\sigma]^{N-1}/(N-1)!$$

And the probability distribution of x_N is

$$P(x_N)dx_N=\rho_{N-1}dx_N/M_N$$
$$=Ndx_N[x_N-(N-\tfrac{1}{2})\sigma]^{N-1}/[(l-N\sigma)^N].$$

We can suppose the boundary at l to be a fixed atom A_{N+1} like the others with center at $l+\sigma/2$. The distance δ_1 between centers of A_{N+1} and A_N would be

$$\delta_1=l+\sigma/2-x_N\geq\sigma.$$

As this distance is more significant than x_N we eliminate the latter, at the same time introducing $\theta=N\sigma/l$ the fraction of the line occupied by atoms. This gives

$$P(\delta_1)d\delta_1=\frac{N}{l(1-\theta)}\left[1-\frac{\delta_1-\sigma}{l(1-\theta)}\right]^{N-1}d\delta_1, \quad \delta_1\geq\sigma, \quad (12)$$

an exact expression for the probability distribution of the end atom among a total of N.

If we use the linear density of atoms $n=N/l$ to eliminate l and allow N to approach infinity we find

$$P(\delta_1)d\delta_1=[n/(1-\theta)]\epsilon^{-n(\delta_1-\sigma)/(1-\theta)}d\delta_1, \quad \delta_1\geq\sigma. \quad (13)$$

$P(\delta_1)d\sigma$ at $\delta_1=\sigma$ is the probability of collision between A_N and the boundary. Its value is $[n/(1-\theta)]d\sigma$. It is greater by virtue of θ than for infinitesimal atoms. The $(1-\theta)^{-1}$ in the exponent shows a correspondingly more rapid

[6] See Jeans, *Dynamical Theory of Gases*, 4th edition, §125ff. Also R. H. Fowler, *Statistical Mechanics*, §1–4.

decrease in probability of large separations. The net result is to give for the mean value of δ_1

$$\bar{\delta}_1 = \int_{\sigma}^{\infty} \delta_1 P(\delta_1) d\delta_1 = 1/n,$$

which is the average separation of adjacent atoms for the whole array and is independent of particle size. That this should be so is not evident *a priori*, since one atom A_{N+1} of the two for which Eq. (13) was derived was fixed in position. But a direct integration for the density in generalized space of

$$\delta_1' = x_{k+1} - x_k$$

gives the same probability distribution for δ_1' as for δ_1. The general conclusion is that the probability distribution of the distance between a pair of adjacent atoms is the same no matter where they are located with respect to the boundary or even if one of them forms a boundary.

An immediate consequence of Eq. (13) is that the equation of state of the linear gas can be calculated. Reasoning similar to that which gave Eq. (2) gives

$$fl = NkT + \sum r\varphi(r)$$

for the force length product. In evaluating $\sum r\varphi(r)$, it is to be noted that an atom A_k can only collide with its two neighbors. The probability of this twofold chance is $[2n/(1-\theta)]d\sigma$ from Eq. (13). This is to be multiplied by $\frac{1}{2}\sigma NkTd\sigma^{-1}$ just as in the two-dimensional case, whence

$$\sum r\varphi(r) = n\sigma NkT/(1-\theta) = \theta NkT/(1-\theta)$$

and

$$fl = NkT/(1-\theta). \tag{14}$$

In the form $f[(1-\theta)l] = NkT$

we can give the equation of state the simple interpretation that product of force by unoccupied length of line equals NkT. Or applying it to a single atom confined to a length l_1 gives

$$f = kT/(1-\theta)l_1, \tag{15}$$

which states that the single atom acting as a gas exerts a force equal to kT divided by the length of its excursions; and although the immediate derivation is not rigorous because Eq. (14) was derived on the assumption that N is large, the end result can be confirmed by applying Eq. (12) directly.

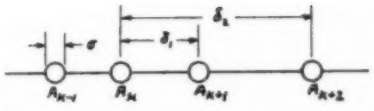

FIG. 3. Relation of atoms in one-dimensional gas.

Thus the force due to the N atoms is the same as that which would result if the line were subdivided into N equal compartments, each containing a single atom.

The separation δ_2 of two adjacent-but-one atoms is of particular interest for present purposes, for they form the boundary of a single-atom gas in the linear gas much as the six neighbors of atom A of the two-dimensional gas do in the plane case. The probability distribution can be found by the change of variable in the phase integral of Eq. (11.5) from x_k to $x_{k+2} - \delta_2$, but more conveniently it can be found directly from δ_1. Referring to Fig. 3, Eq. (13) tells us that the probability of conjointly finding A_{k+1} at a distance δ_1 (within $d\delta_1$) and A_{k+2} at an additional distance $\delta_2 - \delta_1$ (within $d\delta_2$) is

$$[n^2/(1-\theta)^2]\epsilon^{-(\delta_1-\sigma)n/(1-\theta)}\epsilon^{-(\delta_2-\delta_1-\sigma)n/(1-\theta)}d\delta_1 d\delta_2.$$

The distribution of δ_2 is given by the integral of this over all possible values of δ_1, namely from σ to $\sigma_2 - \sigma$. It is

$$P(\delta_2)d\delta_2 = (\delta_2 - 2\sigma)n^2/(1-\theta)^2\epsilon^{-(\delta_2-2\sigma)n/(1-\theta)}d\delta_2. \tag{16}$$

The importance of this expression lies in its derivability on quite another basis. Let us treat the atom A_{k+1} as a gas confined with the boundaries $x_k + \sigma/2$ and $x_{k+2} - \sigma/2$, upon which the gas consisting of all other atoms exerts the gas force

$$f_2 = nkT/(1-\theta).$$

The atom A_{k+1} can move through a distance $\delta_2 - 2\sigma$ and hence the outward force with which it resists compression by the other atoms is

$$f_1 = kT/(\delta_2 - 2\sigma)$$

from Eq. (15). Let us now apply the Boltzmann equation to the whole system considered as composed of the above two portions. The work

done in increasing δ_2 is

$$W=\int_c^{\delta_2}(f_2-f_1)d\delta_2$$

$$=kT\left[(\delta_2-c)\frac{n}{(1-\theta)}-\ln\frac{\delta_2-2\sigma}{c-2\sigma}\right],$$

where c is a constant of integration, so that the distribution of the coordinate δ_2 is

$$P(\delta_2)d\delta_2=\epsilon^{-W/kT}d\delta_2$$

$$=(\delta_2-2\sigma)/(c-2\sigma)\epsilon^{-n(\delta_2-c)/(1-\theta)}d\delta_2. \quad (17)$$

When c is evaluated by

$$\int_{2\sigma}^{\infty}P(\delta_2)d\delta_2=1$$

Eq. (17) becomes identical with Eq. (16).

The significance of this result is the additional confirmation beyond Eq. (15) that statistical relations apply to the time average of single particle relations. There is no reason to expect that this generalization is valid in one dimension only. It lends theoretical justification to the Debye-Hückel theory of electrolytes which depends directly upon the use of time averaging over a few particles in place of instantaneous averages over a large number of particles. It also gives the means for solving the present problem.

3. Equation of State of a Two-Dimensional Gas at High Concentrations

Let us extend the implications of Eq. (15) to a concentrated plane gas by dividing the area into N equal regular hexagonal compartments (neglecting boundary adjustments) as shown in Fig. 4, and placing one atom in each. The length s is a measure of the incompleteness of coverage. Let n be the number of atoms per unit area It is readily found that

$$s/\sigma=(1-\theta^{\frac{1}{2}})/\theta^{\frac{1}{2}}, \quad \sigma+s=2^{\frac{1}{2}}3^{-\frac{1}{4}}n^{-\frac{1}{2}},$$

$$s=2^{\frac{1}{2}}3^{-\frac{1}{4}}n^{-\frac{1}{2}}(1-\theta^{\frac{1}{2}}).$$

The area accessible to each atom center is that of the small hexagon of the figure, namely, $A=3^{\frac{1}{2}}s^2/2$. The tension exerted on the boundaries is, by

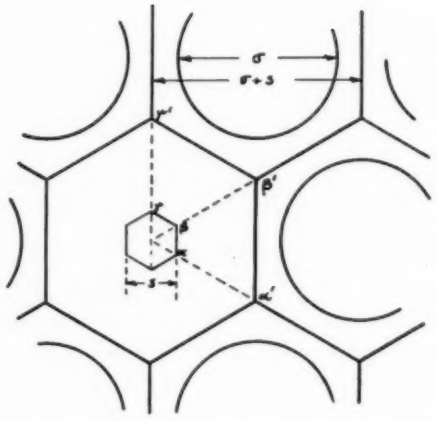

Fig. 4. Partitioning of concentrated two-dimensional gas.

analogy with Eq (15),

$$\tau_1=kT/A \quad (18)$$

and the force on one side of length $3^{-\frac{1}{4}}s$ will be

$$F_{\alpha\beta}=(2/3)kT/s,$$

which is transmitted across the compartment side $\alpha'\beta'$ so that

$$F_{\alpha'\beta'}=(2/3)kT/s$$

also. The force across $\beta'\gamma'$ is the same, but its horizontal component $F_{\beta'\gamma'}$ is only one-half this. Together, the two give the total force F_1 of a single row of atoms:

$$F_1=F_{\alpha'\beta'}+F_{\beta'\gamma'}=kT/s.$$

Two factors of uncertainty are involved in this expression. The first arises from the choice of the size of small area to be used in Eq. (18). Unlike the linear case the excursions of the particles from the regular lattice positions apparently decrease the total space accessible to other atoms. Thus A may not be the correct choice of area, but whatever that area may be it will bear a constant ratio to A, independent of s and σ. The second factor arises from the use of a regular hexagon when it is known that the hexagon is in general of nonequal sides. Thus the average value of $\alpha\beta$ may not be $3^{-\frac{1}{4}}s$. It will, however, bear a constant relation to this.

As only the quotient of these two factors is involved, only one unknown numerical multiplier

μ need be introduced to correct the expression for F_1 so that

$$F_1=\mu kT/s.$$

Since a single row of atoms occupies a transverse length of $3^{\frac{1}{2}}(s+\sigma)/2$, the force per unit length of the gas is

$$\tau=2\cdot 3^{-\frac{1}{2}}\mu kT/[s(s+\sigma)]=\mu nkT/(1-\theta^{\frac{1}{2}}). \quad (19)$$

This is the equation of state. It contains the undetermined numerical coefficient μ which we attempt to evaluate by an alternative calculation based on the virial.

For the two-dimensional gas, in view of the preceding discussion,

$$\sum r\varphi(r)=\sigma N(1/2)6(P_c d\sigma)kTd\sigma^{-1},$$

where $P_c d\sigma$ is the probability of a selected atom A being in collision with a particular neighbor; 6 is the number of neighbors and hence the number of possible colliding pairs involving atom A; and N is the total number of atoms which could be chosen for A.

The same small hexagon as before can be used as a basis for calculating P_c. For it P_c is $2/(3s)$, but the same uncertainties that required the introduction of μ are involved. This time introducing a numerical factor η to take care of these

$$\sum r\varphi(r)=2\eta\sigma NkT/s$$

and for the equation of state, by Eq. (2)

$$\tau a=NkT(1+\eta\sigma/s)$$
$$=NkT[1+(\eta-1)\theta^{\frac{1}{2}}]/(1-\theta^{\frac{1}{2}}). \quad (20)$$

Only if $\mu=1$, $\eta=1$ can both Eq. (19) and Eq. (20) be satisfied. Unfortunately, however, neither equation is exact and both are valid only to the first degree in $1-\theta$. Equality of the two to this approximation requires simply that $\eta=\mu$, and only if it could be proved that there was equality to the second degree in $1-\theta$ would η and μ be limited to unity. But such a proof appears to be extremely difficult.

A consideration which renders it probable that $\eta=\mu=1$ and that consequently

$$\tau a=NkT/(1-\theta^{\frac{1}{2}}), \quad (21)$$

is that this law holds for atoms in a square array. In this case reasoning based on the double approach already used leads to results identical with Eqs. (19) and (20) with the understanding, of course, that θ now refers to coverage in a square array so that actually for the same density θ will be larger. But the result can be found directly from the linear chain calculations. Any row of atoms constitutes a linear gas with $n^{\frac{1}{2}}$ atoms per unit length, and by Eq. (14) the thrust of the row is $n^{\frac{1}{2}}kT/(1-\theta^{\frac{1}{2}})$. Since there are $n^{\frac{1}{2}}$ rows per unit length, Eq. (21) follows directly. This is rigorous. The atoms would certainly tend to assume a triangular arrangement, but in actual cases surface binding forces might tend to hold them in squares; and for the present a square boundary can be assumed which confines the atoms so closely that they cannot rearrange themselves.

A smooth curve for the complete range from $\theta=0$ to unity can be obtained by using for $NkT/\tau a$ of Fig. 2 the formula

$$\frac{NkT}{\tau a}=\frac{1-1.307\theta^3+0.307\theta^4}{1+1.814\theta+2.573\theta^2}. \quad (22)$$

The coefficients of θ^3 and θ^4 were determined so as to give $NkT/\tau a=0$ and its derivative equal to -0.5 at $\theta=1$, and, by using the higher order terms, the second-order approximation at low θ's is preserved.

4. Adsorption Isotherm of Two-Dimensional Gas

The relation which can be determined experimentally is that between vapor pressure p in the gas phase and surface coverage θ, namely the adsorption isotherm. Accordingly it is desirable to have the connection between this relation and the equation of state. Experimental results can then be interpreted in terms of an equation of state, or from a given equation of state the corresponding adsorption isotherm can be calculated.

Thermodynamics gives the desired relation:

$$d\tau=nkTd\ln p, \quad (23)$$

whence
$$d\ln p=(n_0kT)^{-1}d\tau/\theta, \quad (24)$$

where n_0 is the density of close packed adatoms.

If the equation of state be written

$$\tau=n_0kTf(\theta),$$

then
$$d\ln p=\theta^{-1}f'(\theta)d\theta, \quad (25)$$

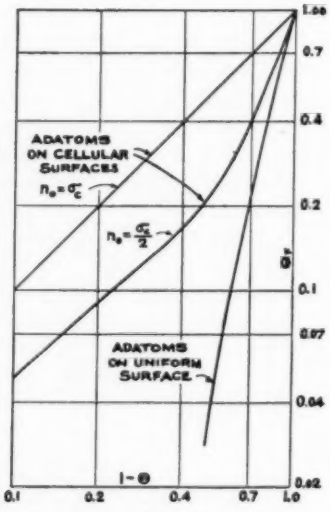

FIG. 5. Adsorption isotherm characteristics.

and integration by parts gives

$$\ln Ap=\theta^{-1}f(\theta)+\int\theta^{-2}f(\theta)d\theta \tag{26}$$

for the adsorption isotherm, A representing a constant of integration which depends upon the detailed mechanism of evaporation and condensation.

From Eq. (22)

$$\theta^{-2}f(\theta)=\frac{1+1.814\theta+2.573\theta^2}{\theta(1-1.307\theta^3+0.307\theta^4)}, \tag{27}$$

This can be integrated by using partial fractions, for $(1-\theta)$ and $(1-0.2372\theta)$ are both factors of the denominator. The result is

$$\ln Ap=\ln[\theta/(1-\theta)^2]+0.578\ln(1-0.2372\theta)+0.2105\ln(1+1.2372\theta+1.2935\theta^2)-0.3239\tan^{-1}(0.648+1.3553\theta)+\frac{1+1.814\theta+2.573\theta^2}{1-1.307\theta^3+0.307\theta^4}. \tag{28}$$

The adsorption isotherm for adsorption on a surface on which the adatoms occupy definite positions is[7]

$$n=Ap\sigma_F, \tag{29}$$

[7] Forthcoming papers by I. Langmuir and L. Tonks.

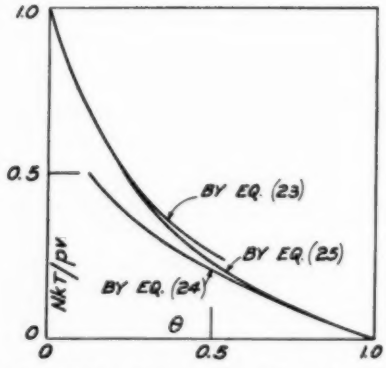

FIG. 6. Equation of state of three-dimensional gas.

where σ_F is the number of such positions or cells per unit area which are free to receive an adatom. Putting σ_c equal to the total number of cells per unit area and denoting the fraction of these that are free by θ_F, so that $\theta_F=\sigma_F/\sigma_c$, the isotherm becomes

$$\theta=(\sigma_c/n_0)Ap\theta_F. \tag{30}$$

Thus the function θ/Ap, adjusted by a factor (which may be considered to be implicit in A) to make it unity at $\theta=0$, gives the fraction of cells which are free.

This concept breaks down for the continuous surface of the present treatment. Nevertheless, for comparison with the other cases in particular, and if only as a representation of Eq. (28), θ_F defined by Eq. (30) is shown in Fig. 5 plotted against $1-\theta$.

For such comparison the θ_F curves have been plotted for the cases where the number of adatoms in a complete film equals the number of cells and where n_0 is half the number of cells, the cells being in square array. For a given degree of coverage the uniform surface requires increasingly greater pressures than the other cases. Thus saturation effects which might be very evident for a cellular surface could be completely absent with a uniform one.

5. Equation of State of a Three-Dimensional Gas

The same methods outlined above will serve to give the complete equation of state for the volume case.

Boltzmann[4] has already given the second-

order correction for small concentrations in terms of $b=2\pi N\sigma^3/3$ as

$$pv=NkT[1+b/v+(5/8)(b/v)^2].$$

The close packed (face-centered cubic) concentration of atoms is

$$n_1=\sqrt{2}/\sigma^3,$$

so that in terms of fractional close packing θ, where

$$\theta=N/n_1v.$$

$$pv=NkT(1+2.9619\theta+5.4830\theta^2). \quad (31)$$

The reciprocal of the coefficient of NkT is plotted in Fig. 6.

Near $\theta=1$ each atom center is confined to a dodecahedron formed by the twelve 110 planes, and the same reasoning as for the two-dimensional case leads now to the formula

$$pv=NkT/(1-\theta^{1/3}). \quad (32)$$

Again, this can be rigorously proved for a plain cubic array.

The appropriate formula which covers the whole range of θ is

$$pv=NkT\frac{1+2.9619\theta+5.4830\theta^2}{1-0.8517\theta^3-0.1483\theta^4}. \quad (33)$$

NOVEMBER 15, 1936 PHYSICAL REVIEW VOLUME 50

Quantum Theory of the Equation of State at Low Temperatures*

LEON GROPPER, *New York University, Washington Square, New York City*

(Received September 28, 1936)

The quantum formulae for the second virial coefficient B are derived, for the case of Boltzmann, Einstein-Bose and Fermi-Dirac statistics. It is shown how these formulae may be expressed in terms of the phases of the Schrödinger wave function. For low temperatures the expression for B is developed in a power series of T, the temperature, which gives formal agreement with the experimental formula in the case of He. Using this series development a potential is fixed to fit the data. The potential agrees with the Slater-Margenau potential in the region where the latter is valid.

1.

IN a fundamental paper on the quantum statistics of a gas, Slater[1] has pointed out that the classical Zustands integral

$$e^{-\beta\psi}=\frac{(2\pi mKT)^{3N/2}}{(2\pi\hbar)^{3N}}\int_V\cdots\int e^{-\beta U}dx_1\cdots dz_N \quad (1)$$

must be replaced by the Zustandsumme in the following form,

$$e^{-\beta\psi}=\int\cdots\int dx_1\cdots dz_N\sum_n e^{-\beta E_n}\Psi_n\Psi_n^*. \quad (2)$$

Here ψ is the free energy of the gas from which is derived the pressure $p=-\partial\psi/\partial V$, Ψ_n is the still to be normalized, time free, wave function for a system of N molecules (we will take N to be the number of molecules in a mole of gas), U is the total potential energy of the system, E the energy, and $\hbar$ is Planck's constant divided by 2π. The integrals in (1) and (2) are over the whole volume V of the gas.

The classical expression for the second virial coefficient which is the B, in the equation of state,

$$p^V/RT=(1+B/V+C/V^2+\cdots) \quad (3)$$

is derived from (1) and is given by,[2]

$$B_{\text{Cl.}}=2\pi N\int_0^\infty drr^2(1-e^{-\beta V}) \quad (4)$$

for the case of monatomic gases, where the force field is radial. Here, V is now the potential between two molecules and is not to be confused with the volume.

It can be shown that the quantum expression for the second virial coefficient is given by:

* The results of the present investigation were submitted in the form of a Letter to the Editor on March 19, 1936. —Editor.

[1] J. C. Slater, Phys. Rev. **38**, 237 (1931).

[2] See R. H. Fowler, *Statistical Mechanics*, Chap. VIII

FIG. 1.

(a) Boltzmann statistics

$$B_B = \sum_{\text{all } l} (l+\tfrac{1}{2})B_l. \tag{5}$$

(b) Einstein-Bose statistics

$$B_{E.B.} = -\frac{N\pi^{\frac{1}{2}}\lambda^3}{2} + 2\sum_{\text{even } l} (l+\tfrac{1}{2})B_l. \tag{6}$$

(c) Fermi-Dirac statistics

$$B_{F.D.} = +\frac{N\pi^{\frac{1}{2}}\lambda^3}{2} + 2\sum_{\text{odd } l} (l+\tfrac{1}{2})B_l, \tag{7}$$

where

$$B_l = 16(\pi)^{\frac{1}{2}}\lambda^3 N \int_0^\infty dk e^{-\lambda^2 k^2} \int_0^\infty dr \times ((\pi kr/2)J^2_{l+\frac{1}{2}}(kr) - v_l^2(k, r)). \tag{8}$$

Here v_l is determined from the radical wave equation in the relative coordinates of two molecules,

$$d^2v/dr^2 + (k^2 - (m/\hbar^2)V - l(l+1)/r^2)v = 0$$

and has already been normalized so as to behave asymptotically like, $v \sim \sin(kr - l\pi/2 + \eta_l(k))$ where η is the phase shift in the wave due to the presence of the force field, and λ, the statistical wave-length of the molecule is given by $(\beta\hbar^2/m)^{\frac{1}{2}}$ where m is the mass of a molecule.[3]

Eqs. (5), (6) and (7), follow from (2) by the same procedure used in deriving (4) from (1). Since the rigorous proofs are long and tedious we leave them to the appendix.[4]

For an ideal gas it is clear that B_l is zero, so that B_B is zero, and $B_{E.B.}$, $B_{F.D.}$ reduce to the well-known expressions for the second virial coefficient of a degenerate, ideal, gas.

2.

With the methods of Uhlenbeck and Gropper,[4] or Kirkwood,[5] both of which depend on the invariance of the Spur,[6] plus the use of the following formulae,[7]

$$\sum_{n=0}^{\infty} (n+\tfrac{1}{2})J^2_{n+\frac{1}{2}}(z) = z/\pi,$$

$$\sum_{n=0}^{\infty} (2n+\tfrac{1}{2})J^2_{2n+\frac{1}{2}}(z) = \tfrac{1}{4}z^2\{J^2_{-\frac{1}{2}}(z) - J_{-\frac{1}{2}}(z)J_{\frac{1}{2}}(z)\},$$

one can verify that as $\lambda \to 0$ (quantum theory $\to$ classical theory) (5), (6), (7), may be evaluated in power series of λ^2,

$$B_B = 2\pi N \int_0^\infty dr r^2 \left\{1 - e^{-\beta V}\left[1 - \frac{\beta^2\lambda^2}{12}\left(\frac{dV}{dr}\right)^2 + \frac{\beta^2\lambda^4}{120}\left(\left(\frac{d^2V}{dr^2}\right)^2 + \frac{2}{r^2}\left(\frac{dV}{dr}\right)^2 + \frac{10}{9}\frac{\beta}{r}\left(\frac{dV}{dr}\right)^3 - \frac{5}{36}\beta^2\left(\frac{dV}{dr}\right)^4\right) + \cdots\right]\right\}, \tag{5'}$$

$$B^{E.B.}_{F.D.} = B_B \pm 2\pi N \int_0^\infty dr r^2 e^{-\beta V} e^{-r^2/\lambda^2}\left(1 + \beta r\frac{dV}{dr} + \cdots\right). \tag{6'}(7')$$

In (6′), (7′), the plus sign is for the E.B. statistics, the negative sign for the F.D. statistics. One sees from this, that as $\lambda \to 0$, (5′), (6′), (7′), reduce to the classical value 4.

In conjunction with Professor Uhlenbeck, the writer has made a graphical study of (5′), (6′), (7′), with different potentials, at low temperatures ($T = 20°$ absolute). For such low temperatures this formulation for B is unsatisfactory because:

[3] Formula (5) was pointed out to me without proof some years ago in a private communication from Professor Uhlenbeck to whom I wish to acknowledge my indebtedness. In a recent paper, August, 1936, in Physica, Uhlenbeck and Beth consider some of the points in this paper, though from a somewhat different point of view.

[4] Uhlenbeck and Gropper, Phys. Rev. **41**, 79 (1932).

[5] Kirkwood, Phys. Rev. **44**, 31 (1933).

[6] F. Bloch, Zeits. f. Physik **74**, 295 (1932).

[7] Watson, *Bessel Functions*, p. 152.

1. Either (5′), (6′), (7′) do not converge or converge too slowly to be useful (as is also mentioned by Uhlenbeck and Beth).

2. (5′), (6′) (7′) are extremely sensitive to the potential V, so that as Wigner[8] remarks, a change of only $\frac{1}{2}$ percent in the parameter of the exponential representing Slater's repulsive force, changes *even the classical part of* B by as much as 20 percent. And it does not seem possible to determine V theoretically to anywhere near that accuracy.

3.

In this paper we shall eliminate these objections by,

1. Deriving an alternate general expression for B.
2. Obtaining a series in power of $1/\lambda^2$ for large λ, which is relatively insensitive to V.

Point (1) depends essentially on the fact that we know the behavior of the wave function at large distances, point (2), on the fact that as $\lambda\to\infty$ we know the expression for the phase shifts.

4.

Consider first, the integral over r in (8). We may write it,

$$\begin{aligned} F&=\lim_{\substack{R\to\infty\\ \partial\to 0}}\int_{\partial}^{R}\left(\frac{\pi kr}{2}J^2_{l+\frac{1}{2}}(kr)-v_l^2\right),\\ &=\lim_{\substack{R\to\infty\\ \partial\to 0}}\int_{\partial}^{R}dr\frac{1}{2\pi i}\oint\frac{((\pi kz/2)J^2_{l+\frac{1}{2}}(kz)-v_l^2(z))}{z-r}dz, \end{aligned} \tag{9}$$

where the z path of integration is indicated in Fig. 1. Since the integrand has no singularities, except $z=r$, in the finite portion of the z plane, we may take the sides of the rectangle as large as we please. Further, since the integral is regular and finite throughout both limits of integration ($z\neq r$), we may permute the integrals. Integrating over r we get

$$F=\lim_{\substack{R\to\infty\\ \partial\to 0}}\frac{1}{2\pi i}\oint dz\left(\frac{\pi kz}{2}J^2_{l+\frac{1}{2}}(kz)-v_l^2(z)\right)\log\left(1+\frac{R-\partial}{z-R}\right). \tag{10}$$

Now the logarithm may be expanded in a convergent series provided

$$\left|\frac{R-\partial}{z-R}\right|=\frac{R-\partial}{((x-R)^2+y^2)^{\frac{1}{2}}}<1.$$

But by taking the rectangle large enough we can assure this condition to be satisfied over the path of integration. Hence, letting $f(z)=((\pi kz/2)J^2_{l+\frac{1}{2}}(kz)-v_l^2(z))$, (10) becomes

$$\begin{aligned} F&=\lim_{\substack{R\to\infty\\ \partial\to 0}}\frac{1}{2\pi i}\oint dzf(z)\left[\left(\frac{R-\partial}{z-R}\right)-\frac{1}{2}\left(\frac{R-\partial}{z-R}\right)^2+\frac{1}{3}\left(\frac{R-\partial}{z-R}\right)^3-\cdots\right]\\ &=\lim_{\substack{R\to\infty\\ \partial\to 0}}\left\{(R-\partial)f(R)-\frac{(R-\partial)^2}{2!}f'(R)+\frac{(R-\partial)^3}{3!}f''(R)-\cdots\right\}, \end{aligned} \tag{11}$$

the last line following from an extension of Cauchy's theorem.

[8] Wigner, Phys. Rev. **40**, 749 (1932).

Going to the limit $\partial=0$ (11) becomes

$$F=\lim_{R\to\infty}\{Rf(R)-(R^2/2!)f'(R)+(R^3/3!)f''(R)-\cdots\}. \tag{12}$$

Putting in the asymptotic values for $f(R)$ and its derivatives,

$$f(R)=\sin^2(kR-l\pi/2)-\sin^2(kR-l\pi/2+\eta_l(b))$$
$$=(-1)^l/2[\cos 2kR(\cos 2\eta-1)-\sin 2kR\sin 2\eta],$$

collecting terms, and summing the two resultant series, (12) becomes

$$F=\lim_{R\to\infty}(-1)^l/k\{-\sin 2\eta+(\cos 2\eta-1)\sin 2kR+\sin 2\eta\cos 2kR\}. \tag{13}$$

Inserting this result in (8), we find, on using the second of the Riemann-Lebesgue lemmas,[9] that the terms with $\sin kR$ and $\cos kR$, after integrating over k, and going to the limit $R\to\infty$, vanish. There remains only the term with $\sin 2\eta$ which is free of R. Therefore (8) becomes

$$B_l-=4\pi^{\frac{1}{2}}\lambda^3N(-1)^l\int_0^\infty dke^{-\lambda^2k^2}\frac{\sin 2\eta_l(k)}{k}. \tag{14}$$

Substituting this in (5), (6), (7) we get

$$B_B=-4\pi^{\frac{1}{2}}\lambda^3N\int_0^\infty dke^{-\lambda^2k^2}\sum_{\text{all } l}(-1)^l(l+\tfrac{1}{2})\frac{\sin 2\eta}{k}, \tag{5''}$$

$$B_{E.B.}=-\frac{N\pi^{\frac{1}{2}}\lambda^3}{2}-8\pi^{\frac{1}{2}}\lambda^3N\int_0^\infty dke^{-\lambda^2k^2}\sum_{\text{even } l}(-1)^l(l+\tfrac{1}{2})\frac{\sin 2\eta}{k}, \tag{6''}$$

$$B_{F.D.}=+\frac{N\pi^{\frac{1}{2}}\lambda^3}{2}-8\pi^{\frac{1}{2}}\lambda^3N\int_0^\infty dke^{-\lambda^2k^2}\sum_{\text{odd } l}(-1)^l(l+\tfrac{1}{2})\frac{\sin 2\eta}{k}. \tag{7''}$$

The integrals here represent a statistical average over the quantity $\sum(-1)^l(l+\frac{1}{2})\sin 2\eta/k$, which is closely related to, although not identical with, the expression for the total elastic collision cross section. Hence, if one knows the phases $\eta_l(k)$, say, from collision data, one can immediately compute the virial coefficient from (5''), (6''), (7'').[10] We shall postpone to a later paper the numerical calculation of the phases and the values of the second virial coefficient obtained with them.

5.

In the absence of a knowledge of these phases, however, we can gain some idea of the correlation between theory and experiment by expressing the second virial coefficient as a power series in $1/\lambda^2$ for the region of low temperature, and then using these expressions to derive a potential which may be compared with that already known. It will be sufficient to deal with (6'').

Letting $f=\sum_{\text{even } l}(-1)^l(l+\frac{1}{2})\sin 2\eta/k$, we have, aside from the factor, $-N\pi^{\frac{1}{2}}\lambda^3/2$, which is very small compared to experimental values, even at very low temperature, $T\leq 20°$ absolute,

$$B_{E.B.}=-8\pi^{\frac{1}{2}}\lambda^3N\int_0^\infty dke^{-\lambda^2k^2}f(k). \tag{14'}$$

[9] Whittaker-Watson, *Modern Analysis*, third edition, p. 172.

[10] These formulae are to be compared with the analogous formulae for viscosity and diffusion. See Massey and Mohr, Proc. Roy. Soc. London **141**, 734 (1933).

Now as $\lambda \to \infty$, the integrand of (14′) is different from zero only in the neighborhood $k=0$. Therefore, since most of the integral comes from the neighborhood $k=0$, we may expand $f(k)$ in a Mac-Laurin series. This series will certainly not represent $f(k)$ for large k, but in that case the integrand is negligible anyway because of the factor $e^{-\lambda^2 k^2}$, so that the error in using the expansion in this region does not matter. Making this expansion and integrating over k we get,

$$B_{\text{E.B.}} = -4\pi\lambda^2 N f(0) - 4\pi^{\frac{1}{2}}\lambda N f'(0) - \pi N f''(0) - \cdots. \tag{15}$$

Remembering that $\lambda^2 = \hbar^2/mKT$, and rewriting (15) in terms of the temperature we have

$$B_{\text{E.B.}} = -\frac{4(\pi\hbar^2/mK)Nf(0)}{T} - \frac{4(\pi\hbar^2/mK)^{\frac{1}{2}}Nf'(0)}{T^{\frac{1}{2}}} - \pi N f''(0) - \cdots. \tag{16}$$

As is shown in the appendix (2) all the odd derivative terms $f'(0)$, $f'''(0)$, etc., are zero; so that we finally have for $B_{\text{E.B.}}$

$$B_{\text{E.B.}} = -\frac{(4\pi\hbar^2/mK)Nf(0)}{T} - \pi N f''(0) - \cdots. \tag{17}$$

Formula (17) agrees in first approximation with the form for B in the expanded van der Waals equation

$$\frac{pV}{RT} = \left(1 + \frac{-a/RT + b}{V} + \frac{5}{8}\frac{b^2}{V^2} + \cdots\right).$$

At the same time, for T less than the boiling point of oxygen, the second virial coefficient, for He in Kammerling-Onnes units, is found to fit very closely the formula,[11]

$$B_{\text{K.O.}} \times 10^3 = -18.905/T + 0.7224.$$

In terms of cc mole this is,[12] $B = -423/T + 16.2$.

The experimental formula may be looked upon as the first two terms of a rapidly converging series in T, for T small. Therefore comparing the coefficients with (17) we find, $f(0) = 4.6\times10^{-8}$, $f''(0) = -8.5\times10^{-24}$. Thus,

$$f = \sum_{\text{even } l} (-1)^l (l+\tfrac{1}{2})(\sin 2\eta/k) = f(0) + kf'(0) + (k^2/2!)f''(0) + \cdots = 4.6\times10^{-8} - 4.25\times10^{-24}k^2 + \cdots.$$

Letting $k = k_0/a_0$, where a_0 is the radius of the first Bohr orbit this becomes,

$$\sum_{\text{even } l} (-1)^l (l+\tfrac{1}{2}) \sin 2\eta = 8.75k_0 - 29k_0^3 + \cdots.$$

For very small values of k_0, we may replace the sum by the first term, $l=0$, and neglect the second term on the right. Thus $\sin 2\eta_0 \cong 17.5k_0$. This formula can only be valid in the region $17.5k_0 \leq 1$. Thus, for $17.5k_0 = 1$ we should find $\eta_0 = \pi/4 = 0.78$. The writer is at present calculating the phases so as to compare the exact formulae (5″), (6″), (7″), with the data.

It is possible also to calculate the first coefficient of (17), $f(0)$ (Appendix 2) by means of the formula

$$f(0) = -m/\hbar^2 \int_0^\infty V r^2 dr. \tag{18}$$

Using a potential

$$V = \left\{7.7e^{-2.43\rho} - e^{-b^2/\rho^2}\left(\frac{0.68}{\rho^6} + \frac{5.37}{\rho^8} + \frac{20.4}{\rho^{10}}\right)\right\} \times 10^{-10} \text{ ergs}$$

[11] G. P. Nyhoff, Leiden Comm. Supp. No. °64C.

[12] The conversion is given by $B = (N/v_0)B_{\text{K.O.}}$ where v_0 is the number of molecules per cc under normal conditions.

and comparing (17) with the first coefficient of the experimental formula, we find, $b=1.71$. This potential is quite reasonable for, (1) since b is quite small it reduces to the Slater-Margenau potential in the region where the latter is known to be valid; (2) it insures that the negative part of the potential vanishes as $\rho\to 0$, as it must; (3) for large ρ the expansion of e^{-b^2/ρ^2} leaves the experimentally determined dipole-dipole term unaltered, and slightly corrects the dipole quadruple, and quadrupole-quadrupole terms.

I am indebted to Dr. I. S. Lowen for his very helpful criticism, and to Professor G. E. Uhlenbeck who first introduced me to the problem in this paper.

Appendix 1.

In the following we shall adopt a derivation, given by Ursell,[5] of the classical second virial coefficient as obtained from the classical Zustands integral.

Boltzmann statistics

Eq. (1) may be written

$$e^{-\beta\psi}=\int_V\cdots\int dx_1\cdots dz_N\sum_n e^{-\beta E_n}\Psi_n\Psi_n^*, \tag{1}$$

where the Ψ_n (still to be normalized) satisfy the Schrödinger equation

$$\sum_{r=1}^{N}\Delta_r\Psi_n+\frac{2m}{h^2}(E_n-U)\Psi_n=0. \tag{2}$$

Let the integrand of (1) be called g. Let Φ^N be the wave function for a system of N free molecules and ϵ^N the corresponding energy, $\Phi^{N-2}\psi(r_ir_j)$ the wave function for $N-2$ free and two interacting molecules, $\Phi^{N-4}\psi(r_ir_j)\psi(r_kr_l)$ the wave function for $N-4$ free and two pairs of interacting molecules, etc. (r stands for the three coordinates x, y, z). Consider the expression,

$$f=\Big[\sum_n e^{-\beta\epsilon_n N}\Phi_n{}^N\Phi_n^{*N}\Big]+\Big[\sum_{i\neq j}\sum_n e^{-\beta\epsilon_n N-2}\Phi_n{}^{N-2}\Phi_n^{*N-2}\sum_{n_in_j}e^{-\beta E_{n_in_j}}(\psi(r_ir_j)\psi^*(r_ir_j)-\varphi(r_ir_j)\varphi^*(r_ir_j))\Big]$$

$$+\Big[\sum_{i\neq j,\,k\neq l}\sum_n e^{-\beta\epsilon_n N-1}\Phi_n{}^{N-4}\Phi_n^{*N-4}\sum_{n_in_jn_kn_l}e^{-\beta(E_{n_in_j}+E_{n_kn_l})}(\psi(r_ir_j)\psi^*(r_ir_j)-\varphi(r_ir_j)\varphi^*(r_ir_j))$$

$$\times(\psi(r_kr_l)\psi^*(r_kr_l)-\varphi(r_kr_l)\varphi^*(r_kr_l))\Big]+\cdots,$$

where $\sum_{i\neq j}$ means the sum over all pairs without repetition, and the (i, j) molecules are not included in Φ^{N-2}. Similarly for the third and higher brackets. We will now show that, for the forces of the range we are considering, $f\leqq g$.

The integral (1) is over all position of all the molecules.

Consider first the case when all the molecules are in a position free from each other's influence. In the region of such a set of values of the coordinates the contribution to the integrand is the same as $g_0\leqq\sum_n e^{-\beta\epsilon_n N}\Phi_n{}^N\Phi_n^{*N}$ in the same region. But in this region all the $\psi(r_ir_j)\leqq\varphi(r_ir_j)$, so that all the brackets of f after the first vanish and we have. $f_0=g_0=\sum_n e^{-\beta\epsilon_n N}\Phi_n{}^N\Phi_n^{*N}$.

Next, take the case when all molecules except one pair are in positions free from each other's influence. In the region of such a set of values of coordinates the contribution to the integrand becomes

$$g_1\leqq\sum_n e^{-\beta\epsilon_n N-2}\Phi^{N-2}\Phi^{*N-2}\sum_{n_in_j}e^{-\beta E_{n_in_j}}\psi(r_ir_j)\psi^*(r_ir_j).$$

But in this region all except one of the $\psi(r_ir_j)\leqq\varphi(r_ir_j)$, so that all the brackets of f after the second vanish. Part of the second cancels with the first, and we have

$$f_1=g_1=\sum_n e^{-\beta\epsilon_n N-2}\Phi^{N-2}\Phi^{*N-2}\sum_{n_in_j}e^{-\beta E_{n_in_j}}\psi(r_ir_j)\psi^*(r_ir_j).$$

The same considerations apply to sets of values of the coordinates where any number of pairs of molecules are under each other's influence. Thus we see for any set of values,[13] the two functions are the same. That is, if we were to plot the "graphs" of f and g they would almost coincide.

These considerations, of course, apply only to short range forces where a boundary can be drawn between the positions where the molecules are or are not under each other's influence, the limiting case being the hard sphere model. For long range forces there is no sharp boundary line, so that one cannot "count" positions of the assemblage.

Replacing g by f in (1) we can now proceed to reduce (1).

Consider the first bracket in f,

$$S_0=\sum_n e^{-\beta\epsilon_n N}\Phi_n{}^N\Phi_n^{*N}=\sum_{n_1=0}^{\infty}\sum_{n_2=0}^{\infty}\cdots\sum_{n_N=0}^{\infty}e^{-\beta\epsilon_n N}(\varphi_{n_1}{}^2\varphi_{n_2}{}^2\cdots\varphi_{n_N}{}^2).$$

For any molecule,

$$\varphi_n=\sin(n_x\pi x/L)\sin(n_y\pi y/L)\sin(n_z\pi z/L),\quad \epsilon_n=(h^2\pi^2/2mL^2)(n_x{}^2+n_y{}^2+n_z{}^2).$$

The normalization furnishes the factor $2^{3N}/V^N$. Replacing the multiple sums by integrals, integrating over the n's and then integrating over the coordinates, we find that the first bracket in f contributes to (1) the amount,[14] $(1/2\pi\lambda^2)^{3N/2}V^N$.

Coming now to the second bracket in f, and taking into account the normalization, we have,

$$S_1=\frac{2^{3(N-1)}}{V^{N-1}}\sum_{i\neq j}\sum_n e^{-\beta\epsilon_n N-2}\Phi_n{}^{N-2}\Phi_n^{*N-2}\sum_{n_in_j}e^{-\beta E_{n_in_j}}\left(\frac{\psi(r_{ij})\psi^*(r_{ij}')}{A}-\frac{\varphi(r_{ij})\varphi^*(r_{ij}')}{B}\right),$$

where

$$A=\int\!\!\int_V\!\!\int d\tau\psi(r_{ij})\psi^*(r_{ij}),\qquad B=\int\!\!\int_V\!\!\int d\tau\varphi(r_{ij})\varphi^*(r_{ij}),$$

and $\psi(r_{ij})$ means the wave function for the relative motion of the (ij) molecules. Similarly for $\varphi(r_{ij})$. These will also be referred to as ψ_R and φ_R.

Summing over the free wave function, as before, and integrating over their coordinates we get

$$2^3V^{N-3}\left(\frac{1}{2\pi\lambda^2}\right)^{\frac{3}{2}(N-2)}\frac{N(N-1)}{2}\sum_{n_in_j}e^{-\beta E_{n_in_j}}\left(\frac{\psi(r_{ij})\psi^*(r_{ij}')}{A}-\frac{\varphi(r_{ij})\varphi^*(r_{ij}')}{B}\right).$$

The factor $N(N-1)/2$ comes from the $\Sigma_{i\neq j}$. For the (ij) molecules we separate into relative and center of gravity coordinates, sum over n and integrate over the coordinates of the latter, so that the above expression becomes

$$2^3V^{N-1}\left(\frac{1}{2\pi\lambda^2}\right)^{3N-1}(\pi\lambda^2)^{\frac{3}{2}}\frac{N(N-1)}{2}\int\!\!\int_V\!\!\int d\tau\sum e^{-\beta E_R}\left(\frac{\psi_R\psi^*{}_R}{A}-\frac{\varphi_R\varphi^*{}_R}{B}\right),$$

where ψ_R, φ_R are the relative wave functions of the two molecules, E_R the relative energy, and the integral is over their relative coordinates. Letting

$$t=2^3(\pi\lambda^2)^{\frac{3}{2}}\int\!\!\int_V\!\!\int d\tau\sum e^{-\beta E_R}\left(\frac{\psi_R\psi^*{}_R}{A}-\frac{\varphi_R\varphi_R{}^*}{B}\right),\tag{3}$$

the above expression becomes

$$V^{N-1}(1/2\pi\lambda^2)^{3N/2}(N(N-1)/2)t.$$

Coming now to the third bracket in f, the reader can verify, by a procedure similar to the evaluation of the second bracket, that its contribution to (1) is

$$V^{N-2}(1/2\pi\lambda^2)^{3N/2}(N(N-1)(N-2)(N-3)/2^2\cdot 2!)t^2.$$

The factor $N(N-1)(N-2)(N-3)/2^2\cdot 2!$ comes from the number of double pairs. And so on, for the higher brackets.

[13] We have considered only binary collisions. Tertiary and higher collisions are completely negligible. See reference 2.

[14] A factor due to the finite size of the box, which is completely negligible, has here been omitted.

By letting $x=Nl/2V$, and by collecting together all the brackets, (1) can be written as the following series[2]

$$e^{-\beta\psi}=\frac{V^N}{(2\pi\lambda^2)^{3N/2}}\sum_{r=0}^{N/2}\frac{N!}{r!(N-2r)!N^r}x^r$$

$$=\frac{V^N}{(2\pi\lambda^2)^{3N/2}}\{1+x+O(x^2)+\cdots\}^N.$$

Taking the logarithm, and differentiating with respect to the volume, and neglecting x^2 with respect to x, we get

$$pV/RT=(1-x)=(1-(N/2V)l), \tag{4}$$

where $R=NK$, and we have replaced β by $1/KT$.

We can now reduce the quantities

$$l=2^3(\pi\lambda^2)^{\frac{1}{2}}\int\int\int_V\int d\tau\sum e^{-\beta E_R}\left(\frac{\psi_R\psi^*_R}{A}-\frac{\varphi_R\varphi^*_R}{B}\right),\qquad A=\int\int\int_V d\tau\psi_R\psi_R^*,\qquad B=\int\int\int_V d\tau\varphi_R\varphi_R^*.$$

On passing to polar coordinates and integrating over the angles, A and B become

$$A=\frac{2\pi}{(l+\frac{1}{2})}\frac{(l+m)!}{(l-m)!}\int_0^R v^2dr,\qquad B=\frac{2\pi}{(l+\frac{1}{2})}\frac{(l+m)!}{(l-m)!}\int_0^R\frac{r}{k}J_{l+\frac{1}{2}}^2(kr)dr,$$

where $k^2=(m/h^2)E_R$ and v satisfies the equation

$$\frac{d^2v}{dr^2}+\left(k^2-\frac{m}{h^2}V-\frac{l(l+1)}{r^2}\right)v=0.$$

For large r, $v\rightarrow\sin\left(kr-\frac{l\pi}{2}+\eta\right)$, so the contribution near the origin to the normalization integral may be neglected, since $\sin^2\left(kr-\frac{l\pi}{2}+\eta\right)$ is always positive and R is very large, compared to the distance around the origin (where v remains finite)

$$\therefore\int_0^R v^2dr\leqq R/2.$$

Similarly for large r, $J_{l+\frac{1}{2}}(kr)\rightarrow\frac{\sin(kr-l\pi/2)}{(\pi kr/2)^{\frac{1}{2}}}$, so that

$$\int_0^R\frac{r}{k}J_{l+\frac{1}{2}}^2(kr)\leqq\frac{R}{\pi k^2}.$$

Inserting the resultant values of A and B in l, and going to polar coordinates in the integral for l, we have,

$$l=\frac{8(\pi\lambda^2)^{\frac{1}{2}}}{\pi R}\int_0^R\int_0^\pi\int_0^{2\pi}\sin\theta drd\theta d\varphi\sum_n e^{-\lambda^2k_n^2}\sum_l(l+\tfrac{1}{2})\sum_{m=-l}^{+l}\frac{(l-m)!}{(l+m)!}\left(P_l^m(\cos\theta)\right)^2\left(v_l^2-\frac{\pi kr}{2}J_{l+\frac{1}{2}}^2(kr)\right)$$

where instead of summing over the three quantum numbers, we now sum over the radial quantum number and the degenerate states.

Since[15]

$$\sum_{m=-l}^{+l}\frac{(l-m)!}{(l+m)!}\left(P_l^m(\cos\theta)\right)^2=1,$$

this reduces, after integrating over the angles, to

$$l=\frac{32(\pi\lambda^2)^{\frac{1}{2}}}{R}\int_0^R dr\sum_n e^{-\lambda^2k_n^2}\sum_{l=0}^{\infty}(l+\tfrac{1}{2})\left(v_l^2-\frac{\pi kr}{2}J_{l+\frac{1}{2}}\right).$$

[15] Jahnke and Emde, second edition.

Converting the sum over n into an integral over k, the conversion factor being given by $dn=(R/\pi)dk$, we have

$$t=32\pi^{\frac{1}{2}}\lambda^3\int_0^\infty dk l^{-\lambda^2k^2}\sum_{l=0}^\infty(l+\tfrac{1}{2})\int_0^R dr\left(v_l^2-\frac{\pi kr}{2}J_{l+\frac{1}{2}}^2(kr)\right).$$

Substituting in (4) we have

$$pV/RT=(1+B_B/V),$$

where

$$B_B=16\pi^{\frac{1}{2}}\lambda^3N\int_0^\infty dk l^{-\lambda^2k^2}\sum_{l=0}^\infty(l+\tfrac{1}{2})\int_0^R dr\left(\frac{\pi kr}{2}J_{l+\frac{1}{2}}^2-v_l^2\right).$$

Since the waves are zero at the boundary and outside the vessel, we may extend the integral over r to ∞, and this gives the expression for B_B which was to be proven.

Einstein-Bose or Fermi-Dirac statistics

For the solutions of (2) we must take the symmetric or antisymmetric linear combinations. That is

$$\Psi_n=\sum_P(\pm1)^P(\psi_{n_1}(r_1)\psi_{n_2}(r_2)\cdots\psi_{n_N}(r_N))$$

the sum being taken over all permutations of the coordinates keeping the quantum numbers fixed.

As before we may replace the integrand g by f. Consider the first term of f,

$$S_0=\sum_n e^{-\beta\epsilon_nN}\Phi_n{}^N\Phi_n^{*N}.$$

Written more fully this is,[16]

$$S_0=\sum_{n_1\geq}\sum_{n_2\geq}\cdots\sum_{n_N}e^{-\beta(\epsilon_{n_1}+\epsilon_{n_2}+\cdots\epsilon_{n_N})}\sum_P(\pm1)^P(\varphi_{n_1}(r_1)\varphi_{n_2}(r_2)\cdots\varphi_{n_N}(r_N))\sum_{P'}(\pm1)^{P'}(\varphi^*{}_{n_1}(r_1)\varphi^*{}_{n_2}(r_2)\cdots\varphi^*{}_{n_N}(r_N)).$$

The normalization will introduce the factor $(2^{3N}/(N!V^N)g(n_1\cdots n_N)$ where $g(n_1\cdots n_N)$ will be defined immediately. Thus

$$S_0=\frac{2^{3N}}{N!V^N}\sum_{n_1\geq}\sum_{n_2\geq}\cdots\sum_{n_N}e^{-(\beta\hbar^2\pi^2/2m)(n_1{}^2+n_2{}^2+n_3{}^2+\cdots)}g(n_1\cdots n_N)\Phi^N\Phi^{*N}.$$

Here $g(n_1\cdots n_N)$ is unity when all the n_i are different (in which case the integral of $(\Phi^N)^2$ consists of only $N!$ terms because of the orthogonality relations); $g(n_1\cdots n_N)=1/2!$ when two of the n_i are the same (in which case the integral of $(\Phi^N)^2$ consists of $2!N!$ terms); $g(n_1\cdots n_N)=1/3!$ when three of the n_i are the same, etc.

We now arrange the terms of $(\Phi^N)^2$ into a series of sums. The first sum will contain all those terms for the identical permutation $P=P'$; the second all those in which the permutation differs only with respect to one pair of molecules, the third with respect to two pairs of molecules, etc. Of all the sums, we write down only those which contribute to the two highest powers of V, the volume, after integration. One can verify that the sums in which the permutations differ with respect to more than one pair of molecules, do not contribute to the two highest powers of V. Writing down S_0, for the first two sums,

$$S_0=\frac{2^{3N}}{N!V^N}\sum_{n_1\geq}\sum_{n_2\geq}\cdots\sum_{n_N}e^{-\beta\epsilon_nN}\sum_P\{(\varphi_{n_1}{}^2(r_1)\cdots\varphi_{n_N}{}^2(r_N))\pm(\varphi_{n_1}{}^2(r_1)\cdots\varphi_{n_{N-2}}{}^2(r_{N-2}))\sum_{i\neq j}\varphi_{n_i}(r_i)\varphi_{n_j}(r_i)\varphi_{n_j}(r_j)\varphi_{n_i}(r_j)+\cdots\}.$$

It is understood that whenever a pair of molecules occurs in the sum (ij) it is missing from the product $\varphi_{n_1}{}^2(r_1)\cdots\times\varphi_{n_{N-2}}{}^2(r_{N-2})$. Now if we permute the order of the relation $n_1\geq n_2\geq\cdots n_N$ we do not change the value of the multiple sum. Thus we can take the multiple sum $N!$ times corresponding to the $N!$ permutations in $n_1\geq n_2\geq\cdots n_N$ and divide by the factor $N!$. The effect of this is to sum over all the n_i independently with the factor $g(n_1\cdots n_N)$ omitted. Again, since the multiple sum is the same for each permutation of the Σ_P we need only take one term and multiply by the factor $N!$, which cancels the $N!$ just introduced. Thus we get,

$$S_0=\frac{2^{3N}}{N!V^N}\sum_{n_1=0}^\infty\sum_{n_2=0}^\infty\cdots\sum_{n_N=0}^\infty e^{-\beta\epsilon_nN}\{(\varphi_{n_1}{}^2(r_1)\cdots\varphi_{n_N}{}^2(r_N))\pm(\varphi_{n_1}{}^2(r_1)\cdots\varphi_{n_{N-2}}{}^2(r_{N-2}))\sum_{i\neq j}\varphi_{n_i}(r_i)\varphi_{n_j}(r_i)\varphi_{n_j}(r_j)\varphi_{n_i}(r_j)+\cdots\}.$$

Letting $\lambda^2=\hbar^2\beta/m$, and carrying out these sums and integrating over the coordinates,[17] we get as the contribution of

[16] This sum was worked out by Uhlenbeck and Gropper, Phys. Rev. **41**, 79 (1932) but we do it here explicitly since the method is used to calculate the other brackets in f. The sums with $n_1\geq n_2\geq n_3\geq\cdots n_N$ insures that no state is repeated.

[17] Again, a term λ^3/V has been neglected with respect to unity, and enters only because of the finite size of the box.

the first bracket in f to (1),

$$\frac{1}{N!}\left(\frac{1}{2\pi\lambda^2}\right)^{3N/2}\left(1\pm\frac{N(N-1)}{2}\frac{\pi^{\frac{3}{2}}\lambda^3}{V}+O\left(\frac{1}{V^2},\frac{1}{V^3},\cdots\right)\right), \tag{5}$$

where O contains all those terms contributing lower powers of V.

Consider now the second bracket in f. The normalization of $\Phi^{N-2}\psi(r_ir_j)$ will furnish the factor

$$\frac{2^{3(N-1)}}{N!V^{N-1}}\frac{g(n_1\cdots n_N)}{A} \qquad \text{where} \qquad A=\int\int_V\int\psi_R\psi^*_R d\tau$$

and ψ_R means the wave function for the relative motion of two interacting molecules.[18] The normalization of $\Phi^{N-2}\varphi(r_ir_j)$ is, as before $(2^{3N}/N!V^N)g(n_1\cdots n_N)$, which we can also write as $(2^{3(N-1)}/N!V^{N-1})(g(n_1\cdots n_N)/B)$, where

$$B=\int\int_V\int\varphi_R\varphi^*_R d\tau$$

and φ_R means the wave function for the relative motion of two free molecules.

As with the first bracket, we write the terms of the expression

$$\Phi^{N-2}\Phi^{*N-2}\left(\frac{\psi(r_ir_j)\psi^*(r_ir_j)}{A}-\frac{\varphi(r_ir_j)\varphi^*(r_ir_j)}{B}\right)$$

as a series of sums, the first containing all terms with the identical permutations, the second, terms in which the permutations differ with respect to a single pair of molecules, etc. One can verify that terms involving permutations between two or more pair of molecules contribute powers of V lower than V^{N-1}. Of the second sum only those terms in which the quantum numbers of the (ij) molecules are permuted give terms with a factor V^{N-1}. These contributing terms are

$$\pm\sum_P(\varphi_{n_1}{}^2(r_1)\cdots\varphi_{n_{N-2}}{}^2(r_{N-2})\left(\frac{\psi_{n_i}(r_i)\psi^*_{n_j}(r_i)\psi_{n_j}(r_j)\psi^*_{n_i}(r_j)}{A}-\frac{\varphi_{n_i}(r_i)\varphi^*_{n_j}(r_i)\varphi_{n_j}(r_j)\varphi^*_{n_i}(r_j)}{B}\right).$$

All of the terms of the first sum will give the factor V^{N-1}. They are

$$+\sum_P(\varphi_{n_1}{}^2(r_1)\cdots\varphi_{n_{N-2}}{}^2(r_{N-2})\left(\frac{\psi_{n_i}(r_i)\psi^*_{n_i}(r_i)\psi_{n_j}(r_j)\psi^*_{n_j}(r_j)}{A}-\frac{\varphi_{n_i}(r_i)\varphi^*_{n_i}(r_i)\varphi_{n_j}(r_j)\varphi^*_{n_j}(r_j)}{B}\right).$$

As before we eliminate the factor $g(n_1\cdots n_N)$ and the sum over the permutations of the contributing terms. With these contributing terms the second bracket in f, written more fully is,

$$S_1=\frac{2^{3(N-1)}}{N!V^{N-1}}\sum_{i\neq j}\left\{\sum_{n_1=0}^{\infty}\sum_{n_2=0}^{\infty}\cdots\sum_{n_{N-2}}^{\infty}e^{-\beta\epsilon_{n^{N-2}}}(\varphi_{n_1}{}^2(r_1)\cdots\varphi_{n_{N-2}}{}^2(r_{N-2}))\sum_{n_in_j}e^{-\beta E_{n_in_j}}\left(\frac{W(r_ir_j)}{A}-\frac{w(r_ir_j)}{B}\right)\right\}+\cdots,$$

where

$$W(r_ir_j)=\psi_{n_i}(r_i)\psi^*_{n_i}(r_i)\psi_{n_j}(r_j)\psi^*_{n_j}(r_j)\pm\psi_{n_i}(r_i)\psi^*_{n_j}(r_i)\psi_{n_j}(r_j)\psi^*_{n_i}(r_j),$$
$$w(r_ir_j)=\varphi_{n_i}(r_i)\varphi^*_{n_i}(r_i)\varphi_{n_j}(r_j)\varphi^*_{n_j}(r_j)\pm\varphi_{n_i}(r_i)\varphi^*_{n_j}(r_i)\varphi_{n_j}(r_j)\varphi^*_{n_i}(r_j).$$

By permuting r_i and r_j we do not change the value of the sums over n_i, n_j, which then becomes

$$\tfrac{1}{2}\sum_{n_in_j}e^{-\beta E_{n_in_j}}\left(\frac{S(r_ir_j)S^*(r_ir_j)}{A}-\frac{s(r_ir_j)s^*(r_ir_j)}{B}\right),$$

where $S=\psi_{n_i}(r_i)\psi_{n_j}(r_j)\pm\psi_{n_j}(r_i)\psi_{n_i}(r_j)$, and s is the corresponding symmetric or antisymmetric function for the φ's.

Performing the multiple sum for the wave functions of the free molecules, and integrating over their coordinates, we reduce to

$$\frac{2^3V^{N-3}}{N!}\left(\frac{1}{2\pi\lambda^2}\right)^{\frac{3}{2}(N-2)}\cdot\frac{N(N-1)}{2}\cdot\frac{1}{2}\sum_{n_in_j}e^{-\beta E_{n_in_j}}\left(\frac{SS^*}{A}-\frac{ss^*}{B}\right).$$

The factor $N(N-1)/2$ enters from the sum over (ij).

In S and s we separate into relative and center of gravity wave functions. The symmetry or antisymmetry will then enter only in the wave function for the relative motion. Summing and integrating over the center of gravity wave functions we reduce to

$$\frac{4V^{N-1}}{N!}\left(\frac{1}{2\pi\lambda^2}\right)^{3N/2}(\pi\lambda^2)^{\frac{3}{2}}\frac{N(N-1)}{2}\int\int\int\sum e^{-\beta E_r}\left(\frac{\psi_r\psi_r^*}{A}-\frac{\varphi_r\varphi_r^*}{B}\right)d\tau, \tag{6}$$

[18] *Not* the symmetric or antisymmetric combinations.

where ψ_r and φ_r, are the symmetric or antisymmetric wave functions[19] for the relative motion, and E_r the relative energy.

Coming to the third bracket in f, one can verify that all terms there will contribute powers of V lower than V^{N-1}. And similarly for all the other brackets

Let
$$t=\int\int\int \Sigma e^{-\beta E_r}\left(\frac{\psi_r\psi_r^*}{A}-\frac{\varphi_r\varphi_r^*}{B}\right)d\tau.$$

Collecting the terms from (5) and (6) we have finally for (1)

$$e^{-\beta\psi}=\frac{V^N}{N!}\left(\frac{1}{2\pi\lambda^2}\right)^{3N/2}\left[1+\frac{N(N-1)}{2}\cdot\frac{\pi^{\frac{3}{2}}\lambda^3}{V}(\pm 1+4t)+O'\left(\frac{1}{V^2},\frac{1}{V^3},\cdots\right)\right], \tag{7}$$

where the factor $O'(1/V^2, 1/V^3, \cdots)$ includes all those terms in lower powers of V, which we have not given explicitly. The second term in the bracket will give the second virial coefficient, but one cannot now, as is sometimes done, take the logarithm and assume the second term of the bracket small with respect to the first, since their ratio is $(N(N-1)/2)\times(\pi^{\frac{3}{2}}\lambda^3/V)(\pm 1+4t)$ and it is only $(N\pi^{\frac{3}{2}}\lambda^3/2V)(\pm 1+4t)$ which we are entitled to assume small. To proceed correctly, let $y_1=(N(N-1)/2)\pi^{\frac{3}{2}}\lambda^3(\pm 1+4t)$, and rewrite (7) in the form

$$e^{-\beta\psi}=\frac{V^N}{N!}\left(\frac{1}{2\pi\lambda^2}\right)^{3N/2}\left[1+\frac{y_1}{V}+\frac{y_2}{V^2}+\frac{y_3}{V^3}+\cdots\right]. \tag{8}$$

The coefficients $y_2, y_3 \cdots y_N$ could laboriously be calculated following the method above. But it is simpler to arrive at them by the correspondence principle. For it has been shown[16] that when we go from the quantum region to the classical region of high temperatures y_1 reduces to the classical coefficient

$$\frac{N(N-1)}{2}\int\int\int(e^{-\beta V}-1)d\tau=(N-1)x,$$

where we have let $x=\dfrac{N}{2}\int\int\int(e^{-\beta V}-1)d\tau$.

But the classical formula is given by[2]

$$\frac{V^N}{(2\pi\lambda^2)^{3N/2}}\left[1+\frac{(N-1)x}{V}+\frac{(N-1)(N-2)(N-3)}{2!}\frac{x^2}{V^2N^2}+\cdots\right].$$

If now in place of x we write $z=(N/2)\pi^{\frac{3}{2}}\lambda^3(\pm 1+4t)$, so as to get the expression

$$\frac{V^N}{(2\pi\lambda^2)^{3N/2}}\left[1+(N-1)\frac{z}{V}+\frac{(N-1)(N-2)(N-3)}{2!}\frac{z^2}{V^2N^2}+\cdots\right],$$

we see that the first two terms agree with the formula (8) we have derived, and the whole expression agrees with the classical expression in the classical region of high temperature since, as previously stated, $z\to x$. We therefore take this to be the correct quantum expression, although this provides only a sufficient but not necessary condition for determining the coefficients, y_2, y_3, etc.

Now, as shown by Fowler,[2]

$$1+(N-1)\frac{z}{V}+\frac{(N-1)(N-2)(N-3)}{2!}\frac{z^2}{N^2V^2}+\cdots=\left(1+\frac{z}{V}+O\left(\frac{z^2}{V^2}\right)\right]^N.$$

And this is an approximation of the desired order, since $(z/V)\ll 1$.

Using this in Eq. (7), taking the logarithm, and differentiating with respect to the volume we get

$$\frac{pV}{RT}=1-\frac{z}{V}=1-\frac{N}{2V}\pi^{\frac{3}{2}}\lambda^3(\pm 1+4t), \tag{9}$$

where in the left side we have replaced β by $1/kT$, and let $R=NK$.

We can reduce the quantities

$$t=\int\int_V\int d\tau\Sigma e^{-\beta E_r}\left(\frac{\psi_r\psi_r^*}{A}-\frac{\varphi_r\varphi_r^*}{B}\right),\qquad A=\int\int_V\int d\tau\psi_R\psi_R^*,\qquad B=\int\int_V\int d\tau\varphi_R\varphi_R^*.$$

[19] ψ_r and φ_r are to be distinguished from ψ_R and φ_R which occur in A and B.

As before, we showed

$$A=\frac{2\pi}{(l+\frac{1}{2})}\frac{(l+m)!}{(l-m)!}\frac{R}{2},\qquad B=\frac{2\pi}{(l+\frac{1}{2})}\frac{(l+m)!}{(l-m)!}\frac{R}{\pi k^2}.$$

Now in polar coordinates the symmetric or antisymmetric relative wave function, ψ_r is

$$\psi_r=\frac{v(r)}{r}(P_l^m(\cos\theta)e^{im\varphi}\pm P_l^m(\cos\theta')e^{im\varphi'}),$$

where $$\theta'=\pi-\theta,\qquad \varphi'=\varphi+\pi.$$

This is so because the interchange of the two molecules sends φ into $\varphi+\pi$, and θ into $\pi-\theta$. One has the corresponding expressions for φ_r. As before instead of summing over the three quantum numbers, we now sum over the radial quantum numbers and the degenerate states. Going to polar coordinates, inserting the above functions and the values of A and B into t, using the addition theorem,[16]

$$P_l(\cos\alpha)=\sum_{m=-l}^{+l}\frac{(l-m)!}{(l+m)!}P_l^m(\cos\theta)P_l^m(\cos\theta')e^{im(\varphi-\varphi')},$$

where $$\cos\alpha=\cos\theta\cos\theta'+\sin\theta\sin\theta'\cos(\varphi-\varphi'),$$

and integrating over the angles, t becomes

$$t=\frac{8}{R}\int_0^R dr\sum_N e^{-\lambda^2k_n^2}\sum_l(l+\tfrac{1}{2})(1\pm(1-)^l)\left(v^2-\frac{\pi kr}{2}J_{l+\frac{1}{2}}^2\right),$$

where $k_n^2=(m/\hbar^2)E_r$. The sum is over all l. For Einstein-Bose statistics the odd ones vanish, for Fermi-Dirac the even ones vanish, thus

$$t=\frac{16}{R}\int_0^R dr\sum_n e^{-\lambda^2k_n^2}\sum_l(l+\tfrac{1}{2})\left(v^2-\frac{\pi kr}{2}J^2\right),$$

where for Einstein-Bose statistics the sum is over even l, and for Fermi-Dirac statistics the sum is over odd l. Again, since the discreteness due to the finite size of the box is negligible, the sum over n may be converted into an integral, the conversion factor, as before, being given from $dn=(R/\pi)dk$. Thus

$$t=\frac{16}{\pi}\int_0^R dr\int_0^\infty dk\sum_l(l+\tfrac{1}{2})\left(v^2-\frac{\pi kr}{2}J_{l+\frac{1}{2}}^2\right).$$

Inserting this in (6), we have finally

$$\frac{pV}{RT}=1+\frac{1}{V}\left\{\mp\frac{N\pi^{\frac{3}{2}}\lambda^3}{2}+32\pi\lambda^3N\int_0^\infty dkl^{-\lambda^2k^2}\sum_l(l+\tfrac{1}{2})\int_0^\infty dr\left(\frac{\pi kr}{2}J_{l+\frac{1}{2}}^2-v^2\right)\right\},$$

where the integral over r has been extended to infinity for the reasons previously given.

Appendix 2.

Since we are going to the actual lim $k=0$, we may use the formula for η in the neighborhood $k=0$,[20] namely,

$$\eta=-\frac{\pi}{2}\frac{m}{\hbar^2}\int_0^\infty rVJ_{l+\frac{1}{2}}^2(kr)dr.$$

Thus in the neighborhood $k=0$[21]

$$f=\sum_{\text{even }l}(-1)^l(l+\tfrac{1}{2})\frac{\sin 2}{k}\eta_l\sim 2\sum_{\text{even }l}(-1)^l(l+\tfrac{1}{2})\frac{\eta_l}{k}=-\frac{\pi m}{\hbar^2}\sum_{\text{even }l}(-1)^l(l+\tfrac{1}{2})\int_0^\infty\frac{rV}{k}J_{l+\frac{1}{2}}^2(kr)=\frac{-m}{2\hbar^2}\int_0^\infty rV\left(r+\frac{\sin 2kr}{2k}\right).$$

From this one sees immediately that $f'(0)$, $f'''(0)$, etc. vanish.

This also gives $f(0)=-\frac{m}{\hbar^2}\int_0^\infty Vr^2dr$. One cannot, however, calculate $f''(0)$, $f''''(0)$, etc. from this formula, since to do so accurately one must know η to higher approximations.

Nor can one be sure that this proof is correct, since it is questionable if the above formula for η is the proper one to apply as $k\to 0$. However, detailed calculations for the rigid sphere, the potential well, and the noise potential models, all confirm the fact that as $k\to 0$, the expression for η contains only odd powers of k.

[20] Mott and Massey, *Theory of Atomic Collisions*.
[21] Watson, *Bessel Functions*, p. 152.

LETTERS TO THE EDITOR

Prompt publication of brief reports of important discoveries in physics may be secured by addressing them to this department. Closing dates for this department are, for the first issue of the month, the eighteenth of the preceding month, for the second issue, the third of the month. The Board of Editors does not hold itself responsible for the opinions expressed by the correspondents.

Communications should not in general exceed 600 words in length

The Paschen-Back Effect—$^3S^3P$ Multiplets in Strong Fields

In a letter to the editor under the above heading[1] P. Jacquinot explains that the article by us[2] with the same title is practically a repetition of his work reported in the *Comptes rendus*.[3] We should like to clear up this matter.

The article cited by Jacquinot in the C.R. reports in several places that the field strength used was 4400 gauss and was repeated as such in *Science Abstracts*. The conclusions drawn are in error if based on this figure. The letter[1] published after our article mentions a field strength of 44,000 gauss and is in agreement with our work at 38,000 gauss. The supposed lack of recognition is therefore the result, not of a lack of information, but of several typographical errors.

In view of these facts it would seem that priority of the results should be given to the excellent work of M. Jacquinot. The important point, however, is that the same result has been obtained by two independent observers using different methods and serves to clear up an outstanding difficulty in the theory of atomic spectra.

J. B. GREEN
R. A. LORING

Ohio State University,
Columbus, Ohio,
October 29, 1936

[1] Jacquinot, Phys. Rev. **50**, 573 (1936).
[2] Green and Loring, Phys. Rev. **49**, 630 (1936).
[3] P. Jacquinot, Comptes rendus **200**, 383 (1935).

The Heavy Particle Component of the Cosmic Radiation

In a recent paper by the above title,[1] Brode, MacPherson and Starr have published a number of cloud chamber photographs of heavy particles which are probably protons. They conclude their paper with the statement that "It is now, however, not possible to say that the failure to observe heavy particles in the cosmic radiation in a cloud chamber is evidence against the existence of primary protons." This conclusion depends upon the fact that it is only near the end of the range of the proton that one may expect to find it in a condition such as to produce observable tracks. However, in a recent paper by W. F. G. Swann[2] the theory of this matter was developed and it was shown how one can utilize such knowledge as we have to find how many observable particles might be expected in terms of the number of rays passing through the apparatus per second. In a further paper by the writers in conjunction with W. E. Ramsey and W. F. G. Swann,[3] experiments were reported in which actual measurements were made on the bursts of ionization in an ionization chamber with the resultant conclusion that not more than 10 percent of the intensity of the hard component, or more than 5 percent of the total number of cosmic rays at sea level, can consist of primary protons.

Now, these same considerations are, of course, applicable to the experiment of Brode, MacPherson and Starr. If, in fact, we assume that the hard component of the cosmic radiation consists of primary protons, then the fraction of these protons which will end their paths within a given distance R is simply μR, where μ is the coefficient of absorption of the radiation. If the relation between the range of a proton and its specific ionization is known, we can find R for a proton which will have a given specific ionization, and so compute the number of particles having a specific ionization greater than this, which we would expect to find in the cloud chamber photographs. Since it is difficult to estimate the age of a track which occurred before the discharge of the counter actuating the cloud chamber, we shall confine our attention to those heavy particles which set off the counters. Brode, MacPherson and Starr found, out of a total of 8500 counter discharges, 7 particles having specific ionization between two and five times that of an electron, and 7 having between 5 and 20 times the electronic ionization. Let us take for μ the value of 0.08 per meter of water, and assume 0.4 as the fraction of the sea-level cosmic-ray intensity which is the hard component.[4] The range of a proton of specific ionization five times that of an electron (160 ion pairs/cm) may be taken from Bethe's theoretical values as 1430 meters of air. Hence we should expect, in 8500 rays, 510 protons having at least this ionization. This expected number is considerably smaller than the observed one, and we can, in fact, conclude from these calculations that an upper limit of 1.4 percent of the hard component of the cosmic radiation can be primary protons. There is considerable uncertainty, it is true, that the range of protons of this high energy (about 3×10^8 ev) is given correctly by Bethe's expression, and it is for this reason that no corresponding estimate can be made from the observations concerning the particles having smaller specific ionization. We therefore should place upon the numerical value of the upper limit here calculated only the significance that it is much smaller than

is required by a theory of cosmic radiation which ascribes the hard component to primary protons. As has been pointed out before, experiments of this nature can not eliminate the possibility of primary protons whose effects are produced chiefly through the agency of their secondaries.

Perhaps the weakest point in the foregoing argument lies in the fact that it is necessary to assume a relation between the range and specific ionization of protons which is not yet verified by experiment. However, we have to realize that it is only in respect of such uncertainty that our experiments and those of Brode, MacPherson and Starr fail to give definite evidence against the existence of primary protons in appreciable amounts in the observed cosmic radiation.

C. G. MONTGOMERY
D. D. MONTGOMERY

The Bartol Research Foundation of the Franklin Institute,
Swarthmore, Pennsylvania,
October 26, 1936.

[1] R. B. Brode, H. G. MacPherson and M. A. Starr, Phys. Rev. **50**, 581 (1936).
[2] W. F. G. Swann, Phys. Rev. **49**, 478 (1936).
[3] C. G. Montgomery, D. D. Montgomery, W. E. Ramsey and W. F. G. Swann, Phys. Rev. **50**, 403 (1936).
[4] A. H. Compton, Rev. Sci. Inst. **7**, 71 (1936).